

FINAL REPORT
ELECTRONIC AND NUCLEAR PARAMAGNETISM
AND
ENERGY TRANSFER MECHANISMS IN CRYSTALLINE SOLIDS

by

WILLIAM A. BARKER
JOHN J. HILL
THOMAS V. HYNES
ROBERT F. O'BRIEN, S.J.

Compiled by
VINCENT P. JACOBMEYER, S.J.
Principal Investigator
SAINT LOUIS UNIVERSITY
St. Louis, Missouri

Contract No. AF 30 (602) - 2204
Project No. 8503
Task No. 850302

Prepared for
Rome Air Development Center
Research and Technology Division
Air Force Systems Command
United States Air Force
Griffiss Air Force Base
New York

LOAN COPY
AEWL
KIRTLAND



20080306249

PATENT NOTICE: When Government drawings, specifications, or other data are used for any purpose other than in connection with a definitely related Government procurement operation, the United States Government thereby incurs no responsibility nor any obligation whatsoever and the fact that the Government may have formulated, furnished, or in any way supplied the said drawings, specifications or other data is not to be regarded by implication or otherwise as in any manner licensing the holder or any other person or corporation, or conveying any rights or permission to manufacture, use, or sell any patented invention that may in any way be related thereto.

DDC NOTICE: Qualified requestors may obtain copies of this report from the Defense Documentation Center (DDC), Cameron Station, Alexandria, Virginia 22314. DDC Services for the Department of Defense contractors are available through the "Field of Interest Register" on a "need-to-know" certified by the cognizant military agency of their project or contract.

~~THIS INFORMATION IS UNCLASSIFIED~~ This information is furnished upon the condition that it will not be released to another nation without specific authority of the Department of the Air Force of the United States, that it will be used for military purposes only, that individual or corporate rights originating in the information whether patented or not will be respected, and that the information be provided substantially the same degree of security afforded it by the Department of Defense of the United States.



0141829

RADC-TDR-63-446

September 1963

AD-425116

FINAL REPORT

Electronic and Nuclear Paramagnetism
and
Energy Transfer Mechanisms in Crystalline Solids

by

William A. Barker
John J. Hill
Thomas V. Hynes
Robert F. O'Brien, S. J.

Compiled by

Vincent P. Jacobsmeyer, S. J.
Principal Investigator

Saint Louis University
St. Louis, Missouri

Contract No. AF 30 (602) - 2204
Project No. 8503
Task No. 850302

Prepared for

Rome Air Development Center
Research and Technology Division
Air Force Systems Command
United States Air Force
Griffiss Air Force Base
New York

PATENT NOTICE: When Government drawings, specifications, or other data are used for any purpose other than in connection with a definitely related Government procurement operation, the United States Government thereby incurs no responsibility nor any obligation whatsoever and the fact that the Government may have formulated, furnished, or in any way supplied the said drawings, specifications or other data is not to be regarded by implication or otherwise as in any manner licensing the holder or any other person or corporation, or conveying any rights or permission to manufacture, use, or sell any patented invention that may in any way be related thereto.

DDC NOTICE: Qualified requestors may obtain copies of this report from the Defense Documentation Center (DDC), Cameron Station, Alexandria, Virginia 22314. DDC Services for the Department of Defense contractors are available through the "Field of Interest Register" on a "need-to-know" certified by the cognizant military agency of their project or contract.

EXISTENCE OF PROPRIETARY INFORMATION NOTICE: This information is furnished upon the condition that it will not be released to another nation without specific authority of the Department of the Air Force of the United States, that it will be used for military purposes only, that individual or corporate rights originating in the information whether patented or not will be respected, and that the information be provided substantially the same degree of security afforded it by the Department of Defense of the United States.

ABSTRACT


The enhancement of the Na^{23} nuclear magnetic resonance signal by means of the Solid Effect has been observed at 78°K in a sample of mono-crystalline NaCl in which Cl_2^- molecular ions had been introduced by X-ray irradiation. A simple saturation theory for electronic transitions has been developed and checked against the data on EPR lines of both Cl_2^- centers in NaCl and KCl and of Mn^{++} ions in calcite. The relaxation times of the five Mn^{++} transitions have been calculated. Values of the microwave field required for such calculations have been measured in a novel fashion. The linewidth, saturability, and the T_1 and T_2 relaxation times for the invisible forbidden transitions have been obtained, and with these the observed variation of enhancement with applied power has been predicted. Having estimated the number of Cl_2^- centers, the number of Na^{23} nuclei polarized per Cl_2^- center was calculated to be of the order of 10^5 . It was also found that the enhanced NMR signal grew under application of power and decayed back to the unenhanced value with the same decay time of 59 seconds. This data indicated the presence of spin diffusion, or diffusion of the polarization to approximately 30 interionic distances from the Cl_2^- center. Double resonance instrumentation is discussed and preliminary experimental data (both single and double resonances) is reported on a variety of liquid and solid samples. A discussion of certain experimental and theoretical aspects of double resonance

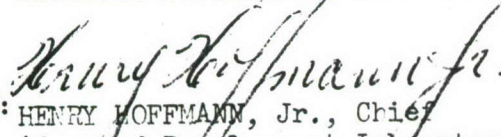
experiments is included. The Report is concluded with a review of this group's theoretical and experimental research effort and some proposals for further research.

Title of Report RADC-TDR-63-446

PUBLICATION REVIEW

This report has been reviewed and is approved. For further technical information on this project, contact Mr. James G. Constantine, RAUAA, Ext. 7671.

Approved: 
 JAMES G. CONSTANTINE
 Advanced Analysis Branch
 Advanced Development Laboratory

Approved: 
 HENRY HOFFMANN, Jr., Chief
 Advanced Development Laboratory
 Directorate of Communications

FOR THE COMMANDER:

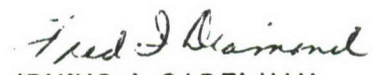

 IRVING J. GABELMAN
 Director of Advanced Studies

TABLE OF CONTENTS

CHAPTER		Page
1.	INTRODUCTION	1
2.	DYNAMIC POLARIZATION OF Na^{23} IN NaCl	5
2.1	Introduction	5
2.2	Saturation Theory	7
2.3	Calculation of Saturation Relaxation Times T_1 and T_2	15
2.4	Measurement of H_1 by Electron Rotary Resonance	17
2.5	Saturation T_1 and T_2 Values For Various EPR Lines	24
2.6	The Cl_2^- Center	37
2.7	Estimate of Number of Centers	42
2.8	Extension of the Saturation Equations to Enhancement of Nuclear Signals	50
2.9	Application of Saturation Theory to Enhancement Data	53
2.10	Prediction of Enhancement as a Function of Power	57
2.11	Dynamic Polarization of Na^{23}	58
2.12	Enhancement of Na^{23} Using Mn^{++} Lines	71

TABLE OF CONTENTS - continued

CHAPTER		Page
	2.13 Relaxation of Polarized Na ²³ Nuclei	72
	2.14 Conclusion	80
	References	82
	Glossary	84
	Appendix	87
3	INSTRUMENTATION	90
	3.1 Introduction	90
	3.2 Experimental Equipment	90
	3.2.1 Nuclear Magnetic Resonance Detector	90
	3.2.2 Microwave Cavity	94
	3.2.3 Low Temperature Apparatus	97
4	RESONANCE EXPERIMENTS	98
	4.1 Introduction	98
	4.2 Experimental Data	99
	4.2.1 DPPH in Benzene	99
	4.2.2 Fuel Oil and Asphalt Dissolved in Pump Oil	101
	4.2.3 Boron	107
	4.2.4 Graphite	112
	4.2.5 Germanium	113
	4.2.6 Potassium Chloride	115

TABLE OF CONTENTS - continued

CHAPTER		Page
5	PREPARATION AND INVESTIGATION OF VARIOUS SAMPLES SUITABLE FOR DMR	120
5.1	General Considerations	120
5.2	Samples Prepared and Under Study	123
5.2.1	Sugar Chars	123
5.2.2	Sodium Dispersion in Mineral Oil	124
6	CONCLUSIONS AND RECOMMENDATIONS	128
6.1	Conclusions	128
6.2	Recommendations	130

LIST OF ILLUSTRATIONS

FIGURE		Page
1 (a)	Typical EPR Spectrum of Cl_2^- Centers in KCl	14
1 (b)	Typical EPR Spectrum of Cl_2^- Centers in NaCl	14
2	Amplitude of Rotary Resonance in H_1 Field as a. Function of Detection Frequency	23
3	Maximum Saturation of an EPR Line as a Function of $P_o/P_{\text{max},A}$	25
4	Ratio of Saturation at Absorption Peak to Saturation at Derivative Peak as a Function of $P_o/P_{\text{max},A}$	26
5 (a)	Typical EPR Spectrum of Mn^{++} in NaCl	27
5 (b)	Typical EPR Spectrum of Mn^{++} in Calcite	27
6	Saturation Data for Mn^{++} in Calcite	29
7 (a)	Room Temperature Saturation Data for Mn^{++} in Calcite	30
7 (b)	78° K Saturation Data for Mn^{++} in Calcite	31
7 (c)	High Power Part of Normalized Saturation Curve	32
7 (d)	Low Power Part of Normalized Saturation Curve	33
8	Saturation Curve for Cl_2^- Centers in NaCl	41
9 (a)	Typical Unenhanced Na^{23} Nuclear Signal Detected at 3.6400 Mc and at 77° K	43

LIST OF ILLUSTRATIONS - continued

FIGURE		Page
9 (b)	Enhanced Na ²³ Nuclear Signal at 77° K and -3 db Microwave Power Detected at 3.6400 Mc	43
9 (c)	Enhanced Na ²³ Nuclear Signal at 77° K and -3 db Microwave Power Detected at 3.6420 Mc	43
10	Enhancement as a Function of Position (Negative Enhancement)	61
11	Enhancement as a Function of Position (Positive Enhancement)	66
12	Enhancement as a Function of Applied Power	67
13	Decay and Rise of Enhanced Na ²³ NMR Signal	73
14 (a)	Relative Number of Nuclei Polarized as a Function of Time	75
14 (b)	Rise of the Number Polarized as a Function of Time	76
15 (a)	Side View: NMR Coil in EPR Cavity	93
15 (b)	End View	93
16 (a)	Effect of Quartz Sheathing on Amplitude of EPR Signal - No Quartz	93
16 (b)	Effect of Quartz Sheathing on Amplitude of EPR Signal - Quartz Sheath	93
17	Enhanced Proton Resonance Signal from Fuel Oil Sample	103

LIST OF ILLUSTRATIONS - continued

FIGURE		Page
18	Percent Enhancement vs Magnetic Field and Frequency	104
19	EPR Saturation of Asphalt in Pump Oil Sample	104
20	Enhanced Proton Resonance Signal from Asphalt in Pump Oil Sample	106
21	EPR Spectra of Crystalline Boron Indicating Temperature and Orientation Dependence	108
22	Crystal Orientation in Magnetic Field	110
23 - 25	B^{11} EPR	110
26	EPR Spectrum from Graphite Single Crystals at Different Microwave Power Levels	114
27 (a)	Ge^{73} EPR	114
27 (b)	Ge^{73} EPR	114
28 (a)	EPR Spectra of Cl_2^- Centers in KCl (Pb^{++}) Crystals at 17 db attenuation	116
28 (b)	EPR Spectra of Cl_2^- Centers in KCl (Pb^{++}) Crystals at 5 db attenuation	116

LIST OF TABLES

TABLE		Page
I	Mn^{++} in Calcite ($\theta = 90^\circ$)	34 - 35
II	Data on Calibration Sample, Calcite (Mn^{++})	45
III	Data on Cl_2^- Centers in NaCl	47
IV	Negative Enhancement Data	62 - 63
V (a)	Positive Enhancement Data	68 - 69
V (b)	Positive Enhancement vs Power Applied	70

CHAPTER 1

INTRODUCTION

In accordance with the Request for Proposal No. 02916 dated January 18, 1960, Saint Louis University submitted a Technical Proposal calling for joint theoretical and experimental research on nuclear polarization. This proposal resulted in the award of a basic research contract by Rome Air Development Command in the Fall of 1960. The work under this contract dealt mainly with the theoretical investigation of static and dynamic nuclear polarization mechanisms, the development of instrumentation for the detection of Double Resonance phenomena, the experimental investigation of a variety of samples, and the analysis and interpretation of the data obtained in such experiments. Technical Note No. 1 was delivered to Rome Air Development Command in September, 1961, and Technical Note No. 2 in September, 1962.

The work reported herein is a continuation of the work described in the preceding Technical Notes. There are six sections in this report, the first of which is this Introduction.

Mr. John Hill presents a detailed report on experimental and theoretical work completed on Cl_2^- centers in NaCl crystals in Chapter 2. By use of double resonance techniques and a low level NMR oscillator-detector, the Na^{23} nuclear magnetic resonance

signal in a sample of monocrystalline NaCl at 77° K was successfully enhanced by a factor of from 2 to 8 both positively (power absorbed) and negatively (power emitted) by means of the Solid Effect. This was accomplished by pumping on forbidden transitions of the electron spin resonance lines of the Cl_2^- molecular ions, introduced by X-ray irradiation. The enhancement was studied by developing a simple saturation theory for the electronic transitions. The theory was checked against the data on EPR lines of both Cl_2^- centers in NaCl and KCl and of Mn^{++} ions in calcite. Some interesting information on the saturation relaxation times of the Mn transitions was found. In order to get more accurate values for the relaxation time from saturation data, a knowledge of the microwave field was required. This was measured in a novel fashion by using a highly saturable EPR line at room temperature and detecting the resonance about the rotating microwave field with the double resonance equipment.

In applying the saturation theory to the Na^{23} enhancement data, the line width, saturability, T_1 and T_2 for the invisible forbidden transition were obtained, based on the assumption of a Lorentzian line shape. With this information it was then possible to predict the observed variation of enhancement with applied microwave power. By estimating the number of Cl_2^- centers present in the sample, the number of Na^{23} nuclei polarized per Cl_2^- center was calculated and found to be quite large of the order of 10^5 . It was also found that the enhanced nuclear signal grew under

application of power and decayed back to the unenhanced value with the same decay time of 58 seconds. This data then indicates the presence of spin diffusion or diffusion of the polarization to about 30 interionic distances from the Cl_2^- center.

In Chapter 3, Mr. Robert O'Brien outlines the work performed on instrumentation during the past year. The sensitivity of the double resonance detection system has been improved and a much better understanding of the instrumental parameters involved in such experiments has been acquired. Particular attention is paid to the double resonance EPR cavity and NMR coil.

The experimental data obtained in experiments on a variety of samples investigated during this past year is presented by Mr. O'Brien in Chapter 4. Slight NMR signal enhancements are reported in several liquid samples. A discussion of some of the critical parameters is included. Experiments on a variety of crystal samples including boron, graphite, germanium, KCl, et al., have yielded considerable information on double and single resonance in solids, although no signal enhancement was observed.

In Chapter 5, Mr. Thomas Hynes has presented some general considerations germane to double resonance experimentation. He discusses the importance of various terms in the Hamiltonian of a general electron-nuclear system. Special consideration is given to the topics of spin concentrations and sample saturability. He concludes with a commentary on a few specific samples and the double resonance problems peculiar to them.

In Chapter 6, Dr. William A. Barker concludes this report with a review of this group's theoretical and experimental research effort. In the light of his review Dr. Barker indicates some guide lines for further research during the next three-year period of the renewal contract.

CHAPTER 2

DYNAMIC POLARIZATION OF Na^{23} IN NaCl

2.1 INTRODUCTION

For a system containing unpaired electrons (or paramagnetic centers in general) in which nuclear spins are coupled to the electrons through hyperfine terms or Zeeman terms in the Hamiltonian of the system, there exists the possibility of enhancing the resonant power absorbed or the power emitted by the nuclear system. In general this is accomplished by pumping sufficient power into an allowed transition (the Overhauser effect) or into a forbidden transition (the solid or Jeffries-Abragam effect) of the electron system in order to over or under populate nuclear levels. Due to space quantization of the energy states this is equivalent to the polarization of nuclei. For electron systems with strong relaxation mechanisms, indicated by a short spin lattice relaxation time, much power is needed to preserve the overpopulation of the levels. For weak relaxation processes, or long relaxation times, overpopulation can be accomplished with low pumping power.

The relaxation times usually increase with decreasing temperature. Most nuclear polarization by dynamic pumping has been accomplished in solids only at very low temperatures (1° to 4° K). Some very large enhancements have been obtained

in liquid samples at room temperature.

The possibility of dynamic nuclear polarization was first suggested in 1953 by Overhauser¹. He predicted that nuclear magnetic resonance signals of metal atoms could be enhanced by pumping strongly on the paramagnetic resonance signal of the conduction electrons. This effect was subsequently observed in Lithium metal by Carver and Slichter² in a field of about 30 gauss. In this case, pumping on the allowed electronic transition overpopulated the nuclear levels and gave rise to an enhanced Lithium nuclear resonance.

In 1958 Erb, Motchane and Uebersfeld³ observed an enhanced proton resonance for protons absorbed on powdered coal containing paramagnetic centers. They observed a positive enhancement when the pumping frequency was lower than the electronic transition frequency, no enhancement when equal to the electronic transition frequency and a negative enhancement when the pumping frequency was higher than the electronic transition frequency. This, the so called solid state effect, is possible due to the fact that in solids the nuclear spin lattice relaxation times are quite long compared to those for liquids. In the solid the probability for pumping on a forbidden transition (in which both electrons and nuclear spin change) is greater than that of the nuclear spin relaxation thus allowing the nuclear states to change in population from the normal Boltzmann distribution.

The solid effect has been observed in many samples, in

polymers containing paramagnetic centers produced by irradiation and in solids containing color centers or paramagnetic ions^{4,5}.

In the following experiment, the electron spin resonance (ESR) spectrometer was used to detect and pump on the electron energy levels in the 9000 Mc range. A low level oscillator-detector operating as a nuclear magnetic resonance spectrometer in the 2 - 15 Mc range was employed to detect the nuclear transitions and the increase in power absorbed or emitted (positive or negative enhancement).

By introducing paramagnetic centers into a NaCl crystal, both a positive and negative enhancement of the Na²³ nuclear magnetic resonance signal was observed at 77° K by pumping on a forbidden transition. An attempt was made to develop and apply a simple theory of saturation of magnetic resonance lines, based on the assumption of a Lorentzian line shape, to the enhancement data and thus to obtain information about the line width and the relaxation time of the forbidden transition. An attempt was also made to measure the effect of the paramagnetic center on the ordinary relaxation time of the Na²³ nuclei in the NaCl crystal and to determine the number of Na²³ nuclei polarized by a single paramagnetic center.

2.2 SATURATION THEORY

The theory of the saturation of an electron spin resonance line was presented in the previous report (RADG-TR 62-436

Technical Note No. 2, September 1961 - August 31, 1962 Contract No. AF 30(602)-2204). At this point the saturation S is redefined to apply to those cases where $h\nu$ is small compared to kT and the Boltzmann populations of levels 1 and 2 are $(n_1)_0$ and $(n_2)_0$. The changes to be made on page 3.7 of the previous report⁶ are as follows.

$$\text{The saturation } S = 1 - \frac{n_1 - n_2}{(n_1)_0 - (n_2)_0} \quad (2.1)$$

where n_1 and n_2 are the populations under pumping with frequency ν and $(n_1)_0$ and $(n_2)_0$ are the normal Boltzmann populations.

Then Eq. 10 becomes

$$\frac{d}{dt}(n_1 - n_2) = \frac{[(n_1)_0 - (n_2)_0] - (n_1 - n_2)}{T_1} \quad (2.2)$$

and Eq. 11 becomes

$$\frac{d}{dt}(n_1 - n_2) = \frac{[(n_1)_0 - (n_2)_0] - (n_1 - n_2)}{T_1} - 2\pi(n_1 - n_2) \quad (2.3)$$

Thus Eq. 12 still remains the same as before, namely:

$$S = \frac{2\pi T_1}{1 + 2\pi T_1} \quad (2.4)$$

where π is the transition probability.

In this same report a factor of $3/2$ was omitted in Eq. 15 and the previous equation (p. 3.8). Thus Eq. 15 should read

$$\pi = \frac{3}{8} \gamma^2 H_1^2 T_2 (1 + \gamma^2 H_1^2 T_1 T_2)^{-1/2} \quad (2.5)$$

Eq. 16 then reads

$$A_0^{(S)} = \frac{P/P_{MAX,A}}{\frac{4}{3}(4 + 2 \frac{P}{P_{MAX,A}})^{1/2} + \frac{P}{P_{MAX,A}}} \quad (2.6)$$

This gives the value for S at $P = P_{max}$ of 23% instead of 17% as indicated on pages 3.9 and 3.11.

If the line under consideration is inhomogeneously broadened it will probably be of Gaussian shape. The Gaussian shape function can be given by

$$g(\omega) = 2T_2 \exp\left(-\frac{T_2^2}{\pi}(\omega - \omega_0)^2\right)$$

which is normalized such that

$$\frac{1}{2\pi} \int_0^\infty g(\omega) d\omega = 1 \quad (2.7)$$

For small values of $(\omega - \omega_0)$ that is, near the peak of the absorption curve, it is expected that the Gaussian and Lorentzian shapes will be about the same, and that the tails of the line shape will show the greatest difference. For $(\omega - \omega_0)$ small, $g(\omega) \rightarrow \frac{2T_2}{1 + \frac{T_2^2}{\pi}(\omega - \omega_0)^2}$ which is Lorentzian.

A similar derivation for the Gaussian shape can be made as follows. The absorption signal B is

$$B = \frac{1}{4} \chi_0 \omega_0 H_1 g(\omega) (1 + \gamma^2 H_1^2 T_1 T_2)^{-1} \quad (2.8)$$

The derivative signal A is given by

$$A = \frac{dB}{d\omega} = -\frac{2}{\pi} T_2^2 (\omega - \omega_0) B \quad (2.9)$$

The peak value of the derivative signal A_0 is found when $\frac{dA}{d\omega} = 0$ or when $\omega = \omega'$. Thus

$$-\frac{2}{\pi} T_2^2 B(\omega') - \frac{2}{\pi} T_2^2 (\omega' - \omega_0) \left(\frac{dB}{d\omega} \right)_{\omega=\omega'} = 0 \quad (2.10)$$

From Eq. 2.9 at the derivative peak,

$$\omega' - \omega = \frac{\sqrt{\pi}}{\sqrt{2} T_2} \quad (2.11)$$

$$g(\omega') = 2 T_2 e^{-1/2} \quad (2.12)$$

and

$$A_o = A(\omega') = \frac{-\chi_o \omega_o H_1 T_2^2 (2\pi e)^{-1/2}}{1 + \gamma^2 H_1^2 T_1 T_2} \quad (2.13)$$

As we saturate the transition by increasing H_1 , the maximum value of the derivative peak, $(A_o)_{\max}$, will occur when

$$\left(\frac{\partial A_o}{\partial H_1} = 0 \right)_{H_1 = (H_1)_{\max, A}}$$

or when

$$\gamma^2 (H_1)_{\max, A}^2 T_1 T_2 = 1 \quad (2.14)$$

Then

$$(A_o)_{\max} = -\frac{1}{2} \chi_o \omega_o (H_1)_{\max, A} T_2^2 (2\pi e)^{-1/2} \quad (2.15)$$

and

$$\frac{A_o}{(A_o)_{\max}} = \frac{2 H_1 (H_1)_{\max, A}}{1 + \gamma^2 H_1^2 T_1 T_2} \quad (2.16)$$

Using Eq. 2.14 we can evaluate the ratio $P/P_{\max, A}$

$$\frac{P}{P_{MAX,A}} = \frac{H_1^2}{(H_1)_{MAX,A}^2} = \frac{\gamma^2 H_1^2 T_1 T_2}{\gamma^2 (H_1)_{MAX,A}^2 T_1 T_2} = \frac{\gamma^2 H_1^2 T_1 T_2}{1} \quad (2.17)$$

Then Eq. 2.16 becomes

$$\frac{A_0}{(A_0)_{MAX}} = \frac{2 (P/P_{MAX,A})^{1/2}}{(1 + P/P_{MAX,A})} \quad (2.18)$$

From Eqs. 2.4, 2.12, 2.17 and

$$\pi_{A=A_0} = \frac{1}{4} \gamma^2 H_1^2 g(\omega') = \frac{1}{2} \gamma^2 H_1^2 T_2 e^{-1/2} \quad (2.19)$$

the saturation S can be found,

$$S_{A_0} = \frac{\gamma^2 H_1^2 T_1 T_2}{\sqrt{2} + \gamma^2 H_1^2 T_1 T_2} = \frac{P/P_{MAX,A}}{\sqrt{2} + P/P_{MAX,A}} \quad (2.20)$$

In order to estimate easily the maximum saturation obtainable for an EPR line with the available power P_0 , Eqs. 2.6 and 2.20 for the Lorentzian and Gaussian lines are used to plot Figure 3.

This shows the saturation at maximum power P_0 for a line whose derivative signal is a maximum at $P_{\max,A}$. At $P = P_{\max,A}$,

$$S = \frac{1}{1 + \sqrt{e}} = .378 \text{ or } 37.8\%, \text{ for the Gaussian line.}$$

Figure 6 (p. 3.14) of the previous report⁶ shows the fit of the Lorentzian theory to the saturation data on two EPR lines. These were due to Cl_2^- centers in KCl and to Fe^{+++} in calcite⁷. Additional data is included here on Mn^{++} lines in calcite and Cl_2^- centers in NaCl. A typical spectrum of Cl_2^- in KCl, Cl_2^- in NaCl, Mn in calcite and Mn in NaCl is shown in Figures 1 and 5.

The EPR spectrum of Mn^{++} ions substituting for Ca ions in CaCO_3 (calcite) has been studied by Hurd, Sachs, and Hershberger⁸. The spectrum consists in five sets of six line groups. The six lines in each set are due to the hyperfine interaction of the electron spin and the $5/2$ nuclear spin of Mn. There are five such sets due to the six possible energy states of the five unpaired Mn electrons. The Hamiltonian and Eigenvalues are given in detail in the reference⁸.

It was found that the transitions between the higher value electronic spin states fit the saturation curve based on a Gaussian shape line rather than the Lorentzian line. The Gaussian shape is similar to the error function and arises due to interactions with surrounding nuclei. Inhomogeneously broadened lines are associated with the Gaussian shape while those lines which are homogeneously broadened with little interaction with the surrounding nuclei are usually closer to the Lorentzian shape.



Figure 1 (a). Typical EPR Spectrum of Cl_2^- Centers in KCl



Figure 1 (b). Typical EPR Spectrum of Cl_2^- Centers in NaCl

In calcite, there are practically no nuclei with magnetic moments except the low abundant isotopes of Ca^{43} , C^{13} , and O^{17} . The saturation data for a single line of each set of the five electron transitions are plotted in Figure 7. The graph shows the value of the derivative peak normalized to the maximum value plotted against the power applied normalized to the value at the maximum derivative signal, $P/P_{\text{max},A}$. The heavy lines are the theoretical relationships:

$$\frac{A_0}{(A_0)_{\text{max}}} = \frac{(P/P_{\text{max},A})^{1/2}}{(\frac{2}{3} + \frac{1}{3} P/P_{\text{max},A})^{2/3}} \text{ for the Lorentzian shape.} \quad (2.21)$$

and

$$\frac{A_0}{(A_0)_{\text{max}}} = \frac{2 (P/P_{\text{max},A})^{1/2}}{(1 + P/P_{\text{max},A})} \text{ for the Gaussian shape.} \quad (2.22)$$

2.3 CALCULATION OF SATURATION RELAXATION TIMES T_1 AND T_2

In order to calculate saturation values of T_1 and T_2 in the above equations, it is only necessary to decide whether the Gaussian or Lorentzian saturation equations apply. Then using the value of $P_{\text{max},A}$ for the line (if the maximum derivative signal can be obtained with the power available), the product T_1 and T_2 can be evaluated. Then knowing T_2 from the line width, T_1 can be

calculated. For the Lorentzian line we have

$$\gamma^2 (H_1)_{\text{MAX},A}^2 T_1 T_2 = \begin{cases} 1/2 & \text{Lorentzian} \\ 1 & \text{Gaussian} \end{cases} \quad (2.23)$$

The line width $\Delta\omega$ or width between points of maximum slope of the absorption signal is then

$$\Delta\omega = 2(\omega_0 - \omega') \quad (2.24)$$

Hence ⁶

$$\Delta\omega = \begin{cases} \frac{(1 + \gamma^2 H_1^2 T_1 T_2)^{1/2}}{\sqrt{3} T_2} & \text{Lorentzian} \\ \frac{\sqrt{2\pi}}{T_2} & \text{Gaussian} \end{cases} \quad (2.25)$$

Now

$$\left(\gamma^2 H_1^2 T_1 T_2 = P/P_{\text{MAX},A} \right)_{\substack{\text{LORENTZ.} \\ P=P_{\text{MAX},A}}} = \frac{1}{2} \quad (2.26)$$

Hence

$$T_2 = \begin{cases} \frac{2}{\sqrt{2} (\Delta\omega)_{P_{\text{MAX},A}}} & \text{Lorentzian} \\ \frac{\sqrt{2\pi}}{\Delta\omega} & \text{Gaussian} \end{cases} \quad (2.27)$$

Thus the saturation T_2 can be obtained directly from line width data. The saturation T_1 can be found if $(H_1^2)_{\max,A}$ can be found. In general the quantity measured at the maximum derivative signal is merely the ratio $\frac{H_1^2_{\max,A}}{(H_1)_0^2}$ or $\frac{P_{\max,A}}{P_0}$ which is the attenuation of the Power P_0 . Calculation of the power P_0 requires knowledge of the cavity Q , and other quantities difficult to measure. A direct measurement of $(H_1)_0$ or the microwave field in the cavity is desirable and is described in the next section. Knowing $(H_1)_{\max,A}^2$ then T_1 is given by

$$T_1 = \begin{cases} (2\gamma^2(H_1)_{\max,A}^2 T_2)^{-1} & \text{Lorentzian} \\ (\gamma^2(H_1)_{\max,A}^2 T_2)^{-1} & \text{Gaussian.} \end{cases} \quad (2.28)$$

2.4 MEASUREMENT OF H_1 BY ELECTRON ROTARY RESONANCE

In the process of studying the saturable lines of Mn^{++} ions in calcite, an attempt was made to saturate a Mn^{++} line and to detect with the Robinson oscillator an enhanced nuclear resonance of C^{13} in the calcite. This was not detectable but upon strongly saturating the EPR line of the Mn^{++} , a resonance signal was observed from the Robinson NMR oscillator. Upon changing the detection frequency of the NMR oscillator within a 2 to 10 Mc range, the observed signal did not shift in field as an enhanced nuclear signal would, but continued to be observed at the same field

position upon passing through the EPR line. The field H_0 was scanned slowly with a fixed EPR detection frequency and a fixed NMR detection frequency. The amplitude of the signal did change with NMR frequency, indicating an electron resonance in the rotating H_1 field. The applied microwave field $(2(H_1) \sin \omega t) \vec{i}$ can be resolved into two counter-rotating fields

$$(H_1) \cos \omega t \vec{i} + (H_1) \sin \omega t \vec{j} \quad \text{and}$$

$$(H_1) \cos (-\omega t) \vec{i} + H_1 \sin (-\omega t) \vec{j}.$$

Only one of these rotating fields is used for detection. The free electron resonates at about 2.8 Mc per gauss. Hence we would expect resonance about H_1 to occur in the range of 1 to 3 Mc.

The resonance of a nucleus in the rotating H_1 field was first observed and explained by Redfield⁹. The rotary resonance was in the audio frequency range. The effect depends upon strongly saturating the resonance signal by applying a large H_1 field. For the rotary resonance of the electron, due to the very small signal being detected, it is preferable to have the sample at room temperature. The gain in saturation at the lower temperatures would probably be lost in increased noise, experimental difficulties in general, and, if liquid nitrogen is used, by bubbling noise. Thus, for the effect to be detected, an easily saturable EPR line at room temperature is needed and one with a small line width of at least the order of magnitude of the rotary resonance frequency or less. The Mn^{++} lines in calcite conform to these requirements although the line width was a little larger than

desired (about 1.3 gauss to 3 gauss, depending on the sample and power applied).

The electron resonance of the $1/2$ to $-1/2$ transition (nuclear spin $5/2$) of Mn^{++} in calcite was detected at very low r.f. levels. A low level Robinson oscillator operating from a coil around the sample in the microwave cavity of the EPR spectrometer was used as the detector. Approximately 35 mv peak to peak on the detection coil will begin saturating the signal. Both a loop type coil with axis perpendicular to H_1 and a solenoid type of several turns with axis along H_1 were effective. As the detection frequency was varied over a wide range (2 - 10 Mc) the rotary resonance signal still appeared as the EPR line was saturated at a fixed static field H_0 , but the amplitude of the signal varied. (A nuclear signal would shift in field as the resonant frequency changed.) The amplitude of the rotary resonance as a function of the detection frequency is shown in Figure 2. All these data points were taken with the solenoid type detection coil. At full power or maximum H_1 value or $(H_1)_0$, the peak occurs at $6.2 \text{ Mc} \pm .2$. At one-half power or $H_1/\sqrt{2}$, the peak occurs at $5.3 \text{ Mc} \pm .1$ and at one-fourth power or $\frac{1}{2}(H_1)_0$ the peak occurs at $4.8 \text{ Mc} \pm .1$. Due to the phase sensitive detection, we expect the recorded signal to appear as the derivative of the absorption line. Thus the peak corresponds to the maximum slope of the resonant absorption line. If we use, as is customary, the line width $\Delta\omega$ as the separation between points of maximum slope, we can write two equations

relating resonant frequency ω_0 and line width $\Delta\omega$, since the derivative peak will occur at $\omega_0 \pm \frac{1}{2}\Delta\omega$. Thus, using

$\omega_0 = \gamma(H_1)_0$, the data indicates

$$\gamma(H_1)_0 + \frac{\Delta\omega_0}{2} = 6.2 \text{ Mc} \pm .05$$

$$\frac{\gamma(H_1)_0}{\sqrt{2}} + \frac{\Delta\omega_3}{2} = 5.3 \text{ Mc} \pm .05$$

$$\gamma \frac{(H_1)_0}{2} + \frac{\Delta\omega_6}{2} = 4.8 \text{ Mc} \pm .05$$

(2.29)

The line used for this data was the transition for the electron $1/2$ to $-1/2$ and nuclear spin of Mn of $5/2$ with the crystal field at 90° to the static field. The γ for this line⁷ was 3.03 Mc/gauss. The observed widths of the original EPR line were 2.80 gauss, 3.03 gauss and 3.40 gauss, all $\pm .2$ gauss at 6 db, 3 db, and 0 db attenuation respectively. These are in the ratio of .82, .89, and 1.00.

A check will show that if we take the line width to be constant, i.e. $\Delta\omega_0 = \Delta\omega_3 = \Delta\omega_6$, that the three data are slightly inconsistent. Clearly, the line is broadening under increasing H_1 . Now if the measured ratios of the actual EPR line widths are inserted in the equations, then

$$\Delta\omega_3 = .89 \Delta\omega_0$$

$$\Delta\omega_6 = .82 \Delta\omega_0$$

(2.30)

Thus the three data equations are

$$\gamma (H_1)_0 + .5 \Delta\omega_0 = 6.2 \pm .05 \text{ Mc}$$

$$\gamma (H_1)_0 + .63 \Delta\omega_0 = 7.5 \pm .07 \text{ Mc}$$

$$\gamma (H_1)_0 + .82 \Delta\omega_0 = 9.6 \pm .1 \text{ Mc}$$

(2.31)

The solution of the first two equations using $\gamma = 3.03 \text{ Mc/g}$

gives the first number and the second two equations the second number

$$\Delta\omega_0 = \begin{cases} 10 \text{ Mc (3.31 gauss } \pm .4) \\ 11 \text{ Mc (3.65 gauss } \pm .2) \end{cases}$$

$$(H_1)_0 = \begin{cases} .43 \text{ gauss } \pm .18 \\ .2 \text{ gauss } \pm .15 \end{cases}$$

This shows that the calculation of $(H_1)_0$ from the resonance data above is not accurate enough due to the effect of small errors in line width producing large errors in $(H_1)_0$. Thus an EPR line which is narrower by at least a factor of 10 would give much better data from the rotary resonance. In order to get a better estimate of $(H_1)_0$, the actual observed values of the line widths in megacycles can be inserted,

$$\gamma (H_1)_0 + 1/2(10.26 \pm .6) = 6.2 \pm .05 \text{ Mc}$$

$$\gamma \frac{(H_1)_0}{\sqrt{2}} + 1/2(9.16 \pm .6) = 5.3 \pm .05 \text{ Mc}$$

$$\gamma \frac{(H_1)_0}{2} + 1/2(8.49 \pm .6) = 4.8 \pm .05 \text{ Mc}$$

(2.32)

The three values obtained for $(H_1)_0$ are $1.07 \text{ Mc} \pm .35$, $1.02 \text{ Mc} \pm .5$, and $1.10 \text{ Mc} \pm .7$. These give values of $(H_1)_0$ of $.354 \pm .12$ gauss, $.337 \pm .17$ gauss and $.364 \pm .23$ gauss. These are consistent within experimental error, and give an average value of $.35$ gauss.

Without a coil in the cavity, the estimated H_1 from cavity size, Q , and power input is of the order of $.7$ gauss. A quartz dewar was used even at room temperature in most other experiments as it was found that the signals increased by $5/3$ with the quartz envelope surrounding the sample. This implies that H_1 was $5/3$ times as large when the quartz dewar is used or about 1.2 gauss. For the rotary resonance experiment a Teflon holder was used, without the quartz dewar and with the solenoidal coil. The introduction of the coil into the cavity lowered the Q . In this case the value of H_1 with the Teflon holder was found to be $.35$ gauss.

In order to use the above value of H_1 in calculating T_1 and T_2 from saturation data, a saturation curve, for the same EPR line of Mn^{++} in calcite as was used for the rotary resonance, was made with the Teflon holder plus coil and also without the coil but in the quartz dewar. Since $\gamma^2 (H_1)_{\text{max},A}^2 T_1 T_2 = 1/2$ at the maximum derivation signal, $P_{\text{max},A}$ is a constant for a given sample and

$$\frac{(H_1)_0 \text{ QUARTZ, NO COIL}}{(H_1)_0 \text{ TEFLON, COIL}} = \frac{\left(P_0 / P_{\text{max},A} \right)^{1/2}_{\text{QUARTZ, NO COIL}}}{\left(P_0 / P_{\text{max},A} \right)^{1/2}_{\text{TEFLON, COIL}}}$$

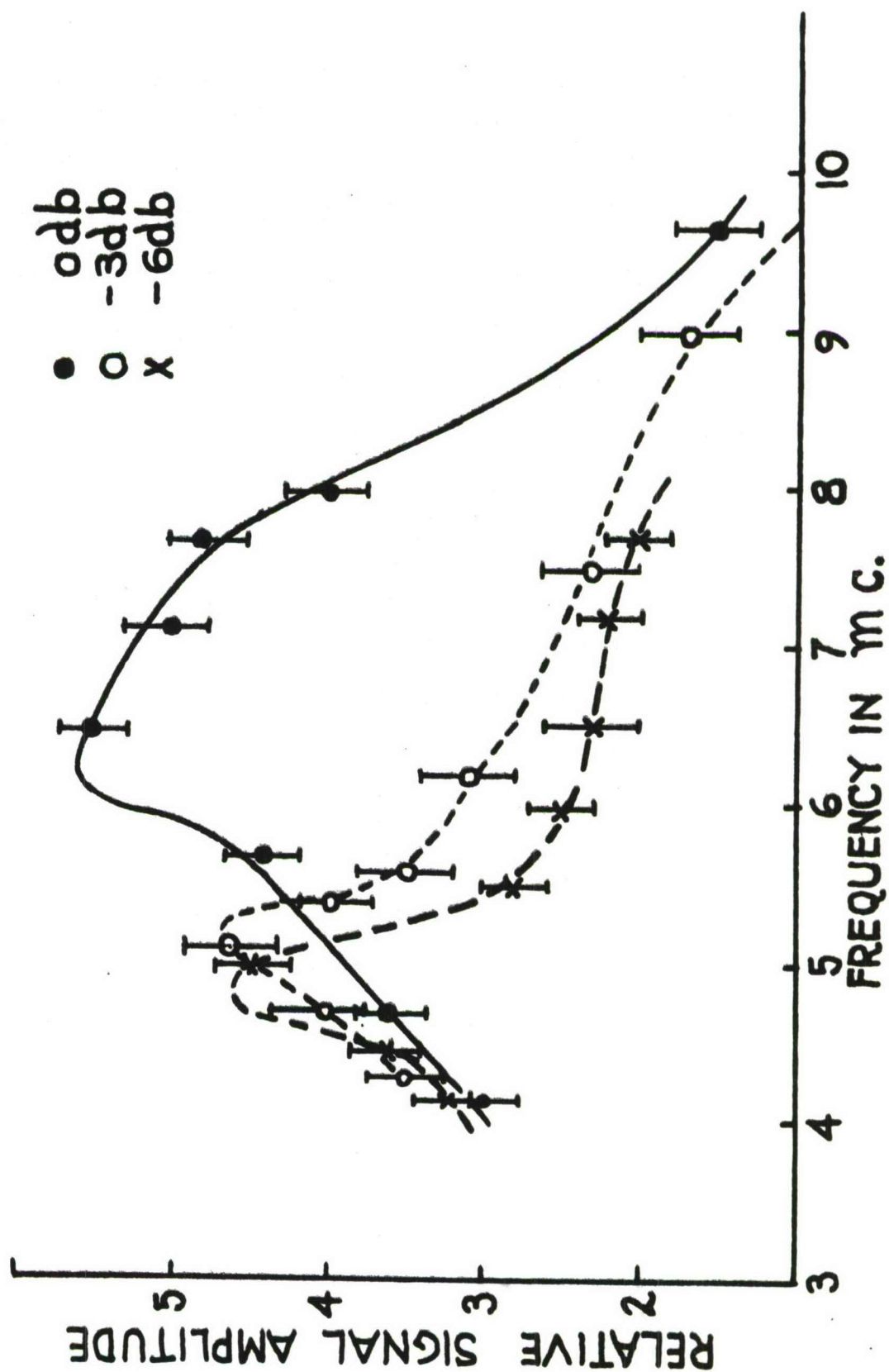


Figure 2. Amplitude of Rotary Resonance in H_1 Field as a Function of Detection Frequency

This ratio was obtained from the decibel attenuation of power at which the maximum derivative signal occurs. With no coil and quartz dewar, the EPR line reached its maximum value at -16.5 db. With the Teflon holder and coil as used in the rotary resonance experiment, the same line reached its maximum at -5 db. Due to the shift of cavity frequency the klystron power mode for the cavity with Teflon holder was 1.3 times that with the quartz dewar. The ratio of the two values of $(H_1)_0$ is then $\sqrt{44.5/[3.16(1.3)]}$ or 3.30. Thus, with the quartz dewar we expect a maximum $(H_1)_0$ of 3.30 times .35 gauss or 1.15 gauss which is the value we will use for calculations of T_1 in the following pages. This value agrees quite well with the value of 1.2 gauss estimated from the cavity Q.

2.5 SATURATION T_1 AND T_2 VALUES FOR VARIOUS EPR LINES

The value of 1.15 gauss as calculated in the previous section will be used as $(H_1)_0$ in the following calculations of saturation parameters T_1 and T_2 . Saturation data, i.e. amplitude of derivative of EPR absorption as a function of applied power to the cavity, were taken for some of the EPR lines of Mn^{++} ions in a natural calcite single crystal in which the Mn appears as a natural substitutional impurity. The spectrum is due to the hyperfine interaction between the five unpaired electrons of Mn^{++} and the 5/2 spin of the Mn nucleus. The lines are orientation dependent and the complete Hamiltonian is given by Hurd, Sacks,

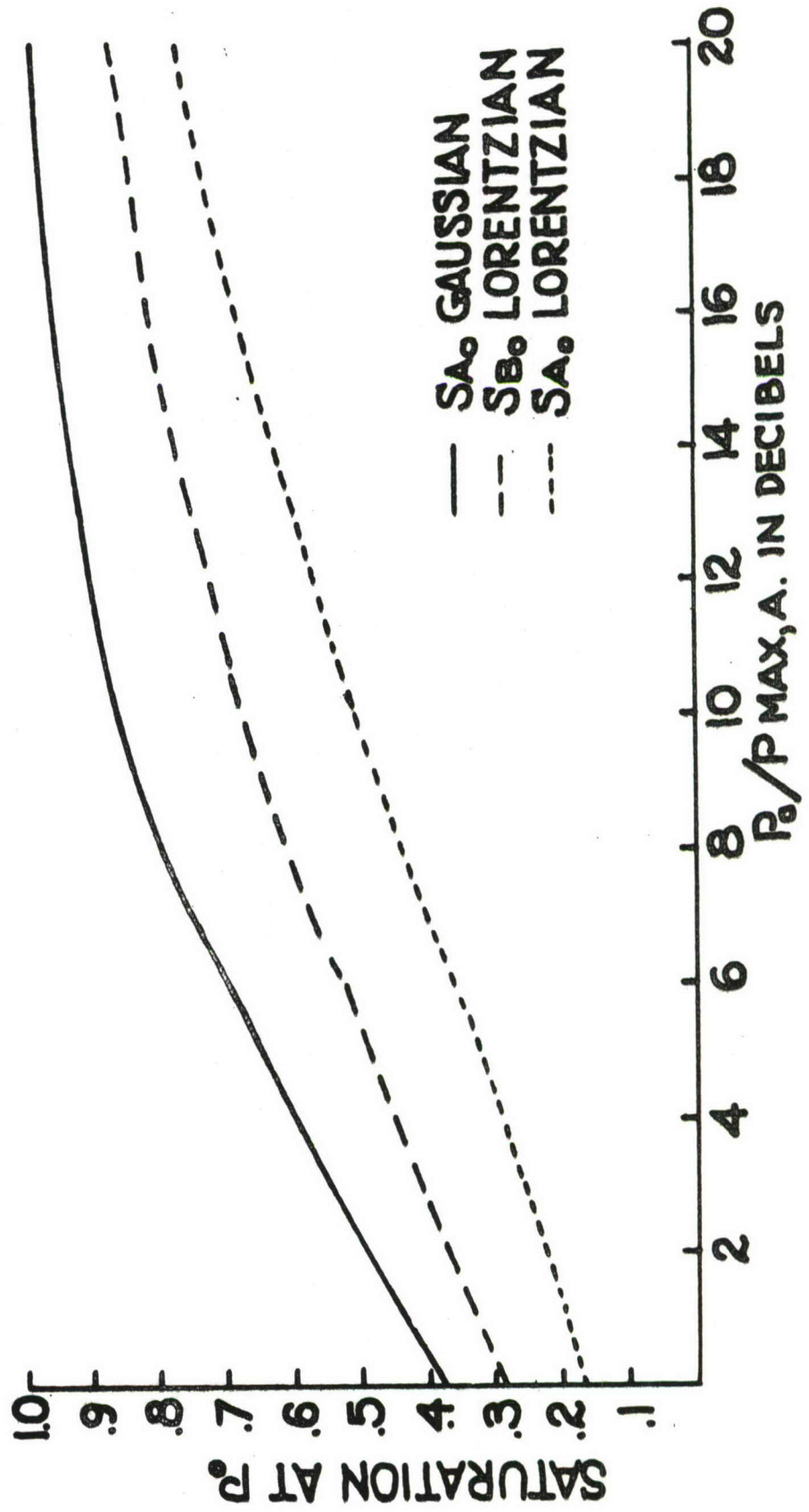


Figure 3. Maximum Saturation of an EPR Line as a Function of $P_0/P_{max,A}$

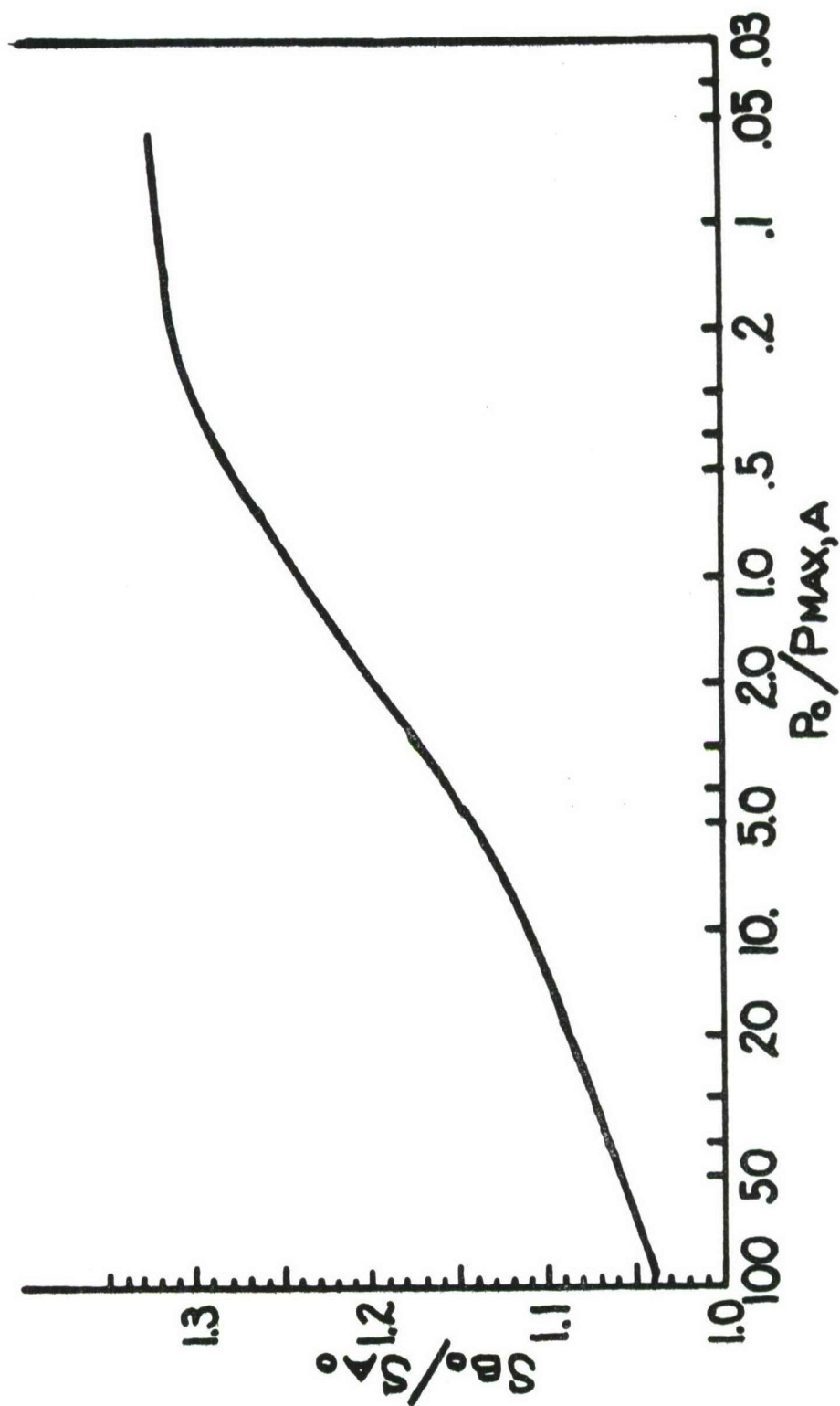


Figure 4. Ratio of Saturation at Absorption Peak to Saturation at Derivation Peak as a Function of $P_0/P_{max,A}$

Figure 5 (a). Typical EPR Spectrum of Mn^{++} in NaCl

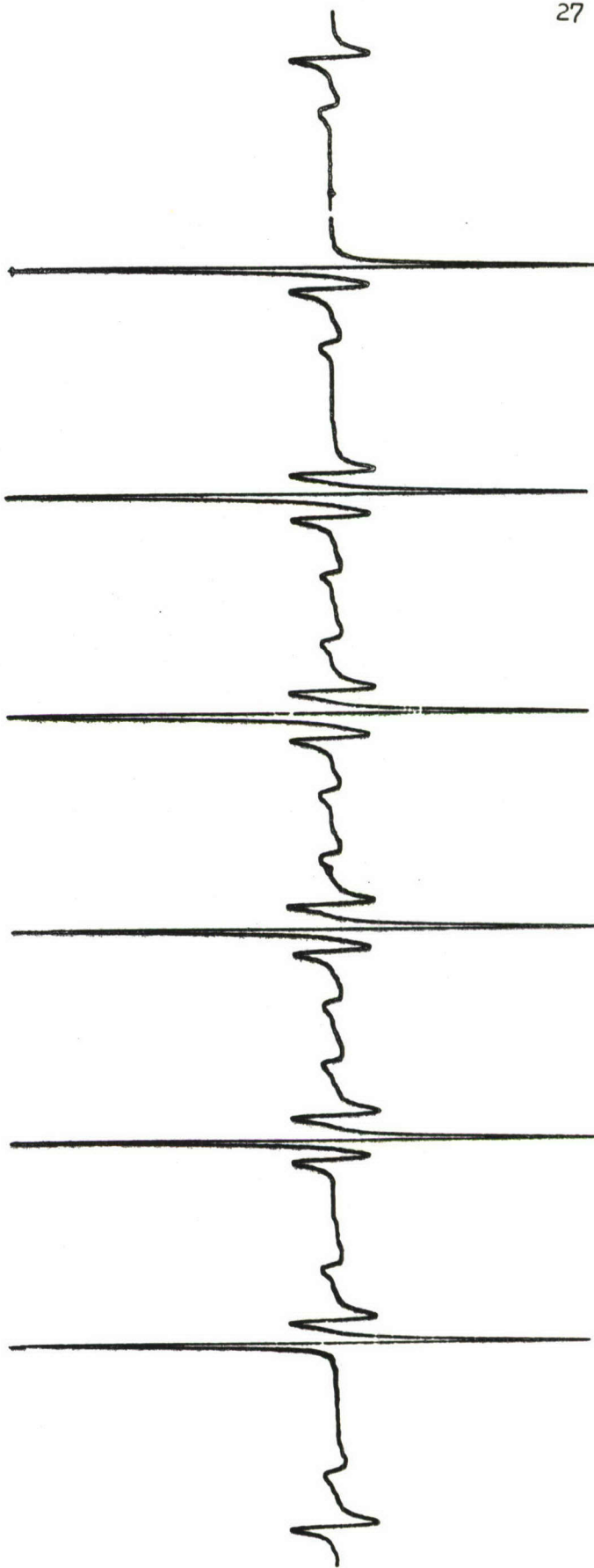
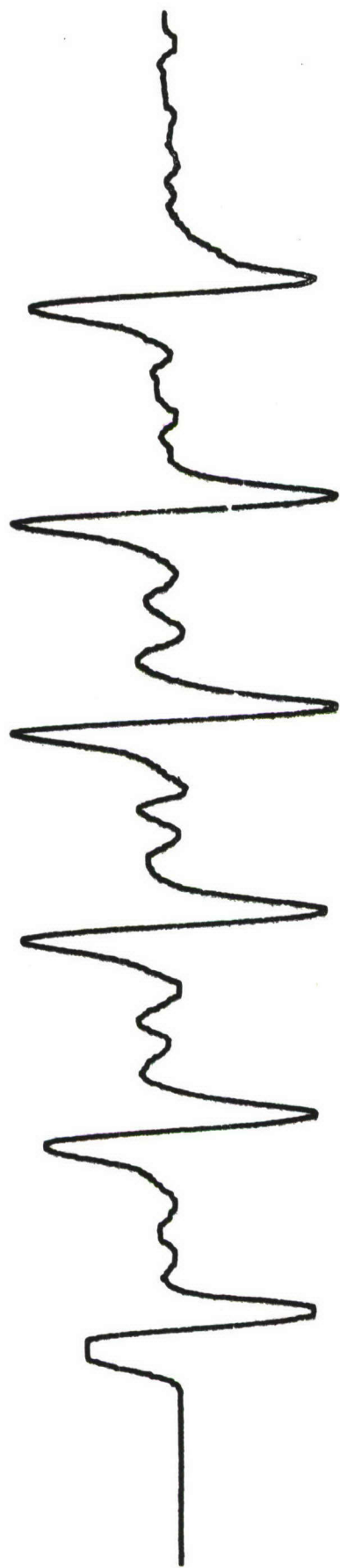
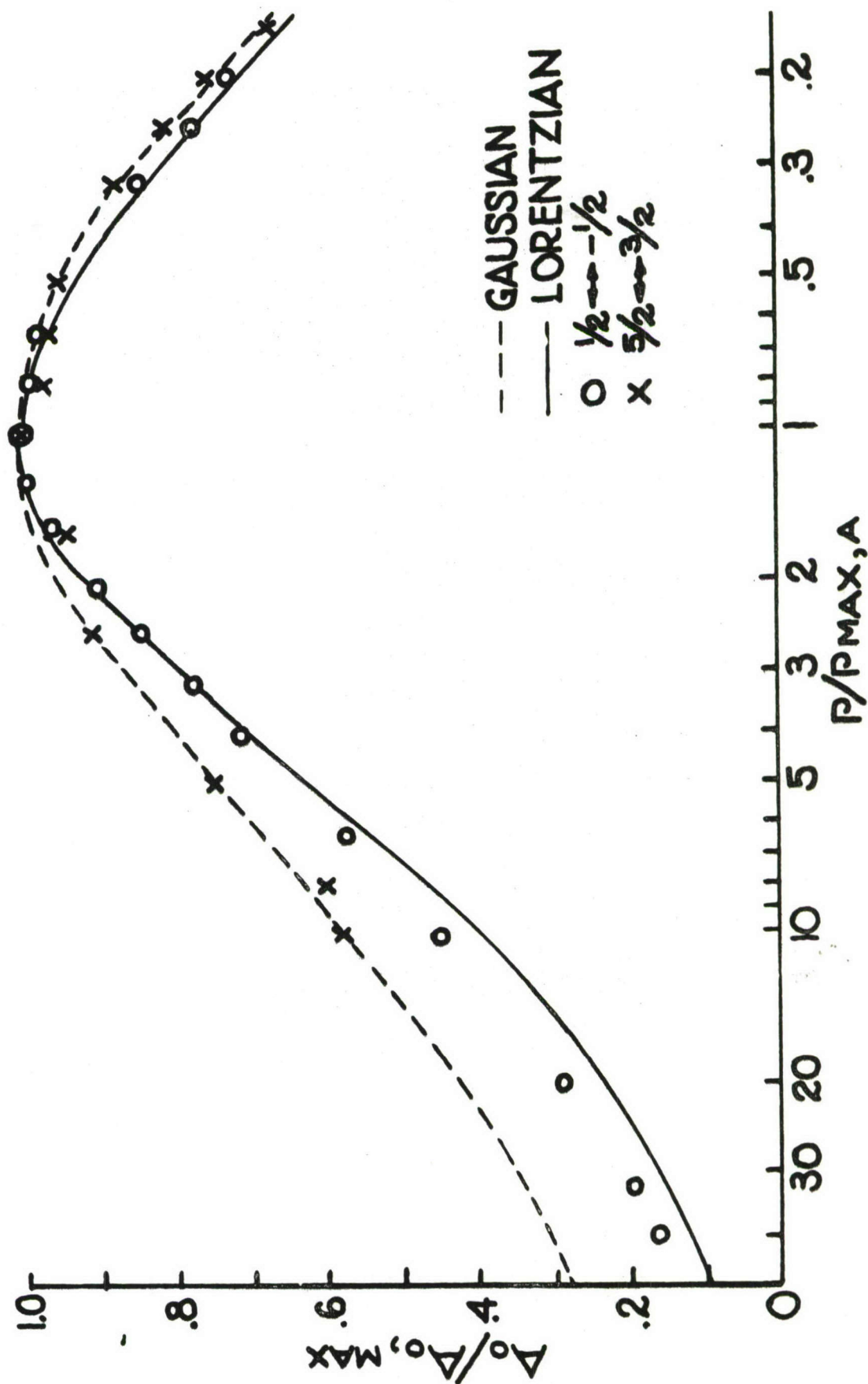


Figure 5 (b). Typical EPR Spectrum of Mn^{++} in Calcite

and Hershberger⁸ and by Kikuchi and Matarrese¹⁰. The main spectrum consists of five sets of six lines each. A typical spectrum is shown in Figure 5. For simplicity, all the data are taken with the optical axis or crystal field axis at 90° to the static magnetic field. The strongest set of six lines is due to the electronic transition of spin 1/2 to spin -1/2, each line corresponding to one of six possible nuclear spin orientations.

The saturation data are listed in Table I with the values of T_1 and T_2 calculated by the methods of the previous two sections. The values are given for both room temperature ($297^\circ \text{K} \pm 2^\circ$) and for liquid nitrogen temperature ($78^\circ \text{K} \pm 1^\circ$). As shown in Figure 7 (a) the room temperature values of relative power at which maximum signal occurs are 18.5 db, 13.5 db and 8.5 db for transition to $+1/2$, $+3/2$, $+5/2$ spin state respectively. The liquid nitrogen temperature values are 32 db, 25.5 db, 9 db (Figure 7 (b)). The room temperature values of power are in the ratio 1, $\sqrt{10}$, and 10, while at the liquid nitrogen temperature, the power for maximum signal is in the ratio 1, $\sqrt{20}$, and 20.

The Gaussian equations for calculations of T_1 and T_2 were used for the 1/2, 3/2 and 5/2 transitions, since Figures 7 (c) and (d) show that the Mn lines lie closer to the Gaussian saturation curve than the Lorentzian. For smaller concentrations of Mn^{++} the 1/2 to -1/2 lines fit very well the Lorentzian curve while the 5/2 to 3/2 line is still inhomogeneously broadened as shown in Figure 6. Actually the two line shapes would give approximately the same

Figure 6. Saturation Data for Mn^{++} in Calcite

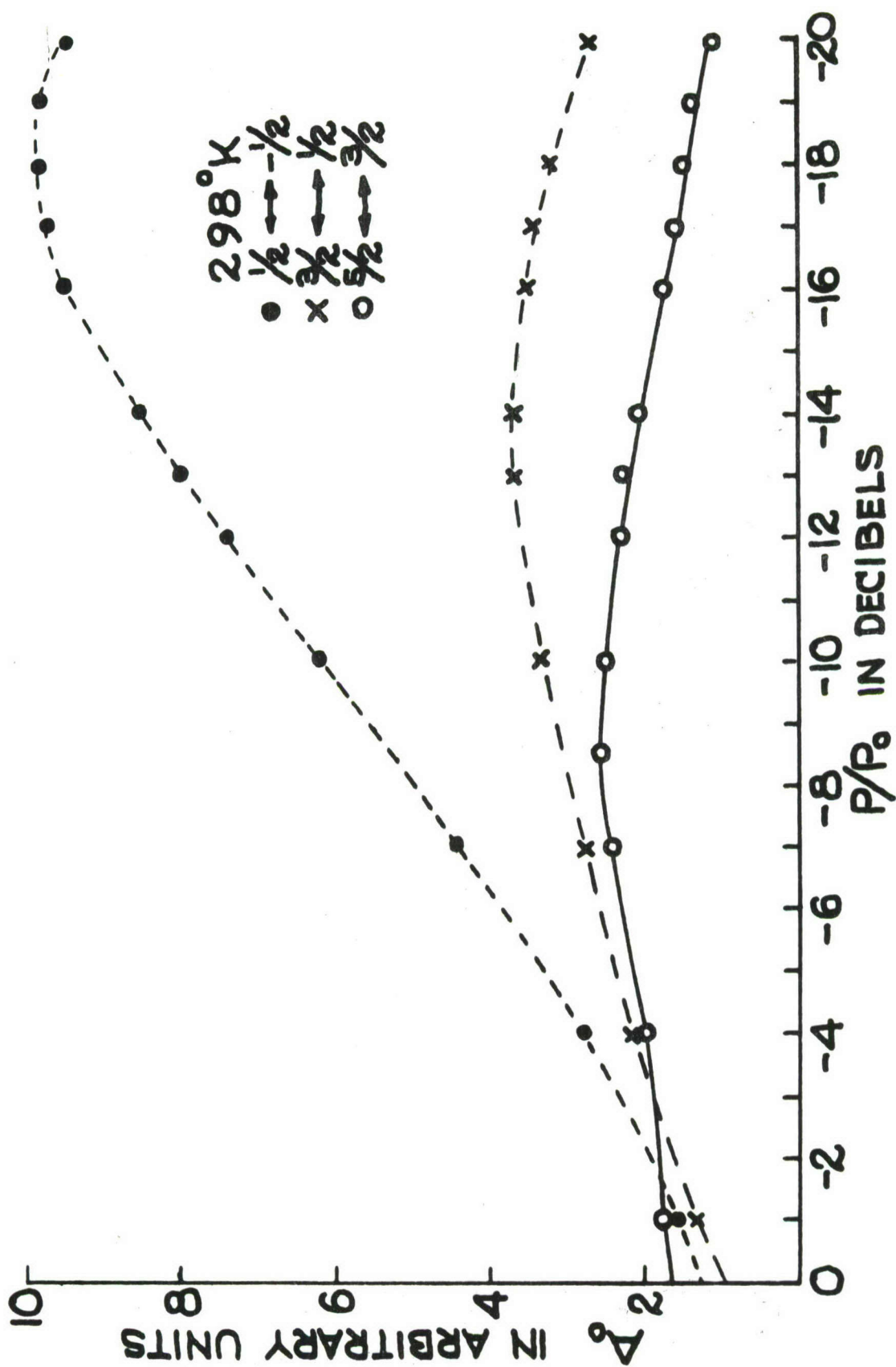


Figure 7 (a). Room Temperature Saturation Data for Mn^{++} in Calcite

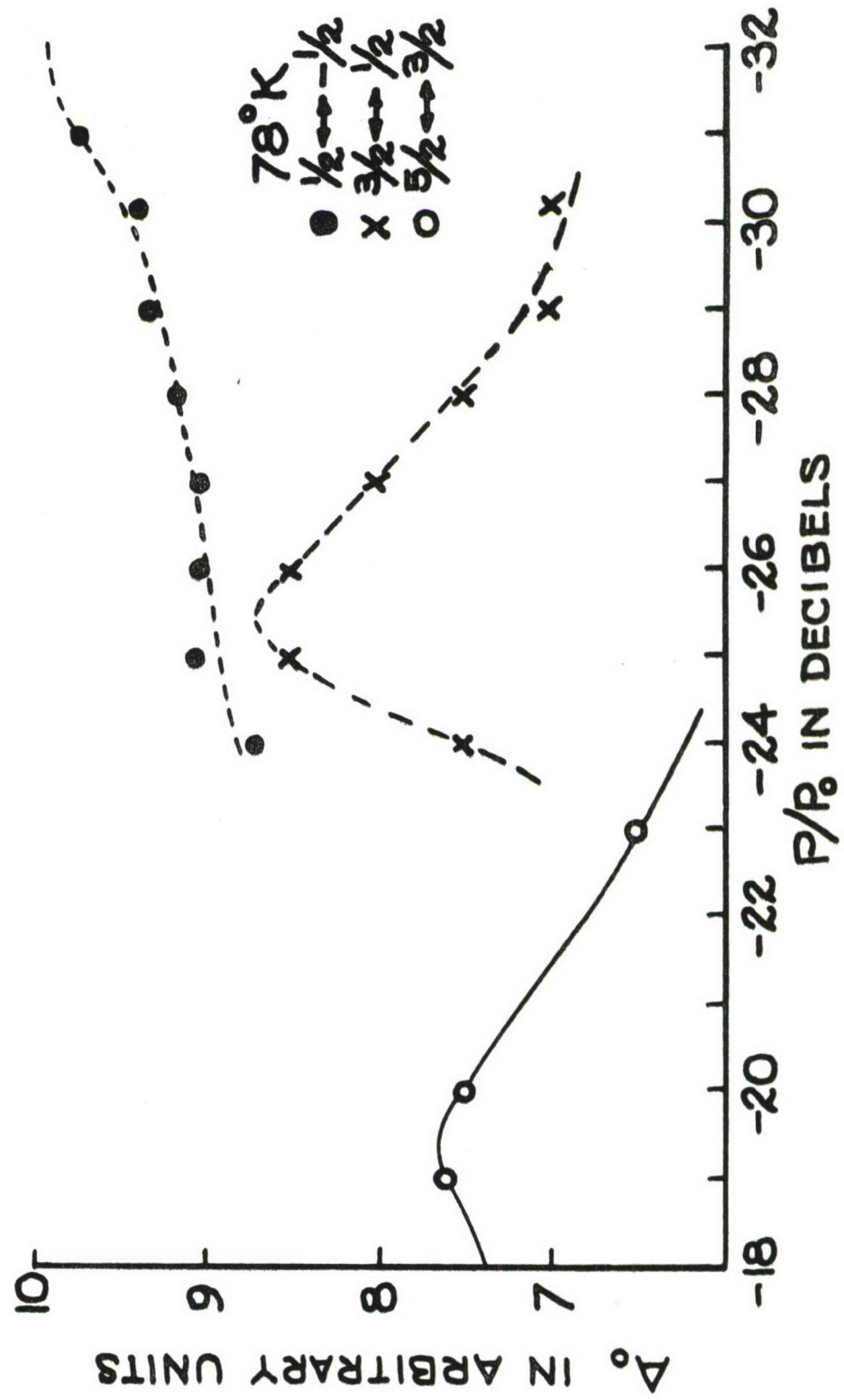


Figure 7 (b). 78° K Saturation Data for Mn⁺⁺ in Calcite

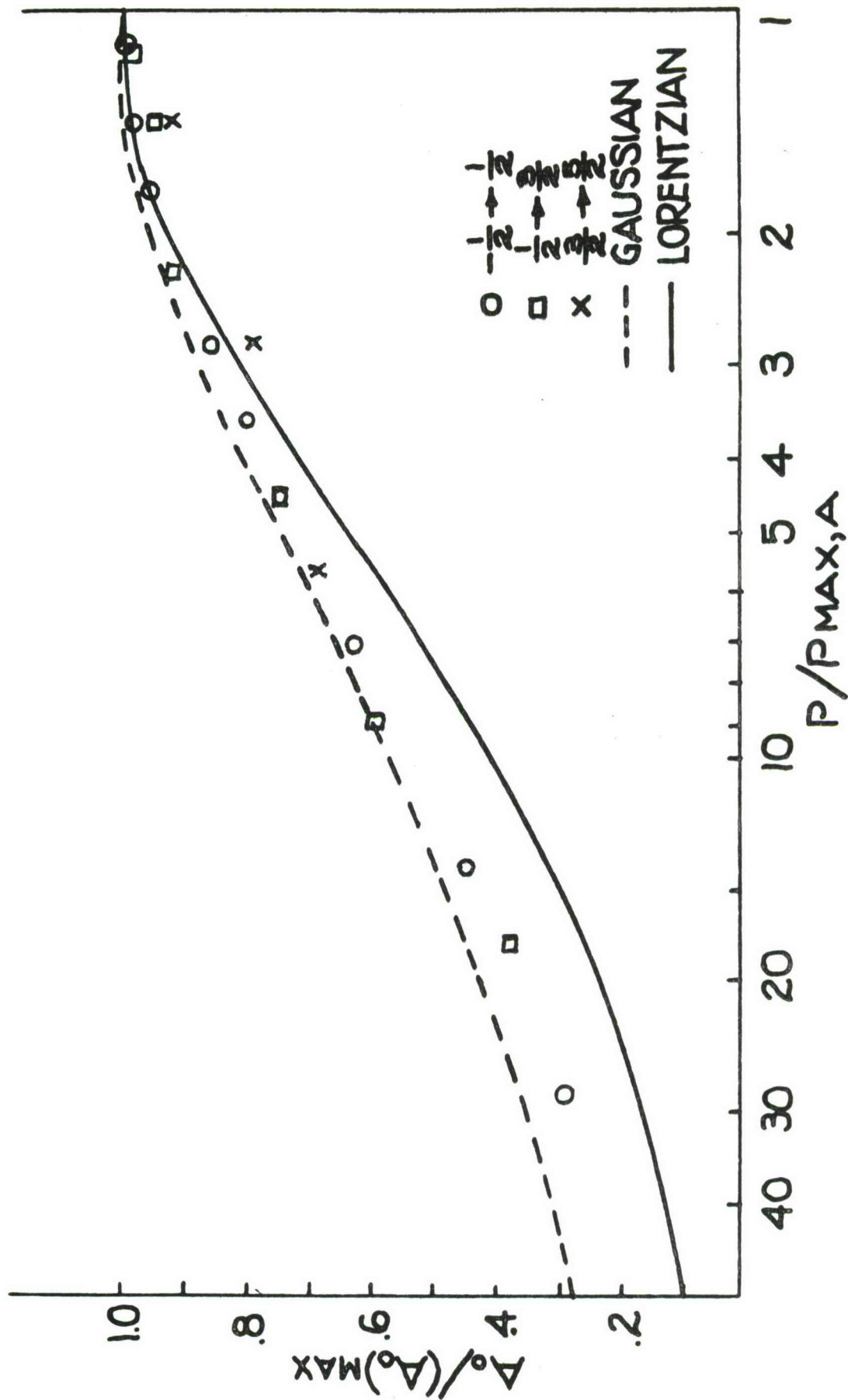


Figure 7 (c). High Power Part of Normalized Saturation Curve

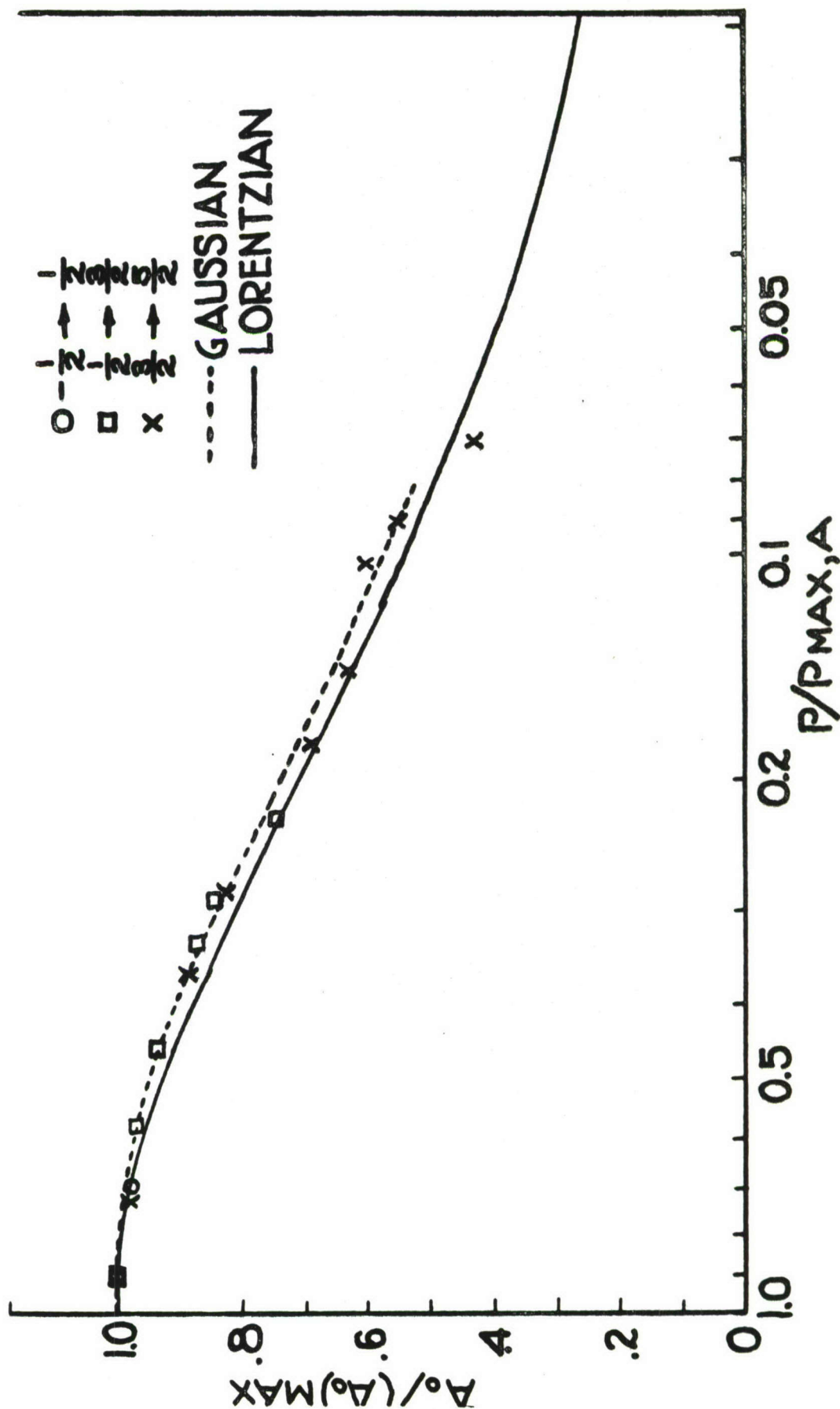


Figure 7 (d). Low Power Part of Normalized Saturation Curve

TABLE I

 Mn^{++} IN CALCITE ($\theta = 90^\circ$)

Temp.	Line	$P_{\max, A/P_0}$	Line Width	T_2 μ sec.	T_1 μ sec.	Transition Probability per sec. at $P_{\max, A}$
297° K	$-1/2 \rightarrow +1/2$	-18.5 db	$1.15 \pm .2g$	$.124 \pm .006$	55.3 ± 3.8	4.31×10^5
297° K	$+1/2 \rightarrow +3/2$	-13.5 db	$3.45 \pm .2g$	$.041 \pm .002$	52.1 ± 2.0	4.06×10^5
297° K	$-3/2 \rightarrow -1/2$					
297° K	$+3/2 \rightarrow +5/2$	-8.5 db	$6.32 \pm .3g$	$.022 \pm .001$	30.8 ± 1.2	4.30×10^5
297° K	$-5/2 \rightarrow -3/2$					
78° K	$-1/2 \rightarrow +1/2$	-32 ± 1 db	$.94 \pm .1g$	$.152 \pm .008$	993 ± 250	$.24 \times 10^5$
		(Predicted value based on T^{-2} law $T_1 =$				804 ± 62)
78° K	$+1/2 \rightarrow +3/2$	-25.5 db	$2.80 \pm .2g$	$.051 \pm .004$	659 ± 94	$.32 \times 10^5$
78° K	$-3/2 \rightarrow -1/2$					
		(Predicted value based on T^{-2} law $T_1 =$				753 ± 31)

TABLE I - continued

Mn⁺⁺ IN CALCITE ($\theta = 90^\circ$)

Temp.	Line	$P_{\max, A/P_0}$	Line width	T_2 μ sec.	T_1 μ sec.	Transition Probability per sec. at $P_{\max, A}$
78° K	$+3/2 \rightarrow +5/2$	-19 ± 1 db	$4.10 \pm .3g$	$.035 \pm .004$	220 ± 125	$.60 \times 10^5$
78° K	$-5/2 \rightarrow -3/2$					
(Predicted value based on T^{-2} law = 446 ± 19)						

Cl₂⁻ IN NaCl (TL) ($\theta = 45^\circ$)

78° K	$m = 0$	-14.5 db	$5.25 \pm .2g$	$.015 \pm .004$	90 ± 12	1.70×10^3
-------	---------	------------	----------------	-----------------	-------------	--------------------

results for T_1 and T_2 . The numerical factors in the Gaussian equations would give a value of T_2 about 1.77 times as large and a value of T_1 about 1.13 times as large as the values calculated from the Lorentzian equations. The γ for the electronic transitions was taken to be 2.8 Mc which is sufficiently accurate since the lines were all measured at approximately the center of the spectrum. The variation of the g value over the spectrum is only of the order of a few percent.

The transition probability for a system of spin I for a transition from the M to $M-1$ state is given by the expression

$$P = \frac{3}{8} \gamma^2 H_1^2 T_2 (1 + \gamma^2 H_1^2 T_1 T_2)^{-1/2} (I+m)(I+1-m) \quad (2.33)$$

This reduces to Eq. 2.5 for $I = 1/2$. For the case of Mn $I = 5/2$ and $m = 5/2, 3/2, 1/2, -1/2, -3/2$. The corresponding values of the factor $(I+m)(I+1-m)$ are 5, 8, 9, 8, 5. The values of the transition probability are calculated at the value of H_1 which gives the maximum derivative signal. For the Lorentzian line $\gamma^2 (H_1)_{\max, A}^2 T_1 T_2 = 1/2$ and for the Gaussian line $(\gamma)^2 (H_1)_{\max, A}^2 T_1 T_2 = 1$.

The values of T_1 for the three transitions as predicted from the room temperature values, by assuming a temperature dependence of $T_1 = aT^{-2}$ is shown also in Table I and agree (within experimental error) with the observed values except in the case of the weak $5/2 - 3/2$ transition. This indicates a probable

dependence on temperature squared. It should be noted that the T_1 values are approximately in the ratio 5,8,9,8,5, for room temperature values, which gives the same value for the transition probability for all the lines. This is only approximately true for the T_1 values at liquid nitrogen temperature, where the accuracy is not as good.

The half field lines of the Mn^{++} in calcite were also observed. These are due to the $\Delta M = 2$ electronic transitions and consist therefore of four sets of six lines corresponding to the six hyperfine terms of the $5/2$ nuclear spin. These lines are more difficult to saturate and no data was obtainable with the power available. The $P_{max,A}$ for these lines is greater than P_o , the maximum applied power. Thus, it can be stated that the values of T_1 for these lines is 10^{-6} sec or less. This sample has possibilities for use as a maser in which either half or twice the pump frequency could be used as the amplified signal frequency.

2.6 THE Cl_2^- CENTER

The following sections describe the polarization of Na^{23} nuclei in a NaCl crystal by overpopulating electronic energy levels of paramagnetic centers introduced into the crystal. The paramagnetic centers can be introduced by doping the crystal during growth with paramagnetic ions, or by radiation damage. Polarization of Na^{23} or enhancement of the nuclear resonance

signal through both types of centers in the same crystal is described below. The NaCl crystal contained Mn^{++} ions as an impurity and was irradiated to produce Cl_2^- molecular ions. The advantage of the center produced by doping is its permanence, while the advantage of the center produced by irradiation is that the concentration can be varied over a wide range by varying the irradiation time. The Cl_2^- center is stable only at liquid nitrogen temperature or below.

The Cl_2^- center is produced by irradiating a NaCl crystal (or other Alkali Chloride) at liquid nitrogen temperature with X-rays. In general the crystal is doped during growth with Pb, Ag, Tl, or other metallic ions which enter substitutionally in the lattice and capture electrons ejected by the X-rays. This decreases the recombination rate and thereby increases the rate of production of the Cl_2^- centers. The capture of ejected electrons also decreases appreciably the production of F-centers or color centers which are electrons trapped in vacant negative ion sites. The F-center is not desirable as it has a very broad interfering EPR line, due to unresolved hyperfine interactions with the neighboring nuclei.

The ejection of an electron from a chlorine ion by the X-ray leaves a neutral chlorine atom which then shares the electron of a neighboring chlorine, forming a singly ionized molecule Cl_2^- . The single unpaired electron has a large hyperfine interaction with

the two chlorine nuclei of spin $3/2$. The total nuclear spin being 3, the resulting spectrum shows seven lines corresponding to the seven space orientations of the total nuclear spin. There is superimposed on this two additional spectra due to the three ways of pairing the isotopes Cl^{35} and Cl^{37} . Since the Cl_2^- has an axis through the two chlorine nuclei, and the hyperfine interaction is orientation dependent, the various Cl_2^- centers are divided between two orientations with respect to an external magnetic field and hence an additional spectrum also appears. In general the four superimposed spectra are easy to distinguish and the EPR spectrum as well as the Hamiltonian and eigenvalues are described adequately and beautifully in the literature¹². A typical spectrum of the Cl_2^- center in KCl and in NaCl is shown in Figure 1. The line widths are much broader in the NaCl sample which is obviously due to the interactions with the surrounding sodium nuclei, which have a magnetic moment about five times as large as the potassium nuclei. It is this interaction that is used below to polarize the Na^{23} nuclei. Since the polarization was accomplished, it is clear that the nuclear Zeeman terms of the neighboring Na^{23} ions must be added to the Hamiltonian describing the Cl_2^- center.

Some saturation data was taken on the Cl_2^- EPR lines. Usually this is of little value in studying the enhancement of the Na^{23} since in the solid effect, the transition of interest is the forbidden transition, i.e. a transition in which both

electron and nuclear spin changes by 1. This transition is either too weak to appear in the EPR spectrum or is hidden beneath the envelope of the allowed line. The T_1 and T_2 values for the Cl_2^- lines in KCl are given in the literature¹³. Data were taken on the Cl_2^- line in NaCl (Tl) and are listed in Table I. The Cl_2^- lines in KCl, fit the Lorentzian saturation curve quite well as shown in the previous report⁶.

The Cl_2^- centers in NaCl seem to fit the Lorentzian saturation curve as shown in Figure 8 which is the $M = 0$ hyperfine line. The line width of the Mn^{++} lines for the $1/2 \rightarrow -1/2$ transition in NaCl is $13.2 \pm .4$ gauss while the Cl_2^- lines in NaCl are $5.25 \pm .2$ gauss wide. The sample used for the saturation parameter determination of the Cl_2^- centers in NaCl was doped with thallium which has no interfering EPR spectrum.

Attempts were made to detect the hyperfine transitions of the Cl_2^- centers in KCl and NaCl which occur in the range of 12 to 150 megacycles depending on the orientation of the center. A simple oscillator operating in the 100 to 130 megacycle range was constructed. The expectation was that the hyperfine transition signals could be enhanced appreciably by pumping on the EPR lines of the Cl_2^- centers. With the 125 megacycle oscillator, it was possible to detect the EPR signal of DPPH at about 30 gauss, as well as a few of the Mn^{++} in calcite lines at this field. Since there were experimental difficulties in operating the high frequency oscillator inside the microwave cavity, a cavity was

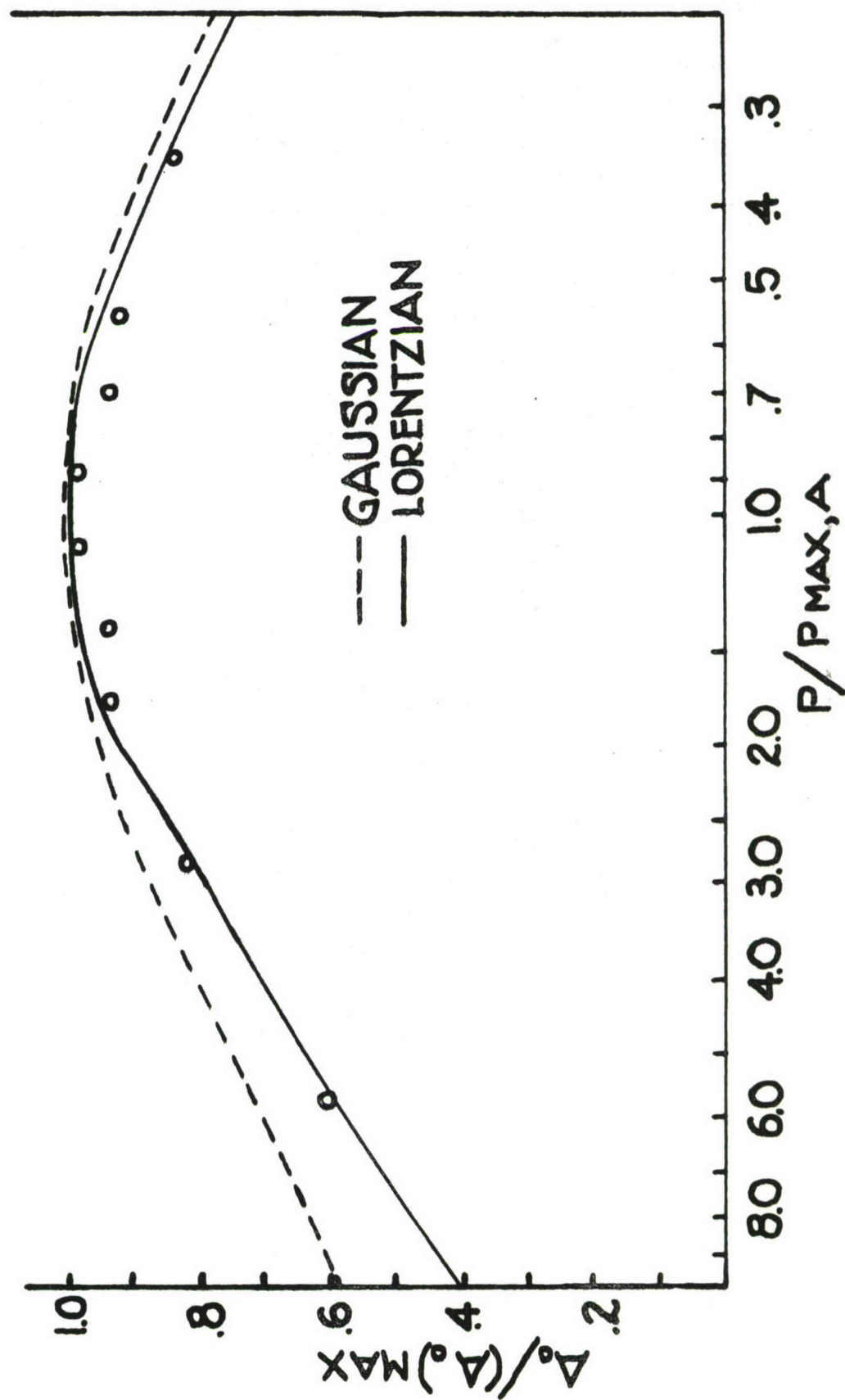


Figure 8. Saturation Curve for Cl_2^- Centers in NaCl

constructed of the KCl crystal itself by using silver paint on the outside of a crystal of appropriate dimensions. The Cl_2^- centers in an irradiated cavity of this type were detected although the Q of the cavity was poor compared to the conventional cavity. The attempts to detect the hyperfine transitions were discontinued eventually in order to study the enhanced Na^{23} signals which were observed in the NaCl sample. The unenhanced Na^{23} resonance signal was easily detected with the low level Robinson oscillator in a sample of NaCl of approximately $.1 \text{ cm}^3$. A typical trace of the Na^{23} signal and the enhanced signal is shown in Figure 9.

2.7 ESTIMATE OF NUMBER OF CENTERS

In order to estimate the number of Cl_2^- centers which are polarizing the Na^{23} nuclei in the NaCl sample, a comparison of the EPR line area was made with that of a calcite sample of known Mn^{++} concentration. Comparison was made with the $1/2$ to $-1/2$ EPR transitions of Mn^{++} which consists of six equal amplitude lines due to the hyperfine interaction with the $5/2$ nuclear spin of Mn. Since the electron spin is also $5/2$, the number of Mn^{++} ions in the six electronic states will be in the ratio $S!/m_s!$ or 1, 20, 120, 120, 20, 1. Hence, $120/282$ of the total will be in state $m_s = 1/2$. Because of the six equal intensity EPR lines associated with this state, one-sixth of these, or $20/282$ of the total will be associated with the single EPR line used in calibration. The number of spins was calculated as follows. The



Figure 9 (a). Typical Unenhanced Na^{23} NMR at 3.6400 Mc and 77° K

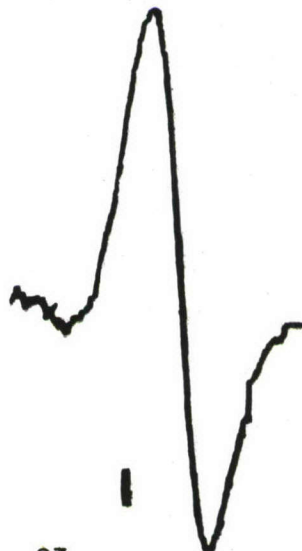


Figure 9 (b). Enhanced Na^{23} NMR Signal at 3.6400 Mc, 77° K and -3 db Microwave Power

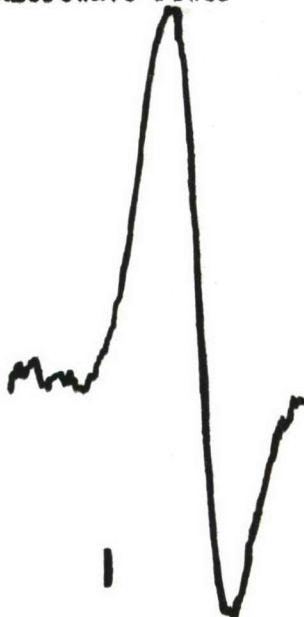


Figure 9 (c). Enhanced Na^{23} NMR Signal at 3.6420 Mc, 77° K and -3 db Microwave Power

percentage of Mn by weight, P , was known from a spectrochemical analysis. The weight of the calcite sample W , the atomic weight M of Mn and Avogadro's number N_0 are known. Hence, the number of Mn ions associated with the single EPR line is

$$N_{m=0} = \left(\frac{W}{M} \right) \left(\frac{P}{100} \right) N_0 \left(\frac{20}{282} \right). \quad (2.34)$$

The data on the observed line was taken with the crystal field or the optical axis at 90° to H_0 , at which angle, rotations of the sample about the axis produce no EPR line shifts. The data obtained on the calcite (Mn^{++}) sample used for calibration are listed in Table II.

To estimate the number of Cl_2^- centers associated with a particular Cl_2^- line by which a nuclear signal is enhanced, we need not consider the total concentration of Cl_2^- centers but only those in the state associated with the line of interest. If we desire, the total concentration of centers, we can observe that the intensities of the seven lines of the Cl_2^- spectrum are in the ratio 1,2,3,4,3,2,1, corresponding to relative concentration $1/16, 2/16, 3/16, 4/16, 3/16, 2/16, 1/16$. Then $N_{total} = (16/4)N_m = 0$. Using the line width as proportional to the amplitude of derivative signal times line width squared (see Appendix), the number of centers is given by

TABLE II

DATA ON CALIBRATION SAMPLE CALCITE (Mn^{++})

Weight, W	71.1 mg
% Mn by weight, P	.01%
Atomic weight, M	54.93
Orientation, θ	90°
(1/2 to -1/2) line width	1.3 gauss \pm .2
P_{max}/P_o	-16 db
Maximum relative amplitude $(A_o)_{\text{max}}$	54.5
Amplification	10
Relative modulation	16
Scan rate	72 gauss/minute
Number Mn ions = N_{total}	7.8×10^{16}
$N_{\text{total}} \times \frac{20}{282} = N_m = o^{(\text{Mn})}$	5.5×10^{15}

$$N_m(Cl_2^-) = N_{m=0}(Mn) \frac{(A_0)_{MAX, Cl_2^-} (\Delta\omega)_{Cl_2^-}^2 K(Mn)}{(A_0)_{MAX, Mn} (\Delta\omega)_{Mn}^2 K(Cl_2^-)} \quad (2.35)$$

Now $K(Mn)/K(Cl_2^-)$ is merely the ratio of the amplification and modulation parameters.

The data for the Cl_2^- centers in NaCl (Pb, Mn), i.e. doped with Pb and Mn, are in Table III. The NaCl sample size was $1.3 \times .28 \times .38$ centimeters.

The number of Na^{23} polarized per center on the average can be calculated as follows:

If the electron levels between which the pumping occurs has populations $(N_1)_0$ and $(N_2)_0$ determined by the Boltzmann distribution, and population N_1 and N_2 under pumping characterized by a saturation S , then the number of nuclei polarized, n , will be the number of electrons pumped, N' , times the number of nuclei, F , polarized per electron. Thus

$$n = N' F. \quad (2.36)$$

Now for $h\nu/kT = \Delta \ll 1$,

$$e^{-\Delta} \approx 1 - \Delta. \quad (2.37)$$

TABLE III

DATA ON Cl_2^- CENTERS IN NaCl (Pb, Mn)

Irradiation time (65 kv, 10 ma)	12 minutes	18 minutes
Sample volume	.14 cm ³	.14 cm ³
Line width	5.7 gauss \pm .16	5.25 gauss \pm .17
Signal amplitude A_0	63. (15 db)	86. (15 db)
Na ²³ Enhancement,	-5.71 (at 3 db)	+7.05 (0 db) +2.57 (10 db)
Amplification	1600	50
Relative modulation	500	800
Scan rate	43 gauss/minute	72 gauss/minute
Number Cl_2^- centers for state \bar{m}	.31 $\times 10^{14}$ (m = 0)	.58 $\times 10^{14}$ (m = 1)
Number $\text{Cl}_2^-/\text{cm}^3$ (state m)	2.2 $\times 10^{14}$ (m = 0)	4.1 $\times 10^{14}$ (m = 1)
Calculated saturation forbidden line	.30	.126
Δ/δ	9190/3.593 = 2560	9200/3.563 = 2580
Number of Na ²³ polarized per center	12.0 $\times 10^5$	3.5 $\times 10^5$

Since

$$S = 1 - \frac{N_1 - N_2}{(N_1)_0 - (N_2)_0} = 1 - \frac{N_1 - N_2}{(N_1)_0 \Delta}, \quad (2.38)$$

then

$$N_1 - N_2 = (1 - S)(N_1)_0 \Delta \quad (2.39)$$

The number pumped is

$$N' = \frac{1}{2} [(N_1)_0 - (N_2)_0 - (N_1 - N_2)]. \quad (2.40)$$

Since the population difference changes by 2 for each transition

$$N' = \frac{1}{2} [(N_1)_0 \Delta - (1 - S)(N_1)_0 \Delta] = \frac{1}{2} S(N_1)_0 \Delta; \quad (2.41)$$

therefore

$$n = \left[\frac{1}{2} S(N_1)_0 \Delta \right] F \quad (2.42)$$

Now the nuclear signal is proportional to $n_1 - n_2$, where n_1 and n_2 are the nuclear populations in the associated nuclear states and we consider $n_1 + n_2 = 2n_1$ to be the total number of nuclei in the sample. The enhancement will be, using $h \nu_{\text{nuc}}/kT = E_{\text{nuc}}/kT = \delta \ll 1$,

$$\mathcal{E} = \frac{(n_1 - n_2) + n}{n_1 - n_2} = 1 + \frac{n}{n_1 - n_2} = 1 + \frac{n}{n_1 \delta} = 1 + \frac{2n}{(n_1)_{TOT} \delta}, \quad (2.43)$$

Thus

$$\mathcal{E} = 1 + \frac{2 \left(\frac{1}{2} S(N_1)_0 \Delta \right)}{n_{TOT} \delta} \quad (2.44)$$

$$\mathcal{E} = 1 + \left[\frac{S(N_1)_0}{n_{TOT}} \frac{\Delta}{\delta} F \right]. \quad (2.45)$$

By introducing the observed enhancement, the number of centers $(N_1)_0$ producing the EPR line, the ratio Δ/δ of the frequencies, the number (n_{tot}) of nuclei in the sample, and the saturation S , it is possible to calculate F , the number of nuclei polarized per electron pumped.

The number of Na^{23} per cm^3 is 3×10^{22} . $(N_1)_0 = N_m(\text{Cl}_2^-)$ and \mathcal{E} , S , and Δ/δ are taken from Table II. The number of Na^{23} nuclei polarized per electron pumped is between 4 and 12 times 10^5 or of the order of 10^6 . This indicates spin diffusion takes place out to about 30 to 50 inter-sodium distances around a Cl_2^- center.

2.8 EXTENSION OF THE SATURATION EQUATIONS TO ENHANCEMENT OF NUCLEAR SIGNALS

In order to apply the saturation equations to the prediction of the variation of the enhancement of a nuclear magnetic resonance signal while pumping at various points on the associated EPR line, the saturation at any position off the center of an EPR line is now calculated. Again for simplicity we assume a Lorentzian line shape, or a shape function

$$g(\nu) = \frac{2 T_2 (1+x)^{1/2}}{1+x+4\pi^2 T_2^2 (\nu-\nu_0)^2} \quad (2.46)$$

where $x = \gamma^2 H_1^2 T_1 T_2$.

The saturation S is given by Eq. 2.4, and the transition probability π , for spin $1/2$,¹¹ is given by

$$\pi = \frac{1}{4} \gamma^2 H_1^2 g(\nu) \quad (2.47)$$

Substituting $g(\nu)$, and π into the saturation equation gives

$$S(\nu, x) = x \left[x + (1+x)^{1/2} + (1+x)^{-1/2} \frac{4\pi^2 T_2^2 (\nu-\nu_0)^2}{1+x} \right]^{-1} \quad (2.48)$$

Now using Eq. 2.26

$$S(\nu, P) = \frac{P}{P_{MAX,A}} \left[\frac{P}{P_{MAX,A}} + \left(4 + 2 \frac{P}{P_{MAX,A}} \right)^{1/2} + 16 \pi^2 T_2^2 (\nu - \nu_0)^2 \left(4 + 2 \frac{P}{P_{MAX,A}} \right)^{-1/2} \right]^{-1} \quad (2.49)$$

The line width at any percent saturation is given for the Lorentzian line by Eq. 2.27. In terms of frequency ν in cycles/sec, the line width $\Delta\nu$ is

$$\Delta\nu = 2(\nu' - \nu_0) = \frac{1}{2\pi} \Delta\omega \quad (2.50)$$

where ν' is the frequency at which the peak of the derivative of the absorption signal occurs, and ν_0 is the frequency at which, the peak of the absorption signal occurs. From Eq. 2.26 and 2.27

$$\Delta\nu = \frac{(1+x)^{1/2}}{\sqrt{3} \pi T_2} = \frac{\left(1 + \frac{1}{2} \frac{P}{P_{MAX,A}} \right)^{1/2}}{\sqrt{3} \pi T_2} \quad (2.51)$$

or

$$T_2 = \frac{\left(2 + \frac{P}{P_{MAX,A}} \right)^{1/2}}{\sqrt{6} \pi \Delta\nu} \quad (2.52)$$

If the value of T_2 in terms of $\Delta\nu$ is inserted in the equation for S , then

$$S(\nu, P) = \frac{P}{P_{MAX,A}} \left[\frac{P}{P_{MAX,A}} + \sqrt{2} \left(2 + \frac{P}{P_{MAX,A}} \right)^{1/2} + \frac{4\sqrt{2}}{3\Delta\nu^2} (\nu - \nu_0)^2 \left(2 + \frac{P}{P_{MAX,A}} \right)^{1/2} \right]^{-1} \quad (2.53)$$

In applying this equation to the study of an enhanced signal, it is merely necessary to compare the saturation at any position on the line to the saturation at the peak of the absorption line where $\nu = \nu_0$. $S(\nu, P)$ can be written in terms of $S(\nu_0, P)$. Eq. 2.53 may be written

$$S_{B_0} = S(\nu_0, P) = \frac{P}{P_{MAX,A}} \left[\frac{P}{P_{MAX,A}} + \sqrt{2} \left(2 + \frac{P}{P_{MAX,A}} \right)^{1/2} \right]^{-1} \quad (2.54)$$

This gives

$$\frac{P}{P_{MAX,A}} = \frac{S_{B_0}}{1 - S_{B_0}} \sqrt{2} \left(2 + \frac{P}{P_{MAX,A}} \right)^{1/2}. \quad (2.55)$$

When this is introduced into Eq. 2.53 above, the saturation at any position ν does not depend on applied power explicitly but only through the dependence of the saturation at the peak of the line. Thus

$$S(\nu) = S_{B_0} \left[1 + (1 - S_{B_0}) \frac{4(\nu - \nu_0)^2}{3 \Delta \nu^2} \right]^{-1} \quad (2.56)$$

where ν_0 is the peak of the absorption signal and $\Delta \nu$ is the distance (in frequency) between points of maximum slope and equals $2(\nu_0 - \nu')$. (As a check, the frequency of the derivative peaks can be inserted; in which case $\nu = \nu'$ and $(\nu' - \nu_0)^2 = \frac{1}{4} \Delta \nu^2$. If the expression for S_{B_0} is inserted from the previous report⁶, $S(\nu') = S_{A_0}$.)

The ratio of the saturation at the center of the line to that at a frequency ν , is

$$\frac{S_{B_0}}{S(\nu)} = 1 + (1 - S_{B_0}) \frac{4(\nu - \nu_0)^2}{3 \Delta \nu^2} \quad (2.57)$$

2.9 APPLICATION OF SATURATION THEORY TO ENHANCEMENT DATA

As shown by Eq. 2.45, the enhancement \mathcal{E} of a nuclear signal is a linear function of the saturation S . Thus,

$$\mathcal{E} = c_1 S + c_2 \quad (2.58)$$

The maximum enhancement, \mathcal{E}_{\max} , will occur when $S = 1$; when $S = 0$, i.e., in the absence of pumping, the enhanced and unenhanced signals are equal, or $\mathcal{E} = 1$. Using these conditions,

the constants c_1 and c_2 can be evaluated to give

$$(\mathcal{E} - 1) = (\mathcal{E}_{\max} - 1) S. \quad (2.59)$$

The maximum enhancement \mathcal{E}_{\max} may be positive or negative.

If \mathcal{E}_{\max} is negative, \mathcal{E} will take on values from 1, through 0, to the negative values as S increases.

Using the $S(\nu)$ from Eq. 2.56 of the previous section, it is now possible to predict how the enhancement should change as the pumping frequency moves off the center of the EPR absorption line. Thus

$$\mathcal{E}(\nu) - 1 = (\mathcal{E}_{\max} - 1) S_{B_0} \left[1 + (1 - S_{B_0}) \frac{4(\nu - \nu_0)^2}{3\Delta\nu^2} \right]^{-1} \quad (2.60)$$

or

$$\frac{\mathcal{E}(\nu_0) - 1}{\mathcal{E}(\nu) - 1} = 1 + (1 - S_{B_0}) \frac{4(\nu - \nu_0)^2}{3\Delta\nu^2} \quad (2.61)$$

and

$$\mathcal{E}(\nu_0) - 1 = (\mathcal{E}_{\max} - 1) S_{B_0}. \quad (2.62)$$

Eliminating S_{B_0} , which in general is not known, from these last two equations, then, for a fixed pumping power, S_{B_0} is

constant and

$$\frac{\mathcal{E}(\nu_0)-1}{\mathcal{E}(\nu)-1} = 1 + \left(1 - \frac{\mathcal{E}(\nu_0)-1}{\mathcal{E}_{\max}-1}\right) \frac{4(\nu-\nu_0)^2}{3 \Delta \nu^2} \quad (2.63)$$

For a fixed EPR frequency, the field H is varied and since frequency is a linear function of H , the equation above may be written in terms of H and the field H_0 at the center of the EPR line on which the pumping occurs. Therefore

$$\frac{\mathcal{E}(H_0)-1}{\mathcal{E}(H)-1} = 1 + \left(1 - \frac{\mathcal{E}(H_0)-1}{\mathcal{E}_{\max}-1}\right) \frac{4(H-H_0)^2}{3 \Delta H^2} \quad (2.64)$$

where ΔH is the width in gauss between points of maximum slope.

If the enhancement is measured at fixed pumping power at various positions H along the EPR line, and if the highest observed enhancement is taken to be the $\mathcal{E}(H_0)$ at the center of the line on which the pumping occurs (which would occur, in the solid effect, at the center of a forbidden transition or in general one nuclear frequency off the center of the observable allowed transition in the EPR spectrum), then a plot of

$(\mathcal{E}(H_0)-1)/(\mathcal{E}-1)$ against $(H-H_0)^2$ should follow a

straight line. The slope of the line, N , would be given by

$$m = \frac{4}{3 \Delta H^2} \left(1 - \frac{\mathcal{E}(H_0) - 1}{\mathcal{E}_{\max} - 1} \right) \quad (2.65)$$

In general, \mathcal{E}_{\max} and ΔH are not known. However, under the assumption of a Lorentzian line, ΔH can be found from the enhancement data. From Eq. 2.59 the ratio of the enhancement at the peak of a Lorentzian line to that at the derivative peak which is half a line width away is

$$\frac{\mathcal{E}(H_0) - 1}{\mathcal{E}(H_0 \pm \frac{\Delta H}{2}) - 1} = \frac{S_{B_0}}{S_{A_0}} \quad (2.66)$$

From the expressions for saturation given previously in terms of applied power P , (Eqs. 2.53 and 2.54),

$$\frac{\mathcal{E}(H_0) - 1}{\mathcal{E}(H_0 \pm \frac{\Delta H}{2}) - 1} = \frac{\frac{P}{P_{\max,A}} + \frac{8}{3} \left(1 + \frac{P}{2P_{\max,A}} \right)^{1/2}}{\frac{P}{P_{\max,A}} + 2 \left(1 + \frac{P}{2P_{\max,A}} \right)^{1/2}} \quad (2.67)$$

The value of this ratio is a slowly varying function of the saturability of the line, or of $P_{\max,A}$. It varies from 1.04 at $P/P_{\max,A} = 100$ which would be an easily saturable line to limiting value of 1.33 for $P_{\max,A} = \infty$. A choice of 1.17 for the ratio $P_0/P_{\max,A}$ would cover most of the situations over a

wide range of saturability. This corresponds to a value of

$P_o/P_{\max} = 3.2$, Figure 4. Thus the line width ΔH can be approximated from the data by

$$\frac{\mathcal{E}(H_o) - 1}{\mathcal{E}(H_o \pm \frac{\Delta H}{2}) - 1} \approx 1.17 \quad (2.68)$$

The line width ΔH can be read off the graph of $(\mathcal{E}_o - 1)/(\mathcal{E} - 1)$ vs $(H - H_o)^2$ by finding the $(H - H_o) = 1/2(\Delta H)$ for which the ratio is 1.17. If the enhancement data is given for other than full applied power P_o , for example at 10 db attenuation then $P/P_o = 1/10$ and $P/P_{\max, A} = (P/P_o)(P_o/P_{\max, A}) = 1/10 P_o/P_{\max, A}$. In this case the ratio of S_{Bo}/S_{Ao} to be used in finding ΔH would be that found at 1/10 the value of $P_o/P_{\max, A}$ or about .32, at which $S_{Bo}/S_{Ao} = 1.30$. Now from the slope and the line width ΔH the value of \mathcal{E}_{\max} can be obtained from Eq. 2.65.

2.10 PREDICTION OF ENHANCEMENT AS A FUNCTION OF POWER

Since the enhancement is given in terms of saturation S_o by Eq. 2.62, and the saturation is given in terms of applied power by Eq. 2.54,⁶ it is now possible to write an expression for the variation of the enhancement $\mathcal{E}(H_o)$ as a function of applied power, i.e.

$$\mathcal{E}(H_o) - 1 = (\mathcal{E}_{\max} - 1) S_{Bo} \quad (2.69)$$

and

$$S_{B_0} = \frac{P}{P_{MAX,A}} \left[\sqrt{2} \left(2 + \frac{P}{P_{MAX,A}} \right)^{1/2} + \frac{P}{P_{MAX,A}} \right]^{-1}. \quad (2.70)$$

Then

$$\mathcal{E}(H_0, P) = (\mathcal{E}_{max} - 1) \frac{P}{P_{MAX,A}} \left[\sqrt{2} \left(2 + \frac{P}{P_{MAX,A}} \right)^{1/2} + \frac{P}{P_{MAX,A}} \right]^{-1} + 1. \quad (2.71)$$

In terms of the maximum applicable power of the equipment,

P_0 , this becomes

$$\mathcal{E}(H_0, P) = (\mathcal{E}_{max} - 1) \frac{P}{P_0} \left(\frac{P_0}{P_{MAX,A}} \right) \left[\sqrt{2} \left(2 + \frac{P}{P_0} \frac{P_0}{P_{MAX,A}} \right)^{1/2} + \frac{P}{P_0} \frac{P_0}{P_{MAX,A}} \right]^{-1} + 1. \quad (2.72)$$

This equation gives the theoretical variation of the enhancement at the center of the forbidden line as a function of the relative applied power to the cavity, P/P_0 .

2.11 DYNAMIC POLARIZATION OF Na^{23}

In the experimental study of the enhancement of the Na^{23} nuclear resonance signal in NaCl, the sample used was a single crystal of NaCl doped with Pb^{++} and containing Mn^{++} ions as an impurity. The EPR spectrum of the Cl_2^- centers, produced in the NaCl crystal by irradiation with 65 kv X-rays, was observed with

the Varian EPR spectrometer. The EPR frequency is fixed by the resonant frequency of the cavity. The nuclear magnetic resonance signal of the Na^{23} , which is 100% abundant, was observed with the Robinson low level oscillator detector. This is a positive feedback, limiter controlled oscillator with the sample placed in the coil of the resonant LC circuit. The coil was made of ten or twelve turns of light copper wire wound flat and placed around the sample in the EPR cavity with its axis perpendicular to H_1 and H_0 . The nuclear resonance signal was easily detected at liquid nitrogen temperature in a sample of .1 to .15 cm^3 volume.

The experiment was performed by centering the field H_0 on the EPR line to be used. By varying the frequency of the Robinson oscillator, the Na^{23} signal could be detected at any field position H near H_0 . By slowly scanning the field across the EPR line, the position of pumping varied continuously. The Na^{23} signal was then observed in any one scan at a particular field H at which the EPR line was pumped. By varying the NMR frequency, the enhancement of the Na^{23} signal was measured for various positions of pumping over the width of the EPR line. The scan rate and line widths were then obtained by using the variation of the Na^{23} frequency with position. The γ for the Na^{23} was taken to be 1.1262 kc per gauss and the frequency of the NMR oscillator was read to five digits with a Hewlett Packard 524C Frequency Meter. The enhancement \mathcal{E} was defined to be the ratio of the signal under pumping to that with no pumping. Thus data was taken on enhancement as a function

of position on the EPR line, and as a function of applied microwave power at a fixed position.

Two sets of data are described, one for negative enhancement and one for positive enhancement. The data for negative enhancement was taken at 3 db attenuation or one-half maximum power. The maximum enhancement observed was -5.71. The line widths are shown in Table IV.

The enhancement was plotted against position with respect to the center of the forbidden transition. Thus H_0 was taken to be the field at which maximum enhancement \mathcal{E}_0 occurred. The ratio of $\mathcal{E}_0 - 1$ to $\mathcal{E} - 1$ was then plotted against $(H - H_0)^2$ as shown in Figure 10. Eq. 2.63 predicts a straight line relationship. We see that this is straight near the center of the line but the enhancement does not fall off as rapidly as predicted. (This could be due to a deviation from Lorentzian shape, or to an overlap with a nearby line, or since there are actually four Zeeman levels for the $3/2$ spin of Na^{23} , to the possibility that some pumping could occur at two sodium frequencies away from the center of the allowed EPR line.) The line width of the forbidden transition was obtained from Eq. 2.68 by using $P/P_0 = 1/2$. The line width of the forbidden transition was found to be approximately that of the nuclear signal. From the slope of the straight line in Figure 10, and the previously estimated value of the line width, the quantity \mathcal{E}_{max} was determined from Eq. 2.65. This is the expected enhancement with 100% saturation of the forbidden line.

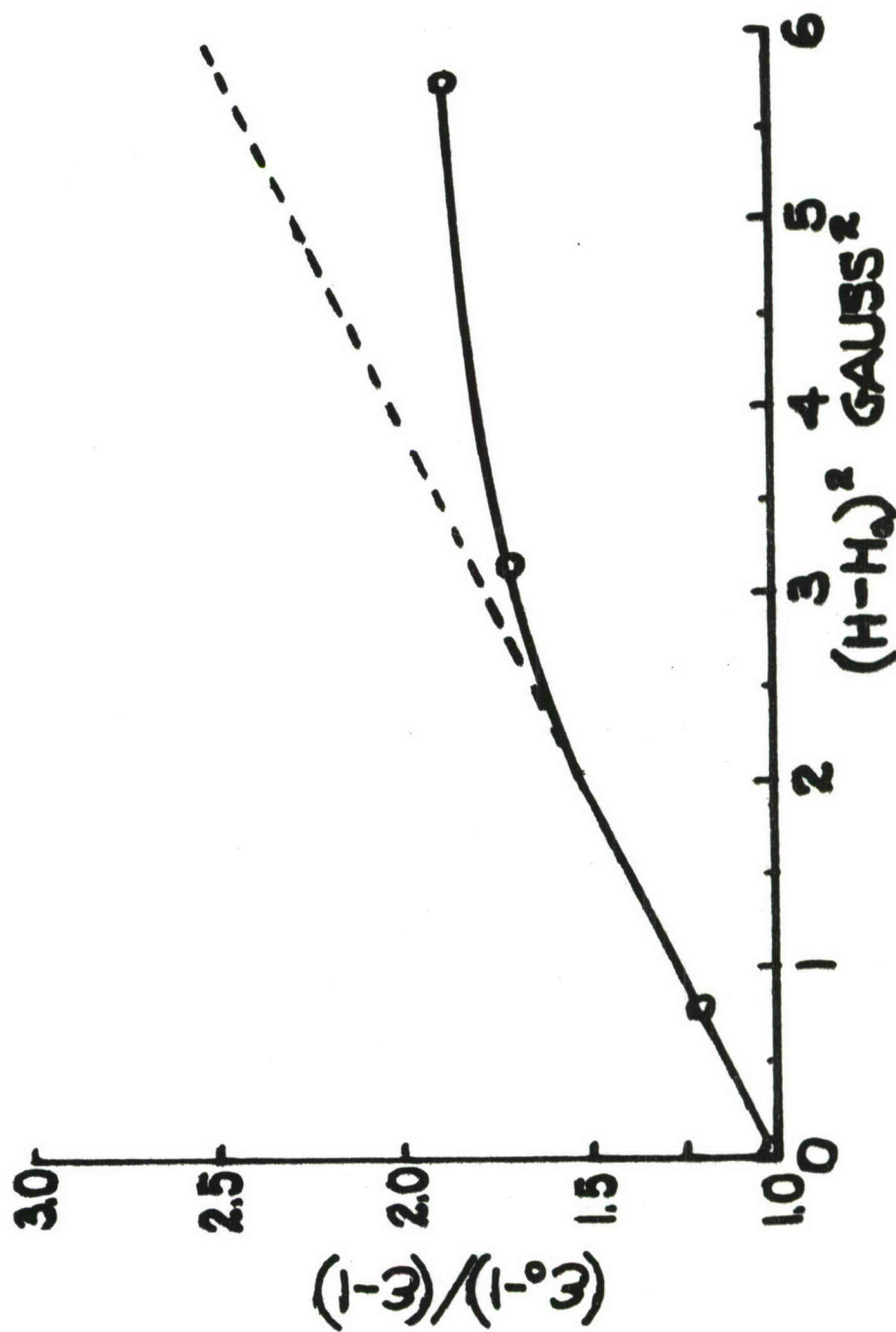


Figure 10. Enhancement as a Function of Position (Negative Enhancement)

TABLE IV

NEGATIVE ENHANCEMENT DATA

Nucleus Polarized	Na^{23} (100% abundant)	
Sample	Cl_2^- in NaCl (Pb, Mn) irradiated 12 minutes (65 kv - X-ray)	
Sample size	1.3 x .28 x .38 cm	
EPR line $m = 0$	$(\theta = 45^\circ)$	
Number of Cl_2^- centers/cm ³ (Table II)	2.2×10^{14}	
Temperature	78° K	
Position EPR line (allowed)	3191.3 gauss	
Microwave frequency	9190 \pm 10 Mc	
EPR line width (allowed line)	5.7 \pm .16 gauss	
Na^{23} NMR line width	1.9 \pm .15 gauss	
Power applied	(-3 db) $1/2 P_0$	
Maximum Enhancement \mathcal{E}_0	-5.71	
<u>Nuclear Frequency Na^{23}</u>	<u>\mathcal{E}</u>	<u>$H - H_0$</u>
3.5903 \pm 0001 Mc	-2.61	-2.395 gauss
3.5910	-2.96	-1.775 gauss
3.5920	-4.57	- .889 gauss
3.5930	-5.71	0
S_{Bo}/S_{Ao} (at -3 db)	1.215	

TABLE IV - continued

NEGATIVE ENHANCEMENT DATA

Width of forbidden line	1.84 gauss \pm .3
Slope m (Figure 10)	.253/gauss ²
\mathcal{E}_{max} (calculated)	-21.4
Saturation of forbidden line	30%
$P_o/P_{\text{max},A}$	2.14
T_2 forbidden line	.043 μ second
T_1 forbidden line	2.3 μ second
Number of Na ²³ polarized per center	1.2×10^6

In this case $\epsilon_{\max} = -21.4$. Thus we would expect the enhancement obtained by increasing the klystron power not to exceed -21.4 .

The percent saturation, 30%, used in calculating the number of Na^{23} polarized per electron pumped, was obtained by using

$$\frac{S_{B_0}}{1} = \frac{\epsilon_0 - 1}{\epsilon_{\max} - 1}$$

Since

$$S_{B_0} = \frac{P/P_{\max, A}}{\sqrt{2} (2 + P/P_{\max, A})^{1/2} + P/P_{\max, A}} = .30$$

then the value of $P/P_{\max, A}$ can be obtained. In this case

$P/P_{\max, A} = 1.07$. Using this value of $P/P_{\max, A}$ and assuming a Lorentzian shape, T_2 can then be found from the expression:

$$T_2 = \frac{(2 + P/P_{\max, A})^{1/2}}{\sqrt{6} \pi W} \quad (2.73)$$

where W is the line width in cycles/sec. Thus $T_2 = .043 \mu \text{sec}$.

Now for the Lorentzian line $\gamma^2 H_1^2 T_1 T_2 = 1/2 P/P_{\max, A} \approx 1/2 (1.07)$.

Hence

$$T_1 \approx \frac{.535}{\gamma^2 H_1^2 T_2} \quad (2.74)$$

Since $(H_1)_0^2 = (1.15 \text{ gauss})^2$, the value of H_1^2 at 3 db attenuation is $1/2(1.15)^2 \text{ gauss}^2$ or $.66 \text{ g}^2$. The value of γ is 2.876 mc/gauss .

Therefore, T_1 is $2.3 \mu \text{sec}$. These values as well as pertinent

data from Table III are listed in Table IV.

In the second sample, the positive enhancement of the Na^{23} was studied. This occurred at a field higher than the center of the allowed EPR line, or at an equivalent lower frequency, indicating overpopulation of the lower nuclear energy state. In this case the enhancement \mathcal{E} was measured at a fixed microwave power of -10 db (or $1/10 P_0$) at various pumping positions on the EPR line. Then, having found \mathcal{E}_0 or the maximum enhancement at fixed pumping power, which was assumed to occur at the center of the forbidden line, the enhancement \mathcal{E}_0 was measured as a function of microwave power. Having found the line width and \mathcal{E}_{max} as in the previous experiment, the data of \mathcal{E}_0 vs P/P_0 was plotted and compared with Eq. 2.72. The agreement of the theory is shown in Figure 12. Data taken on this sample is given in Table V. Figure 11 shows the plot of the ratio $\mathcal{E}_0 - 1 / \mathcal{E} - 1$ as a function of the square of the distance from the center of the forbidden line. The line width of the forbidden line was obtained as indicated in the first sample except here the power applied was $1/10 P_0$ and the value of $S_{\text{Bo}}/S_{\text{Ao}}$ used to obtain the line width was therefore adjusted to 1.3. From the line width and slope of the straight line position of Figure 11, the value of \mathcal{E}_{max} was obtained as before. The percent saturation was then found and used in the calculation of number of nuclei polarized in Section 2.7. The value of $P_0/P_{\text{max},A}$ was found from the saturation S_{Bo} as before. The value of \mathcal{E}_{max} and $P_0/P_{\text{max},A}$ were then used

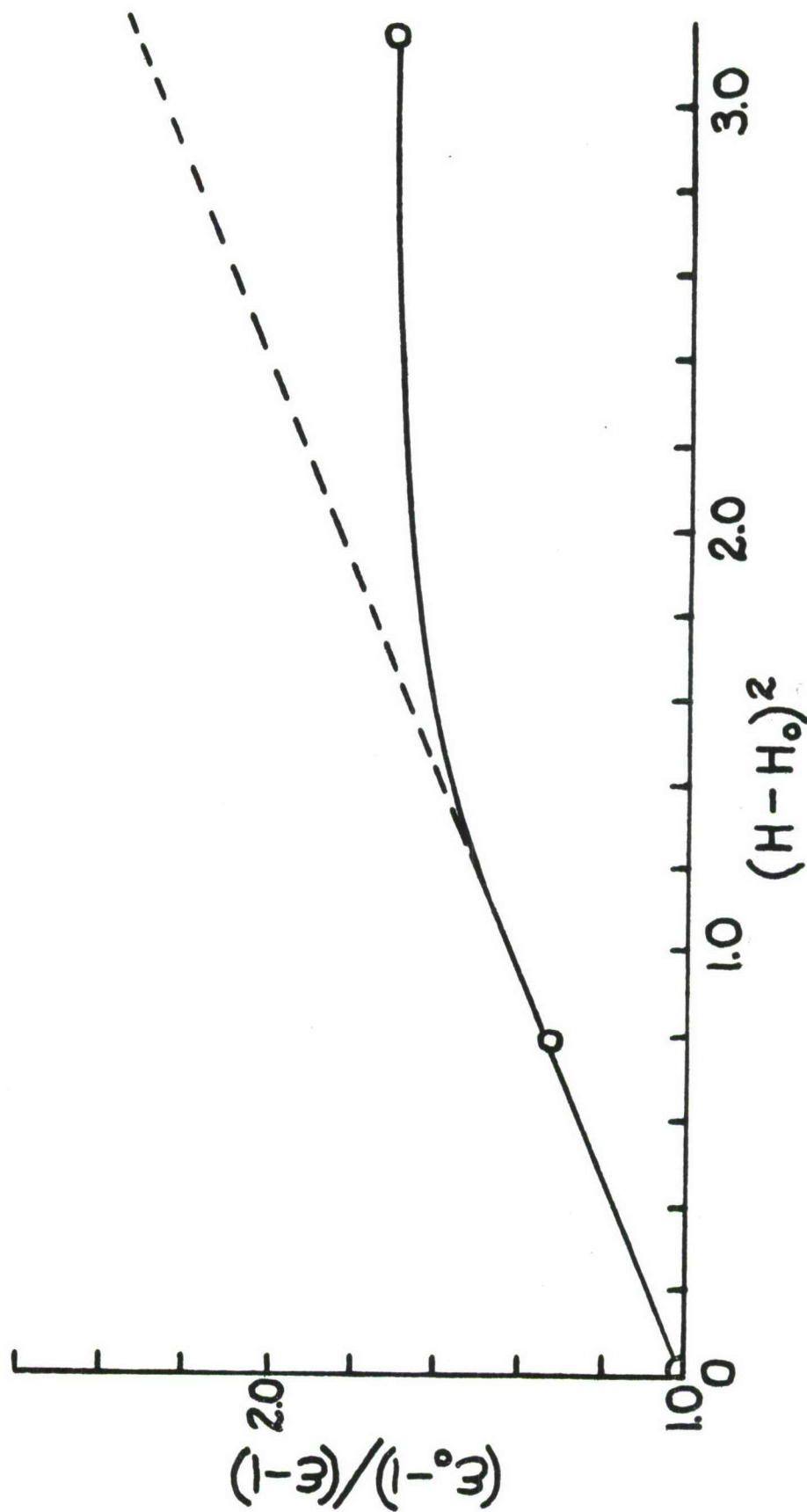


Figure 11. Enhancement as a Function of Position (Positive Enhancement)

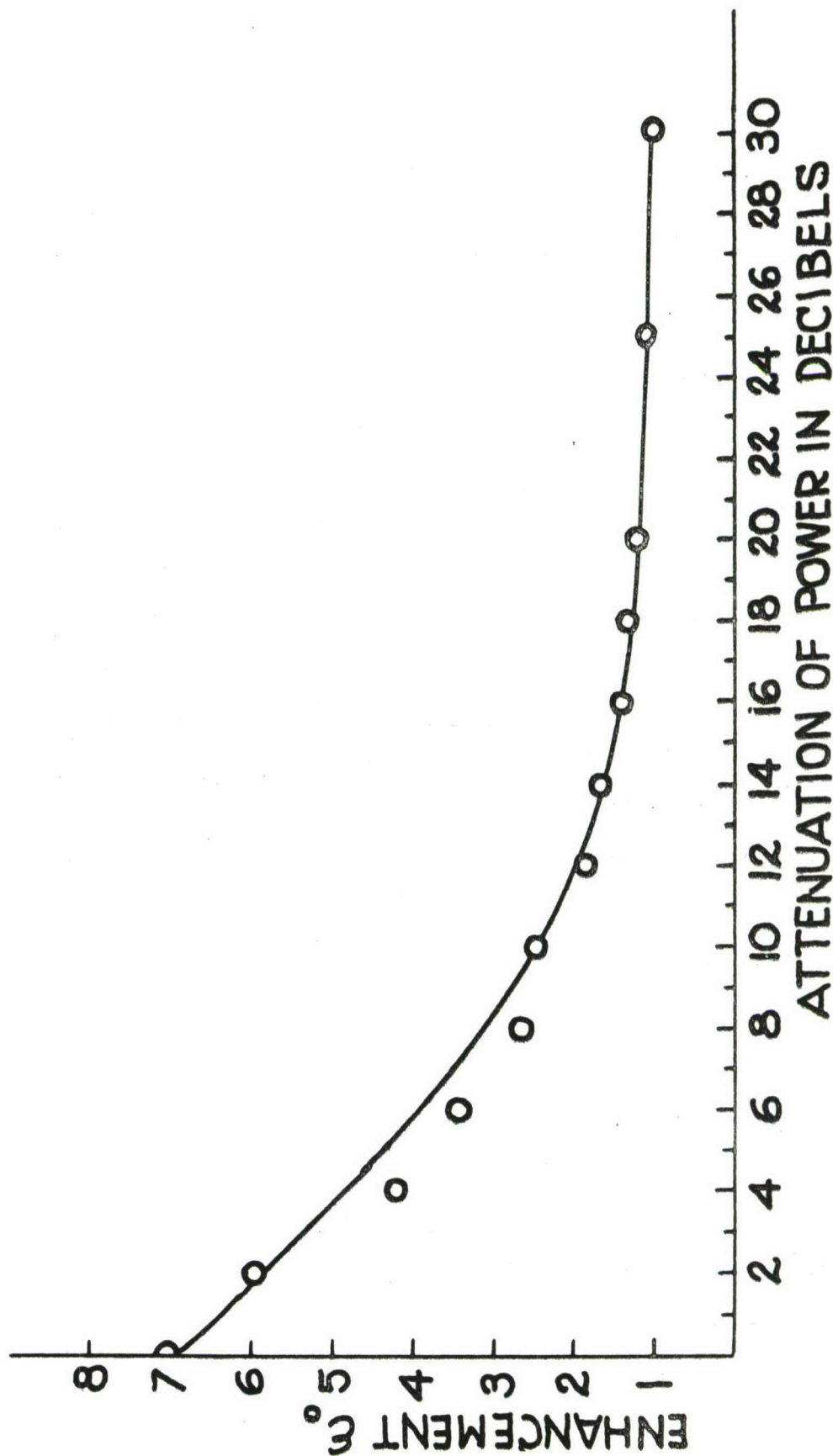


Figure 12. Enhancement as a Function of Applied Power

TABLE V (a)

POSITIVE ENHANCEMENT DATA

Nucleus polarized	Na^{23} (100% abundant)	
Sample	Cl_2^- in NaCl (Pb, Mn) irradiated 18 minutes (65 kv - X-ray)	
Sample size	1.3 x .28 x .38 cm	
EPR line	$m = 1$	$(\theta = 45^\circ)$
Number of Cl_2^- centers/cm ³ (Table II)	4.1×10^{14}	
Temperature	78° K	
Position of EPR line (allowed)	3156.6 gauss	
Microwave frequency	9200 \pm 20 Mc	
EPR line width (allowed line)	5.25 \pm .17 gauss	
Na^{23} NMR line width	2.10 \pm .13 gauss	
Power applied	(-10 db) 1/10 P_0	
Maximum Enhancement of Na^{23}	\mathcal{E}_0 (-10 db)	+2.25
<u>Nuclear Frequency Na^{23}</u>	<u>\mathcal{E}</u>	<u>$H - H_0$</u>
3.5620 Mc \pm .0001 Mc	+2.03	- .889 gauss
3.5630 Mc	+2.25	0
3.5640 Mc	+1.94	+ .889 gauss
3.5650 Mc	+1.73	+1.778 gauss
3.5670 Mc	+1.33	+3.556 gauss

TABLE V (a) - continued

POSITIVE ENHANCEMENT DATA

S_{Bo}/S_{Ao} (-10 db)	1.30
Width of forbidden line	1.67 gauss \pm .3
Slope m (Figure 11)	.417/gauss ²
ϵ_{max} (calculated)	+10.94
Saturation of forbidden line	.126 (12.6%)
$P_o/P_{max,A}$	3.1
T_2 of forbidden line	.042 μ second
T_1 of forbidden line	3.5 μ second
Number of Na ²³ polarized per center	3.5×10^5

TABLE V (b)

POSITIVE ENHANCEMENT vs POWER APPLIED

<u>Attenuation in db</u>	<u>P/P₀</u>	<u>ϵ_0</u>	<u>Predicted by Eq. 2.72</u>
0	1.000	7.05	6.95
- 2	.630	5.92	5.85
- 4	.400	4.18	4.84
- 6	.251	3.40	3.87
- 8	.158	2.65	3.06
-10	.100	2.48	2.42
-12	.063	1.85	1.93
-14	.040	1.65	1.63
-16	.025	1.40	1.405
-18	.016	1.33	1.260
-20	.010	1.20	1.166
-25	.003	1.08	1.053
-30	.001	1.00	1.017
∞	0	1.00	1.00

in Eq. 2.72 to plot a theoretical curve of the variation of enhancement \mathcal{E}_0 with relative power P/P_0 . The result is shown in Figure 12 with the data points falling quite close to the values predicted by the equation. The enhancement obtained at full microwave power was 7.05.

2.12 ENHANCEMENT OF Na^{23} USING Mn^{++} LINES

Since the previously described samples contained Manganese as an impurity, probably introduced as an impurity in the PbCl_2 used for doping the NaCl, attempts were made to enhance the Na^{23} by pumping on the $1/2$ to $-1/2$ lines due to Mn^{++} . A small enhancement of 2.0 was obtained (at liquid nitrogen temperature) with 5 db attenuation of power using the unirradiated NaCl (Pb, Mn) sample showing the EPR spectrum of Mn^{++} as in Figure 5 (b). The allowed EPR line was $13.2 \pm .4$ gauss wide. This sample contained no Cl_2^- centers.

To determine if the presence of the Manganese lines had an effect on the enhancement due to the Cl_2^- centers, a crystal of NaCl, doped with Thallium and showing no Mn^{++} spectrum, was irradiated with X-rays. The rate of production of Cl_2^- centers was not as great as in the NaCl (Pb, Mn). However, sufficient centers were obtained and an enhancement of the Na^{23} of approximately 2.0 was observed by pumping on a Cl_2^- line.

In a sample of NaCl (Pb, Mn) irradiated with X-rays, both the Cl_2^- lines and the Mn^{++} line could be observed in the EPR

spectrum. With such an irradiated sample an enhancement of Na^{23} of +3 and -3 was obtained by pumping on the Cl_2^- center. By resetting the EPR spectrometer on an isolated Mn^{++} line, an enhancement of +1.7 was observed in the same sample by pumping on the Mn^{++} line. No detailed study of these enhancements was made at this time.

2.13 RELAXATION OF POLARIZED Na^{23} NUCLEI

In discussing the effect of paramagnetic centers on the relaxation time of nearby nuclei, Bloembergen¹⁴ indicates that spin diffusion plays an important part in relaxing nuclear spins. He states that Purcell, prior to 1949, suggested an experiment to study this effect, namely "that the spin temperature of the paramagnetic center may be raised above the lattice temperature by a strong field in the microwave region at the magnetic resonance of the electronic spins." Thus the diffusion of "spin temperature" from such a site could be studied through the nuclear relaxations. Such a suggestion is an indication of early ideas on double resonance experiments.

Such an experiment can be carried out easily by dynamic nuclear polarization techniques. An attempt was made to measure the relaxation of the enhanced Na^{23} signal in NaCl. Figure 13 shows the decay of the enhanced Na^{23} resonance peak back to normal after the microwave pump was turned off. It also shows the growth of the enhanced signal to full enhancement in about the

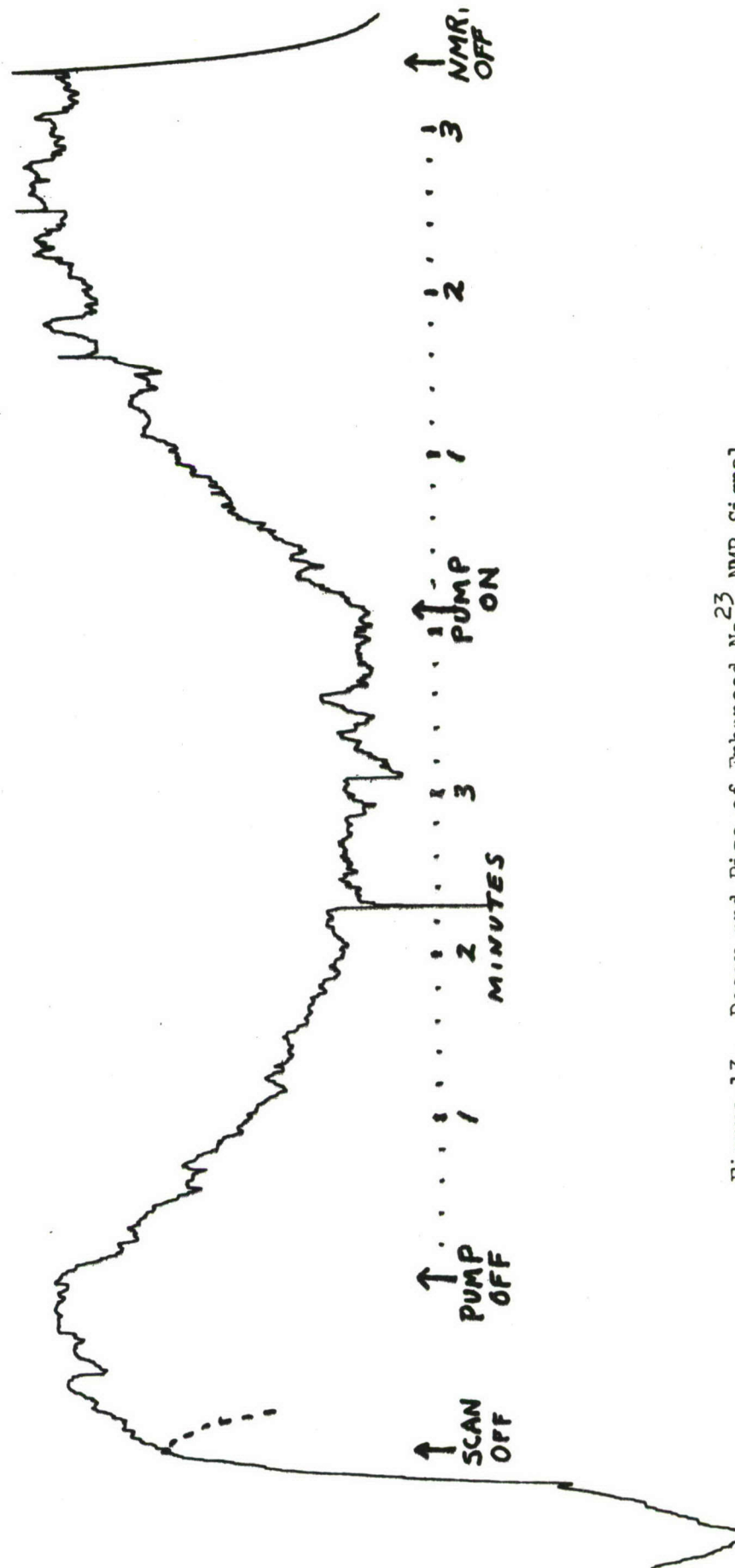


Figure 13. Decay and Rise of Enhanced Na^{23} NMR Signal

same time period upon turning the microwave pump on. The microwave power was turned off and on merely by turning the attenuator in the waveguide from 0 db to 30 db attenuation.

Figure 14 (a) shows the relative number of nuclei polarized as a function of time, after the pump was turned off. Since the signal is proportional to population difference, the change in signal is proportional to the change in population difference or to the number polarized. Hence the relative number of nuclei polarized will equal the quantity $S - S_0$ where S is the enhanced signal and S_0 is the equilibrium signal under no pumping. Thus Figure 14 (a) is a plot of $S - S_0$ against time. It is approximately exponential with a decay constant τ of 59 ± 6 seconds.

Figure 14 (b) shows the relative number of nuclei polarized as a function of time, after the pump was turned on. Here the difference between n_∞ the number polarized after infinite time, and n , the number polarized at time t , is plotted against time. Here again the curve is approximately exponential with a time constant τ of 60 ± 6 seconds.

This indicates that n , the number of nuclei polarized, follows a rate equation of the type:

$$\frac{dn}{dt} = P - \frac{n}{\tau} \quad (2.75)$$

where P is a constant rate of polarization due to the pump. The solution of this equation, using the conditions then $n = n_0$ at

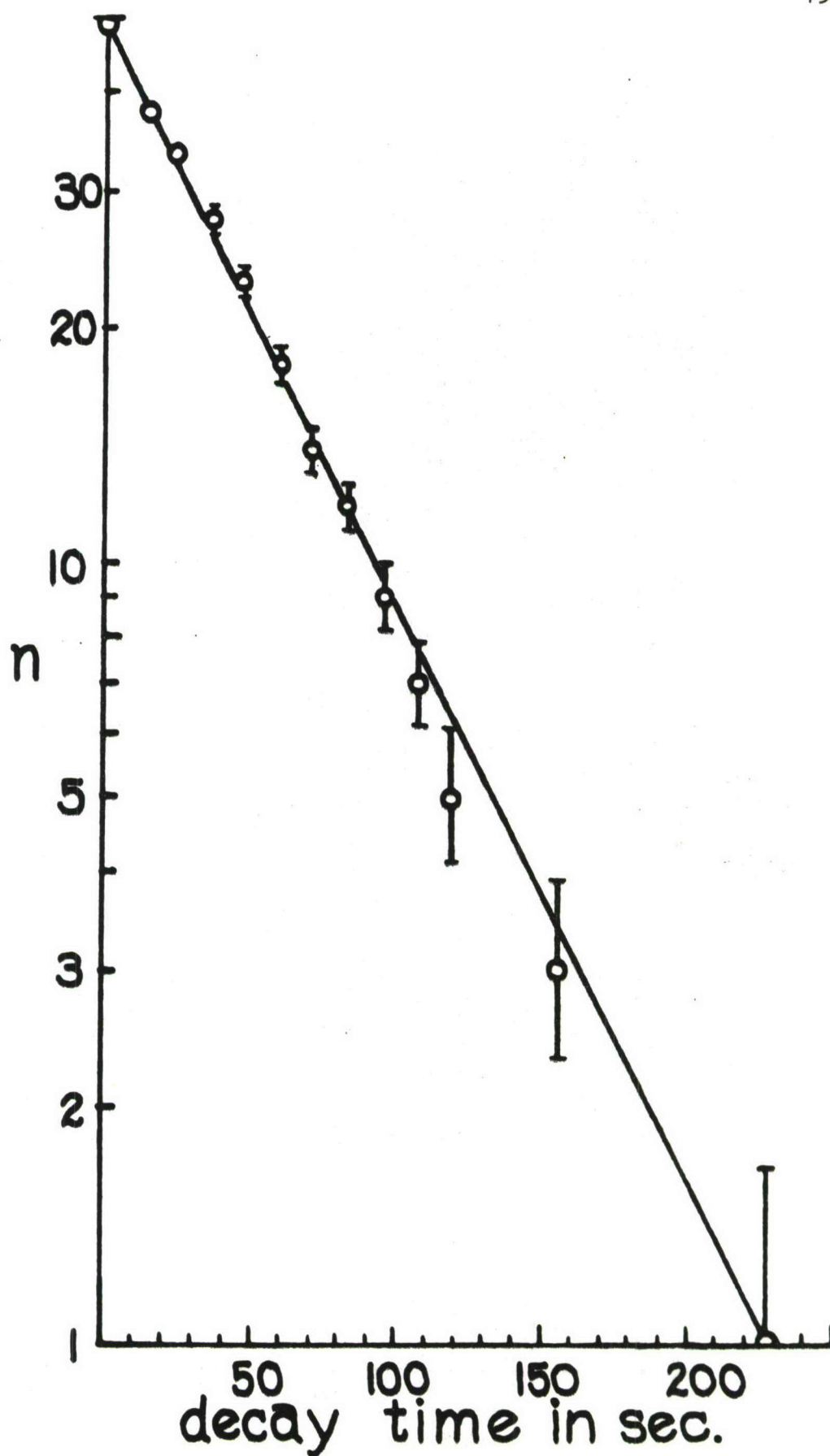


Figure 14 (a). Decay of the Relative Number of Nuclei Polarized as a Function of Time

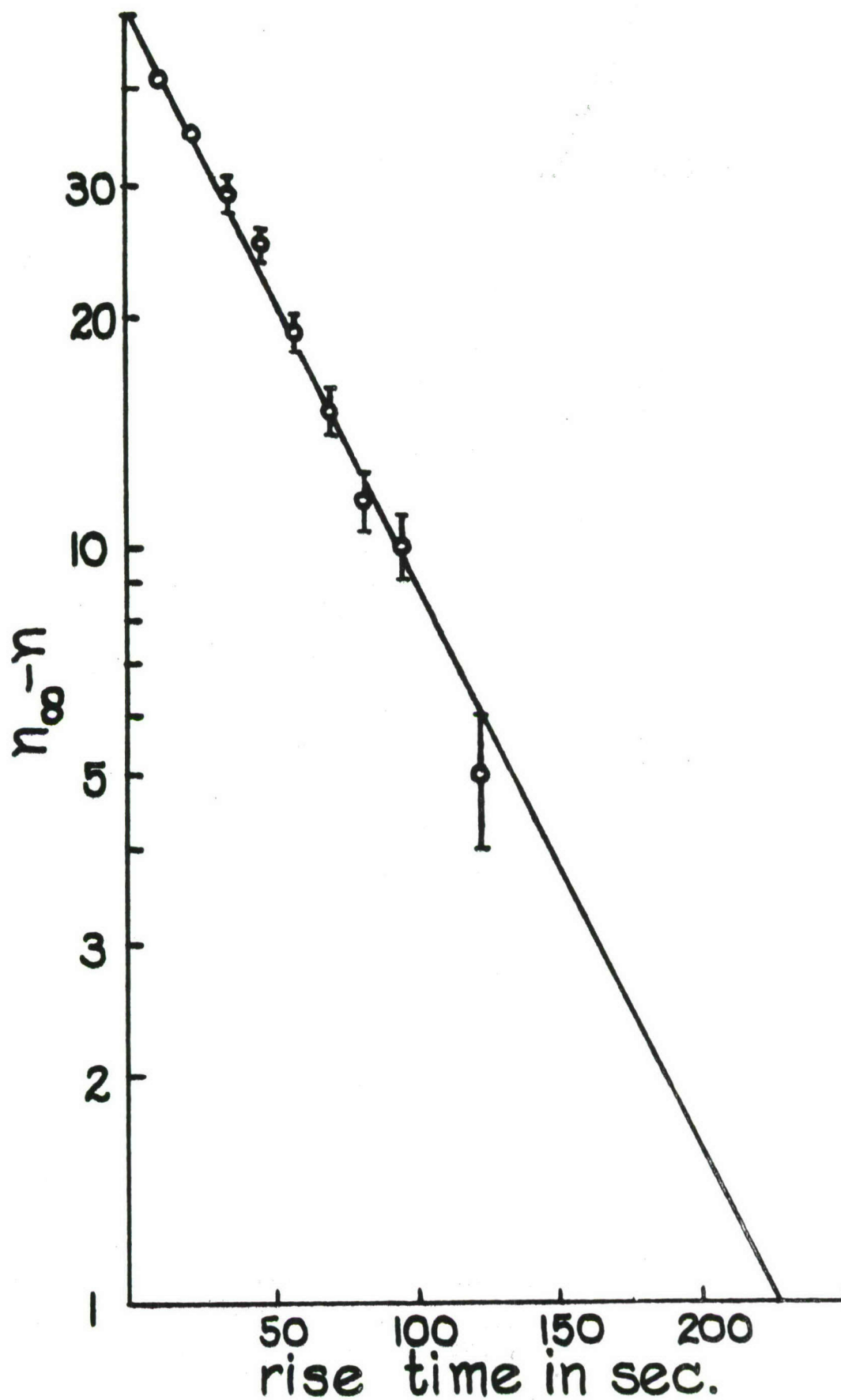


Figure 14 (b). Rise of the Number Polarized as a Function of Time

$t = 0$, is:

$$n = P\tau + (n_0 - P\tau)e^{-t/\tau} \quad (2.76)$$

The two cases above correspond to a) the statement that when $P = 0$, $n_0 = n_0$ and the number of nuclei decay in time according to

$$n = n_0 e^{-t/\tau} \quad (2.77)$$

and b) the statement that if $P \neq 0$ and $n_0 = 0$ the polarization will grow in time according to

$$n = P\tau(1 - e^{-t/\tau}) \quad (2.78)$$

or

$$n = n_\infty(1 - e^{-t/\tau}) \quad (2.79)$$

Thus Eq. 2.75 indicates the enhanced signal should decay or rise with the same time constant.

Now this decay of polarization back to the normal Boltzmann distribution is equivalent to the spin temperature of the nuclei returning to the equilibrium lattice temperature, where spin temperature is defined as that temperature which would produce by Boltzmann statistics the existing population of states. Thus the polarized nuclei return exponentially with the time constant to equilibrium with the lattice. The relation of T to T_1 is

discussed by Andrew, Swanson and Williams¹⁵. They performed an experiment in which, using only nuclear resonance, they saturated the resonance signal of Na^{23} in NaCl and observed the decay of the signal back to normal. They used a Pound-Watkins type detector, (which has a fairly high level of oscillation compared to the Robinson oscillator) and showed that the relaxation time τ is related to T_1 of the Na^{23} line by

$$\tau = T_1 (1 + \gamma^2 H_1^2 T_1 T_2)^{-1} \quad (2.80)$$

where H_1 is the detection field of the NMR oscillator. Thus approaches T_1 as the detector level approaches zero.

The Robinson low level oscillator detector was used in the dynamic polarization experiment described in the previous sections. In the experiments it appeared that the Na^{23} resonance signal was near saturation as an increase or decrease of the level of oscillation gave a smaller resonance signal. If such is the case, the quantity $\gamma^2 H_1^2 T_1 T_2$ is approximately 1/2 for a Lorentzian line and 1 for a Gaussian line. Examination of Figure 9 will show that the Na^{23} nuclear signal is essentially Gaussian. The derivative of a Gaussian line drops to 20% of peak value at a position 2.5 times the position of the peak from the center of the line, while the derivative of a Lorentzian line drops to 20% at a greater distance, namely 3.8 times the peak position from the center. Therefore we can take $\gamma^2 H_1^2 T_1 T_2$ to be approximately 1 for the Na^{23}

line. This gives

$$\tau = T_1(2)^{-1} \quad (2.81)$$

Since the measured value of τ was 60 ± 6 seconds, the value of T_1 associated with the polarized Na^{23} nuclei is twice this or 120 ± 12 seconds. This value may now be compared with observed values of T_1 for Na^{23} in NaCl. Wikner, Blumberg and Hahn¹⁶ have measured the T_1 values for Na^{23} in NaCl at 195°K up to room temperature, by pulse techniques. The values are given as 12 seconds (298°K), 14.5 seconds (273°K) and 28 seconds (195°K). Mahendroo and Nolle¹⁷ measured T_1 for Na^{23} in NaCl as 12.3 seconds at room temperature (approximately 300°K). They claim that it has a temperature dependence given by

$$(T_1)^{-1} = aT^2 + b \quad (2.82)$$

for ranges above room temperature. Extrapolation of the values given by Wikner, Blumberg and Hahn¹⁶ down to 77°K by a plot of $1/T_1$ against T^2 gives $T_1 = 143 \pm 10$ seconds. This compares favorably with the value obtained from the relaxation time of $T_1 = 120 \pm 12$ seconds. Thus within the accuracy of the experiment, the relaxation time of the polarized nuclei is given by Eq. 2.80.

2.14 CONCLUSION

The indications of the above experiment are that the use of irradiation induced centers to enhance nuclear signals in alkali halide crystals can be a very powerful tool for studying relaxation processes in the crystal. Of course large negative enhancements are useful in practical applications to the amplification of radio frequencies as well. The data indicates that higher enhancements should be possible at higher concentrations of Cl_2^- centers. It would be of interest to study the enhancement of Na^{23} as a function of the concentration of Cl_2^- centers in NaCl and to determine the optimum concentration. It would also be interesting to study the enhancement at a given concentration due to each of the seven major lines in the EPR spectrum since the relative number of centers in each state can be determined. A more thorough study of the enhancement as a function of time should also be undertaken in order to study the spin diffusion in the crystals.

It is quite probable that the effect of increasing the concentration of Cl_2^- centers in the sample would produce much larger enhancements than would be obtained by an increase in saturation of the lines in the present samples studied, by using higher klystron power. By decreasing the temperature below liquid nitrogen temperature, an increase in enhancement would be expected due to the greater saturability of the line and to the changes in nuclear relaxation times.

The increase of concentration of Cl_2^- centers at 77°K would require better irradiation equipment than was used in the above experiment. Also other types of metallic-doping of the NaCl could be useful. Parfianovich¹⁸ indicates a large increase in the rate of production of F and V centers in NaCl by doping with Copper or Nickel ions.

It would be exceedingly interesting to attempt a dynamic polarization of Na^{23} by using F_2^- centers in NaF. The F_2^- center has a much more simple spectrum consisting of three EPR lines. This is due to the hyperfine interaction of the electron and the two fluorine nuclei of total spin 1. Since F^{19} is 100% abundant the spectrum is that of only the one isotope. It would be of interest to compare the enhancements of Na^{23} in NaF and in NaCl. Another possibility is the enhancement of Li^6 and Li^7 in LiF by using the F_2^- center. It would be useful to compare results on these two isotopes.

In conclusion we would like to express our appreciation of the encouragement and helpful suggestions of Dr. Bernard Smaller, Dr. P. H. Yuster and Elston Hutchison of the Argonne National Laboratory.

REFERENCES

1. A. W. Overhauser, Phys. Rev. 91, 476 (1953); Phys. Rev. 92, 411 (1953).
2. T. R. Carver and S. P. Slichter, Phys. Rev. 92, 212 (1953).
3. E. Erb, J. L. Motchane, and J. Uebersfeld, C. R. Acad. Sci. 246, 2121 (1958).
4. J. A. Cowen, W. R. Schafer, and R. O. Spence, Phys. Rev. Letters 3, 13 (1959).
5. M. Abraham, M. A. H. McCausland, and F. N. H. Robinson, Phys. Rev. Letters 2, 449 (1959).
6. RADC-TR 62-436, Technical Note No. 2 Sept. 1961-Aug. 31, 1962, Contract No. AF 30(602)-2204.
7. Report No. ARF-A 1216-7 "Investigation of Narrow Line Paramagnetic Resonance Absorption Spectrum in Single Crystal Calcite," (Armour Research Foundation).
8. F. K. Hurd, M. Sachs, and W. D. Hersberger, "Paramagnetic Resonance Absorption of Mn^{++} in a Single Crystal of $CaCO_3$," Phys. Rev. 93, 373 (1954).
9. A. C. Redfield, Phys. Rev. 98, 1787 (1955).
10. C. Kikuchi and L. M. Matarrese, "Paramagnetic Resonance Absorption of Ions with Spin 5/2: Mn^{++} in Calcite," Jour. Chem. Phys. 33, 601 (1960).
11. RADC-TR 62-436, Technical Note No. 2 Sept. 1961-Aug. 31, 1962, Contract No. AF 30(602)-2204, p. 3.11.
12. T. G. Castner and W. Kanzig, "The Electronic Structure of V-Centers," J. Phys. Chem. Solids 3, 178 (1957).
13. T. G. Castner, "Saturation of the Paramagnetic Resonance V-Center," Phys. Rev. 115, 1506 (1959).
14. N. Bloembergen, "Nuclear Magnetic Relaxation," W. A. Benjamin Press (1961) p. 161.

REFERENCES - continued

15. E. R. Andrew, K. M. Swanson, and B. R. Williams, "Angular Dependence of Nuclear Spin Lattice Relaxation Time for Several Alkali Halide Crystals," Proceed. London Phys. Soc. 77, 36 (1961).
16. E. G. Wikner, W. E. Blumberg, and E. L. Hahn, "Nuclear Quadrupole Spin Lattice Relaxation in Alkali Halides," Phys. Rev. 118, 631 (1960).
17. P. P. Mahendroo and A. W. Nolle, "Nuclear Magnetic Relaxation in Ionic Crystals at High Temperature," Phys. Rev. 126, 125 (1962).
18. I. A. Parfianovich, Optika i Spektrosk 4, 253 (1958).

GLOSSARY OF TERMS

A	- Derivative of the absorption signal
A_o	- Peak value of A
$(A_o)_{\max}$	- Maximum value of A_o during saturation
B	- Absorption signal
B_o	- Peak value of B
$(B_o)_{\max}$	- Maximum value of B_o during saturation
\mathcal{E}	- Enhancement of nuclear resonance signal
\mathcal{E}_o	- at center of forbidden electronic transition
$\mathcal{E}(H_o)$	- at center of forbidden electronic transition
\mathcal{E}_{\max}	- at 100% saturation of forbidden line
F	- Number of nuclei polarized per electron pumped
$g(\omega)$	- The shape function for a resonance signal
$g(\gamma)$	- The shape function for a resonance signal
H_o	- Static magnetic field
H_1	- Detection field
$(H_1)_{\max, A}$	- Value of H_1 at which A_o is a maximum
M	- Magnetic moment per unit volume
n	- Excess number of nuclei polarized
n_i	- Population of the i^{th} level
$(n_i)_o$	- Population of the i^{th} level for equilibrium Boltzmann distribution
n_{tot}	- Total number of nuclei in sample per cm^3

GLOSSARY OF TERMS - continued

$N_m = i$	- Number of electron spins in state $m = i$
P	- Applied microwave power
P_o	- Maximum microwave power available
$P_{\max, A}$	- Power at which A_o reaches a maximum
$P_{\max, B}$	- Power at which B_o reaches a maximum
S	- Saturation of EPR line
S_{A_o}	- Saturation of line with power applied at peak of derivative signal
S_{B_o}	- Saturation of line with power applied at peak of absorption signal
$S(\nu, P)$	- Saturation with power P applied at frequency
T_1	- Spin-lattice relaxation time
T_2	- Spin-lattice relaxation time
W	- Line width
X	- $\gamma^2 H_1^2 T_1 T_2$
γ	- Gyromagnetic ratio
δ	- $h\nu / kT$ at nuclear transition frequency
Δ	- $h\nu / kT$ at electronic transition frequency
ΔH	- Line width in gauss
$\Delta \nu$	- Line width in cycles per second
$\Delta \omega$	- Line width in angular frequency
θ	- Angle between crystalline field and H_o
ν	- Frequency
ν_o	- Resonant frequency in cycles per second

GLOSSARY OF TERMS - continued

- π - Transition probability
- χ'' - Imaginary part of complex susceptibility associated with absorption
- χ_0 - Static magnetic susceptibility
- ω - Angular frequency of detection field
- ω_0 - Resonant frequency in radians per second

APPENDIX

AREA OF A LORENTZIAN LINE

In order to calculate the number of spins in an EPR sample by comparison with a known sample, it is convenient to assume both samples show Lorentzian EPR lines. Then it will be shown below that the number of spins, which is proportional to the area under the absorption curve, will be merely proportional to the amplitude of the derivative signal times the line width squared. The area is independent of H_1 because, for the Lorentzian line, the line broadens with an increase in H_1 but in such a way that the product of line width squared and amplitude of derivative remains constant upon saturation.

The Lorentzian absorption signal is of the form

$$B = \frac{C}{D + E(\omega_0 - \omega)^2}$$

The area under the absorption curve is KN , where N is the number of spins detected and K is a proportionality constant depending on modulation and other factors:

$$KN = \int_{-\infty}^{+\infty} B d\omega = \pi C (DE)^{-1/2}$$

The derivative signal $A = \frac{dB}{d\omega}$ is given by

$$A = \frac{2CE(\omega_0 - \omega)}{[D + E(\omega_0 - \omega)^2]^2}$$

At the peak of the derivative signal, $A = A_0$, $\omega = \omega'$ and $dA/d\omega = 0$.

Hence

$$D = 3E(\omega_0 - \omega')^2$$

$$A_0 = \frac{9}{8}C(3E)^{1/2}D^{-3/2}$$

and

$$\omega_0 - \omega' = D^{1/2}(3E)^{-1/2} = \frac{1}{2}W$$

where W = the line width between points of maximum slope.

Substituting for C and D from these equations,

$$D = \frac{3}{4}EW^2$$

$$C = \frac{8}{9}D^{3/2}(3E)^{-1/2}A_0 = \frac{1}{3}A_0EW^3$$

the area becomes

$$KN = \pi C (DE)^{-1/2}$$

$$KN = \pi \left(\frac{1}{3}\right) A_0 E W^3 \left(\frac{3}{4} E^2 W^2\right)^{-1/2}$$

$$KN = \frac{2\pi}{3\sqrt{3}} A_0 W^2 = \frac{2\pi}{3\sqrt{3}} (\text{PEAK SIGNAL})(\text{WIDTH})^2$$

Hence the ratio of spins on two different samples

$$\frac{N_1}{N_2} = \frac{K_2}{K_1} \frac{(A_0)_1}{(A_0)_2} \frac{W_1^2}{W_2^2}.$$

Now K contains factors relating the number of spins to the size of the EPR line, and hence will contain the effect of modulation, the amplification of the system, the Q of the cavity, and the saturation factor $\gamma^2 H_1^2 T_1 T_2$. In comparing two samples, therefore, the modulation difference should be taken into account and the amplification should be known. For similar crystalline samples, the Q of the cavity will not change appreciably with change of sample. In order to avoid the difficulty with the saturation factor, both signals should be compared at the same value of $\gamma^2 H_1^2 T_1 T_2$. This can be accomplished easily if H_1 is increased in the case of each sample until the maximum derivative signal is obtained. Samples compared at the point of maximum derivative signal therefore have the same value of $\gamma^2 H_1^2 T_1 T_2$, assuming both have the same shape. If this is done, then in general the ratio of the K's in the equation for calculating the ratio of the number of spins, reduces to a ratio of the relative amplification at which the signals are detected.

CHAPTER 3

INSTRUMENTATION

3.1 INTRODUCTION

After separate EPR and NMR experiments with a great variety of samples and preliminary double resonance experiments at room temperature, the demands and problems of double resonance instrumentation were more clearly defined and better understood. Considerable time and effort have been devoted to maintaining and improving our present apparatus, to studying and to experimenting with new double resonance techniques and to extending our experiments to the variable-temperature and low-temperature ranges.

3.2 EXPERIMENTAL EQUIPMENT

3.2.1 Nuclear Magnetic Resonance Detector

In previous technical notes the theory, design, construction and modification of a "Robinson" oscillator were presented. As proposed in Technical Note No. 2, the range of this detector has now been extended to cover 500 Kc to 15 Mc. Furthermore, the stability and sensitivity (signal-to-noise ratio) have been improved by at least a factor of three in the center portion of the

frequency range. With circuit adjustment this can be extended to the extremities of the frequency range. A second Robinson oscillator is under construction at present. All the modifications of the prototype have been incorporated into this second detector; the design has been further improved and, in particular, optimized for the low frequency portion of the frequency range. This has been done to facilitate our work on such nuclei as germanium, silicon, potassium, boron, etc.

The design of the NMR detector coil for use in double resonance experiments continues to be a problem. This coil forms part of the ordinary LC tuning circuit of the Robinson oscillator and provides the NMR alternating magnetic field. The chief instrumental problem is combining the EPR microwave field and the NMR r.f. field inside the microwave resonant cavity. A number of requirements must be kept in mind in approaching this problem.

- a) The size of the resonant cavity is limited. The dimensions are dictated in general by the microwave frequency of the system. The size is limited both by the magnet gap and especially by the added requirements of cryogenic work. With liquid helium, for example, a double quartz cryostat is needed.
- b) A small microwave cavity limits the dimensions and configuration of the NMR coil. When mounted inside the

cavity the coil must be so positioned as to fulfill the boundary conditions for producing a standing wave in the cavity. This requirement necessitates that the coil be wound in a rectangular shape so that the magnetic induction lines of the microwave field will always be parallel to the conducting surfaces of the coil, while the electric lines of force will always be perpendicular to these surfaces. The coil must be very accurately positioned in the plane between the two standing half-waves of the Varian TEL02 mode cavity which is employed in our equipment. Finally, some space must be left between the coil and the cavity walls in order that the induction lines of the alternating field of the coil may form a closed loop around the edges of the coil. In Technical Note No. 2 the difficulty of detecting narrow NMR signals from samples located in the Varian cavity was erroneously attributed to the inhomogeneous broadening of the signals resulting from magnetic impurities in the large mass of metal employed in the construction of the cavity. Further experiments with coil shapes and sizes indicated that the coil windings were too close to the cavity walls, resulting in a considerable reduction of the NMR alternating magnetic field. Figures 15 (a) and 15 (b) illustrate our present technique of locating the NMR coil in the microwave cavity.

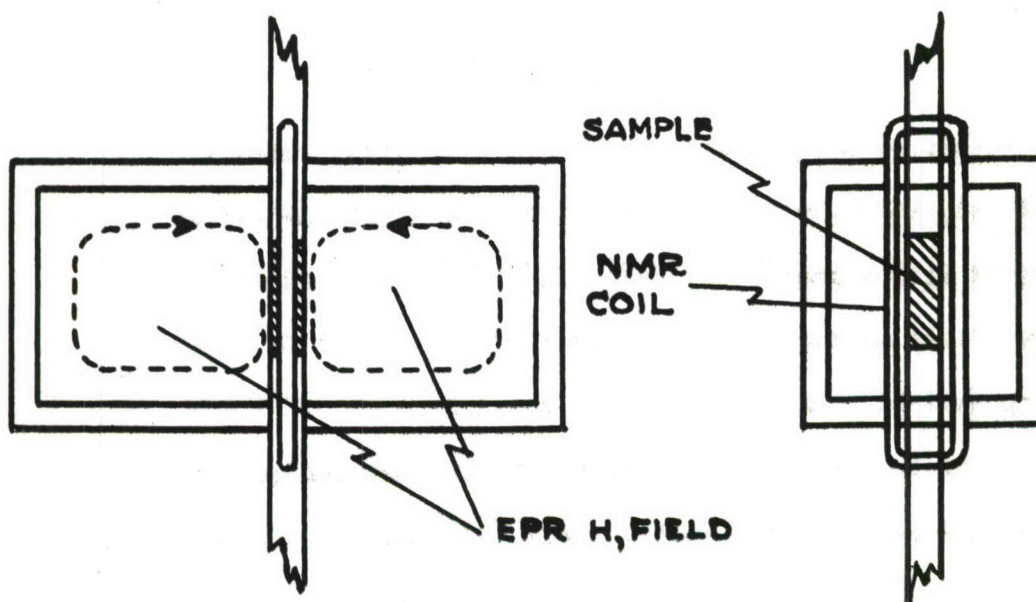


Figure 15(a). Side View: NMR
Coil in EPR Cavity

Figure 15(b). End
View

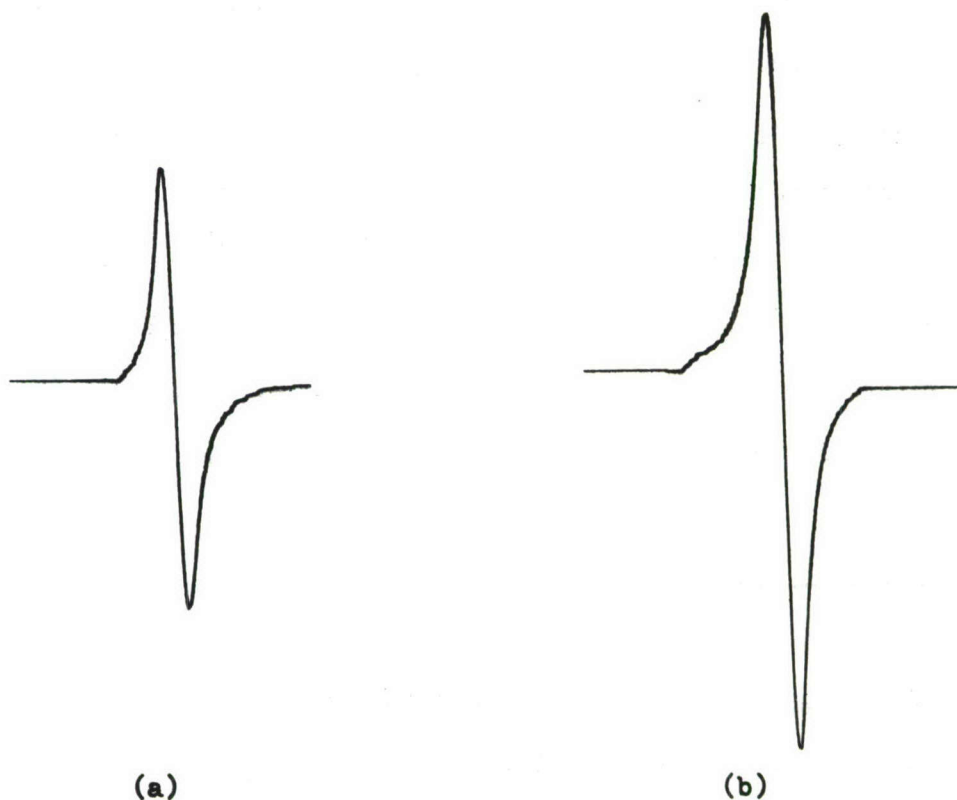


Figure 16. Effect of Quartz Sheathing on Amplitude of EPR Signal.
(a) No Quartz (b) With Quartz Sheath

- c) The filling factor of both the EPR cavity and NMR coil should be high, i.e. the sample should occupy as much as possible of the volume containing the alternating fields. A solenoidal type of NMR coil would guarantee a much better filling factor than the rectangular type described above, but such a coil drastically reduces the Q of the resonant cavity. For a given sample the presence of a rectangular coil in the cavity reduces the EPR signal to 0.93 of its amplitude in the cavity when no coil is present. However, if a solenoidal coil is employed and all other parameters remain constant, the amplitude of the signal is reduced to 0.075 of its original value.
- d) Both the coil and the cavity should have the highest possible Q . This high Q of the microwave cavity is absolutely necessary in order to achieve saturation of the EPR signal, since the power from an X-band klystron is limited. Furthermore, the detection sensitivity of both the NMR and EPR detectors is in general proportional to the quality factor Q .

3.2.2 Microwave Cavity

Experiments with epoxy cavities¹ have been continued. The Q of such cavities did not reach the hoped-for values. The optimum Q obtained was 4000, or about the same as that of the Varian cavity. Two very critical parameters are the polishing of the

cavity walls before silvering and the silvering process itself. Evaporation processes, chemical deposition processes and silver paint were all tried. Silver paint is quite satisfactory, but should be baked onto a surface at high temperatures for best results. It is impossible to heat epoxy above 200°C without affecting the cavity dimensions and the thermal properties of the epoxy. It has been recommended that we heat the finished cavity for 24 - 48 hours in a furnace at 125°C .

In view of the necessity of saturating electron resonance signals in double resonance experiments, the question of a maximum microwave power output is a critical one. The V-58-C Varian klystron power output is approximately 600 milliwatts, one half of which is incident on the sample. For certain samples this is sufficient power to achieve a high percent of saturation. However, greater power and larger alternating magnetic fields constitute a major concern and interest for this group. A number of considerations might be mentioned here in this regard.

- a) At the risk of abbreviating the lifetime of the klystron, the resonator and reflector voltage may be adjusted to higher than average operating values. The power output may be doubled in this manner.
- b) Concentric cylinders of quartz may be used to support and surround the sample in the cavity. For example, even at room temperature the Varian Liquid Nitrogen Dewar (double quartz wall) may be positioned in the cavity and then the

quartz sample tube holding the sample inserted into this dewar. Thus the sample will be sheathed in a triple quartz wall. Figure 16 (a) shows the record of a standard EPR signal from a 0.1% pitch in K Cl sample. Figure 16 (b) shows the record of the same sample when located inside the quartz dewar walls. A signal amplitude improvement of 1.6 has been obtained due to this quartz sheath. By careful adjustment of the quartz sheath diameter and of the number of layers of quartz the signal amplitude may be improved by a factor of two.

- c) A Circulator may be employed in place of the "magic T" bridge of the Varian EPR Spectrometer. Such a change would provide a two-fold increase in the power incident on the sample.
- d) A travelling-wave helix might be employed in place of the resonant cavity for double resonance work.² Such a helix is essentially frequency independent; little power is dissipated in it (high Q, low heating); and the helix serves both as the EPR cavity and as the NMR coil. With such a helix a high Q NMR coil is possible without loss of the saturating microwave power. In one of the several articles on this type of device Webb comments, "We have achieved Overhauser enhancements 50% greater than those possible with the same sample in cavities, and raised our NMR signal-to-noise ratios by a factor of 10 at the same time."³

3.2.3 Low Temperature Apparatus

The instrumentation for double resonance experiments at liquid nitrogen, liquid helium and intermediate temperatures has been completed.

Numerous experiments have been conducted at liquid nitrogen temperatures. Data is reported in other sections of this Technical Note. During the past year the Varian Variable Temperature apparatus was employed for experiments in the 77° K - 300° K range.

No experiments have been conducted yet at liquid helium temperatures. The instrumentation is completed, but room temperature and liquid nitrogen temperature experiments and equipment maintenance and repair work proved to be a full time program. It was decided to concentrate on obtaining more satisfactory and adequate data in the current experiments before inaugurating the considerable task of liquid helium temperature experiments.

References:

1. See Technical Note No. 2, p. 4.2
2. R. H. Webb, "Use of Travelling Wave Helices in ESR and Double Resonance Spectrometers," Review of Scientific Instruments, 33, 732 (1962).
3. Ibid. p. 735

CHAPTER 4

RESONANCE EXPERIMENTS

4.1 INTRODUCTION

Experiments have been conducted on all of the samples proposed for investigation in our Technical Proposal (Response to Request for Technical Proposal PR 175219) with the exception of the beryllium sample. A number of liquid samples not listed in the Proposal have also been investigated when a need for clearer understanding of the polarization processes or for standardization or calibration data dictated such a course of action.

The coupling between unpaired electrons and nuclei in a given system, while absolutely necessary for double resonance, may differ significantly from sample to sample. Such coupling may be a "static" or a "dynamic" interaction. Or, such coupling may be considered in terms of the interaction of the magnetic fields of the nuclear and electronic spins. In the latter scheme the strength of the interaction will depend on the separation of the spins, thus giving rise to "dipole-dipole" and "contact" interaction classifications. In a given sample the nuclear-electronic coupling can be due to either of these interactions separately, or both simultaneously, or a mixture of the two. Accordingly, there are a variety of double resonance effects which

in turn necessitate a variety of detection schemes or techniques depending on the nature of the coupling or interaction. Signal enhancements may be positive or negative. Microwave pumping may be done at any one of several frequencies. The effect of microwave power, of temperature, of sample concentration, of the presence of other nuclei, and of the various relaxation processes differs from sample to sample. A great amount of preliminary study of such processes and their effect on the results of double resonance experiments was found to be necessary before meaningful data analysis could be expected. Much of the data presented in this part of the report was obtained in the process of seeking a better understanding of such double resonance parameters.

The first two samples discussed are liquid samples. They were selected initially because of expected ease of EPR saturation, NMR detection, etc.

4.2 EXPERIMENTAL DATA

4.2.1 DPPH in Benzene

A positive enhancement of the proton resonance signal in solid DPPH has been reported in the literature.¹ The enhanced signal was nine times the unenhanced signal. This experiment is an example of the Overhauser Effect. When DPPH is dissolved in benzene, however, the nuclear-electronic type of coupling changes and a negative enhancement of the proton resonance was reported by this group in the Technical Note No. 1. With improved

instrumentation it was hoped that we might improve the magnitude of the negative enhancement. The previous experimental results (slight negative enhancement), however, were only duplicated. No improvement was achieved. The experiment did serve to clarify the role of sample concentration in the "Liquid" or "Underhauser" type of double resonance experiment (allowed transitions are pumped; dipole-dipole coupling predominates). Sample concentrations from 0.1 to 10^{-5} M. were prepared in sizes ranging from 5mm^3 to 50mm^3 . EPR spectra were recorded at varying microwave power levels (0 - 30 db). Up to approximately 30% saturation of the signal was obtained at full power in the most dilute samples. However, only in samples of slightly less than 10^{-3} M. concentration was any enhancement of the proton signal (NMR frequency = 14.2019Mc) observed. Thus it becomes evident that no coupling occurs in such a solution until a certain minimum concentration of electrons is obtained. As the concentration is further increased the enhancement increases to a certain optimum value. Beyond this little is gained by increasing the concentration. At the same time, however, the increased concentration of electrons makes saturation of the EPR signal more difficult. In DPPH in benzene the minimal concentration for observing an enhancement seems to be between 10^{-3} and 10^{-4} M. Unfortunately, this is also the concentration at which a reasonable percent of saturation is achieved. The saturation and concentration parameters, therefore, are competing and nullifying one another. For a more quantitative analysis of this dependence

samples of smaller volume might be used as long as they contain sufficient nuclei to yield an NMR signal; or steps might be taken for increasing the available microwave power. Since our interest in DPPH in benzene was not so much in an analysis of the sample itself as in obtaining a suitable sample for calibration purposes, we have not continued this experiment.

4.2.2 Fuel Oil and Asphalt Dissolved in Pump Oil

The excellence of the NMR proton signal from pump oil samples combined with the reported successes of Poindexter² and Anderson³ in the double resonance experiments with natural crude oil and asphalt solutions motivated this group to select this type of sample for our next experiment with liquid samples. A sample of natural crude oil unfortunately was not available at the time of this experiment. In its place a sample of heavy fuel oil was employed. The asphalt solution sample was prepared by dissolving roofing tar in heated pump oil. Enhancement of the proton NMR signal was obtained from both of these samples.

It may be noted that in this type of sample, the same electron-nuclear system can exhibit one double resonance effect at low static magnetic fields and a different double resonance effect at high magnetic fields. Poindexter and Uebersfeld⁴, using the same asphalt sample have observed the "Underhauser" effect at low fields and the "Solid State" effect at high fields. In this latter case one has a static dipole-dipole interaction and pumps on the

"forbidden" energy level transitions.

In these experiments all measurements were obtained at a static magnetic field of approximately 3400 gauss. However, in view of instrumental difficulties this magnetic field was scanned or varied instead of the NMR frequency. Since the experimental procedure in such an experiment has been described previously in the literature, it does not seem necessary to include such details here.

A sample of 90mm³ of heavy fuel oil was placed in a 3mm I.D. quartz tube on which a rectangular NMR coil had been wound previously and positioned in the microwave cavity. No saturation of the EPR signal was visible at full power. The unenhanced proton signal was easily detected. After all instruments had been stabilized, careful measurements were made of the field-frequency values. Finally, the proton NMR signal was traced and re-traced at the frequencies ($\nu_e \pm \nu_n$) for a range of microwave power settings. Positive enhancement of the signal was observed at ($\nu_e - \nu_n$); negative enhancement at ($\nu_e + \nu_n$), as predicted theoretically. A typical record is illustrated in Figure 17. Figure 18 illustrates the enhancement behaviour in relation to the magnetic field and frequency. Enhancement is defined

$$E = \frac{(P - P_o)}{P_o}$$

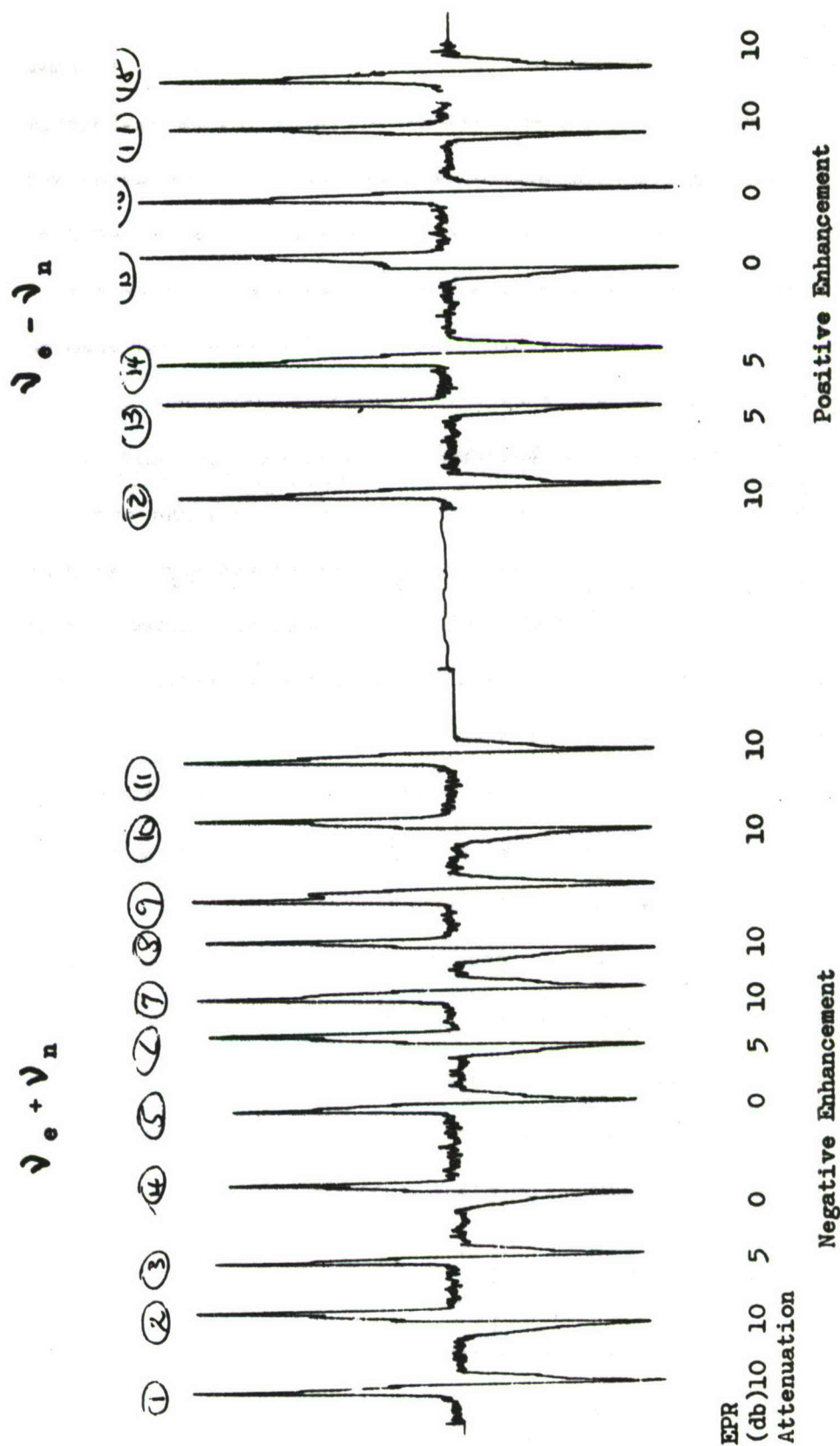


Figure 17. Enhanced Proton Resonance Signal from Fuel Oil Sample

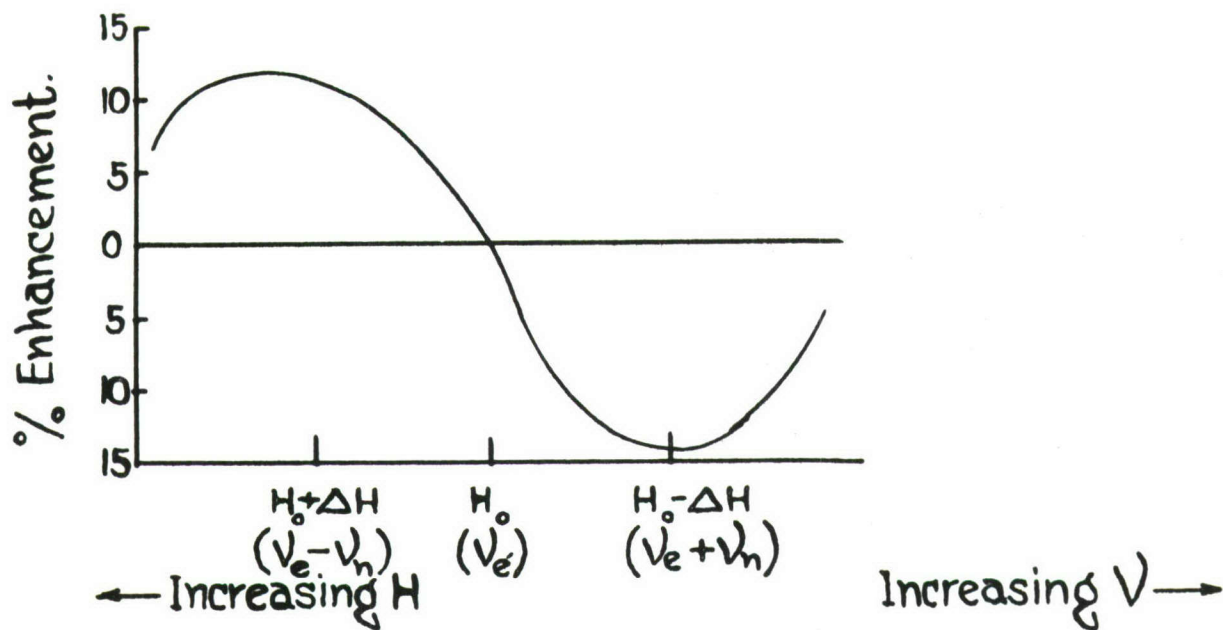


Figure 18. Percent Enhancement vs. Magnetic Field and Frequency

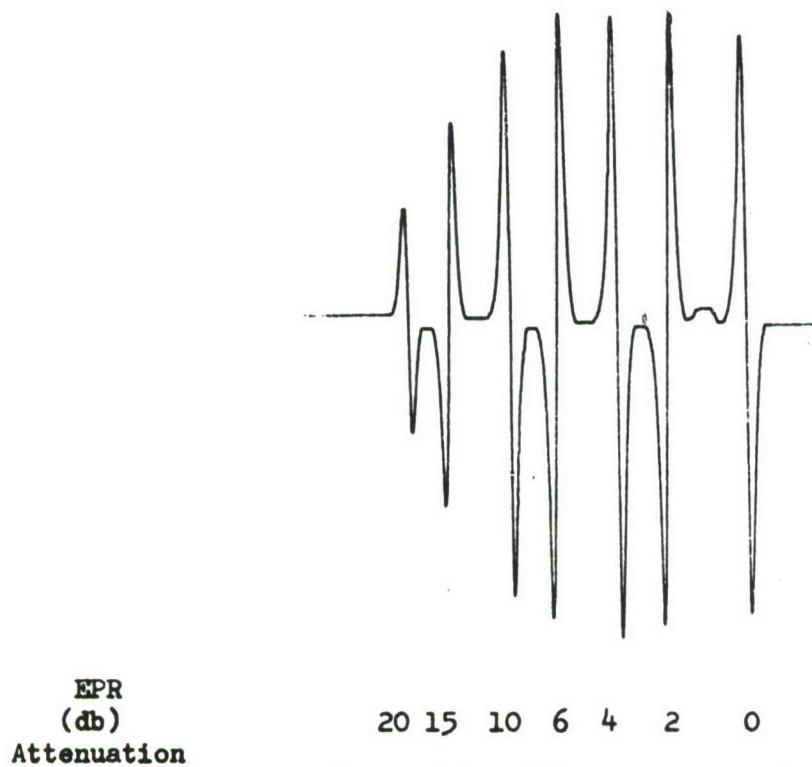


Figure 19. EPR Saturation of Asphalt in Pump Oil Sample

where P_0 is the polarization (as determined by nuclear resonance) at thermal equilibrium. Typical values are

$$\begin{aligned} H_0 \text{ (static magnetic field)} &= 3399 \text{ gauss} \\ \nu_e \text{ (EPR frequency)} &= 9539.50 \text{ Mc} \\ \nu_n \text{ (NMR frequency)} &= 14.474 \text{ Mc} \end{aligned}$$

A negative enhancement of 15% and a positive enhancement of 13% were observed. These values may be compared with those reported by Anderson⁵ for Brookhaven crude oil, namely, a positive enhancement of 50% and a negative enhancement of 65%.

A sample of approximately 500mm³ of roofing tar dissolved in heated (Cenco) pump oil (0.3 gm. of tar in 1.0 ml of oil) was analyzed in the same manner as the fuel oil. With this sample, however, saturation of the EPR signal was observed. The saturation behaviour is illustrated in Figure 19. Assuming a Lorentzian line shape this record indicates 38% saturation. Again, a positive enhancement was detected at $(\nu_e - \nu_n)$ and a negative enhancement at $(\nu_e + \nu_n)$. Figure 20 is a typical record of proton NMR signal obtained in this experiment. This record differs from that shown in Figure 17 in that all proton resonance signals shown here were recorded with maximum microwave power incident on the sample. The static magnetic field (H_0) was altered very slightly from signal to signal. In Figure 17, on the other hand, the magnetic field was kept constant and the microwave power varied step by step. Notice in Figure 20 the broadening of the resonance line during positive enhancement and narrowing during

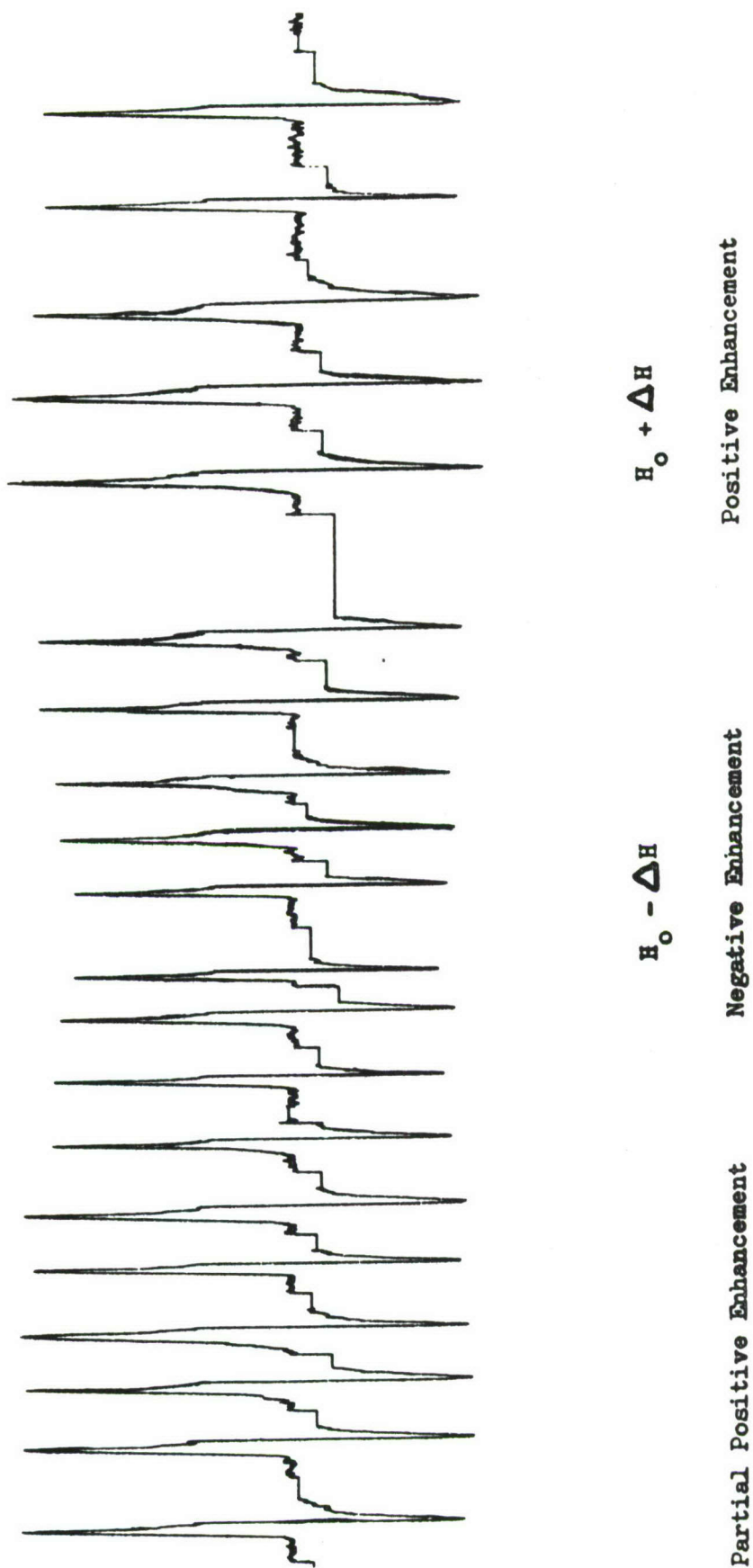


Figure 20. Enhanced Proton Resonance Signal from
Asphalt in Pump Oil Sample

negative enhancement. By measuring the areas under the NMR curves a positive enhancement of approximately 44% is obtained here and a negative enhancement of approximately 57%.

It would be interesting to carry this experiment further, under conditions of higher microwave power, scanning frequency instead of field and over a broader range of temperatures. Preliminary experiments with pump oil at low temperatures have shown that the proton resonance line width, which at room temperature is approximately 45 milligauss, broadens to approximately 13 gauss at liquid nitrogen temperatures. The amplitude of the signal is reduced by a factor of 100 over the same temperature range.

4.2.3 Boron

No magnetic resonance data has yet been reported on pure boron. The considerable amount of information compiled to-date has been obtained in experiments on kernite, borine carbonyl, borates, borides, and the like. This section of the report will contain the experimental data from our preliminary EPR and NMR experiments on boron.

The EPR signal from a double crystal of boron has been detected and the spectrum recorded at both room and liquid nitrogen temperatures. The spectrum is very complex. A broad scan of the magnetic field (approximately 500 - 4000 gauss scan) at 9.4 KMc/S revealed many components whose relative positions, line widths and amplitudes depend strongly both on the orientation of the crystal

$T = 77^{\circ}\text{K}$ $\theta = 0^{\circ}$ $T = 300^{\circ}\text{K}$ $\theta = 0^{\circ}$ $T = 77^{\circ}\text{K}$ $\theta = 45^{\circ}$ $T = 300^{\circ}\text{K}$ $\theta = 45^{\circ}$ $T = 77^{\circ}\text{K}$ $\theta = 90^{\circ}$ $T = 300^{\circ}$ $\theta = 90^{\circ}$

Figure 21. EPR Spectra of Crystalline Boron indicating temperature and orientation dependence.

axes in the external magnetic field and on the temperature of the sample. Figure 21 illustrates typical records of the data from this sample. Further data must be obtained before analysis of such spectra can be undertaken. We hope to complete a program whose objective will be to understand the spectrum observed, identify and locate the paramagnetic sites and interactions responsible for the spectra and to correlate these EPR results with experimental and theoretical data previously reported on boron in other forms and compounds. Temporarily, however, this program has been postponed in view of other experiments which are more closely allied with double resonance phenomena.

The sample employed is a double crystal whose width dimension corresponds to the $[101]$ direction and whose thickness dimension corresponds to the $[010]$ direction. The length dimension corresponds to a crystal direction parallel to the (101) family of planes. The crystal is rhombohedral, belonging to the β -rhombohedral polymorph of boron. The X-ray pattern obtained with the X-ray beam parallel to the $[010]$ crystal direction clearly showed a three-fold symmetry plane. The crystal parameters are

$$a = b = c = 10.145 \text{ \AA}$$

$$\alpha = \beta = \gamma = 65^\circ 17'$$

The dimensions of this sample are 0.8 x 2.2 x 6.6mm.

The sample was positioned rigidly at the end of a narrow quartz rod, and located in the Varian liquid nitrogen quartz dewar which in turn was carefully positioned in the microwave cavity.

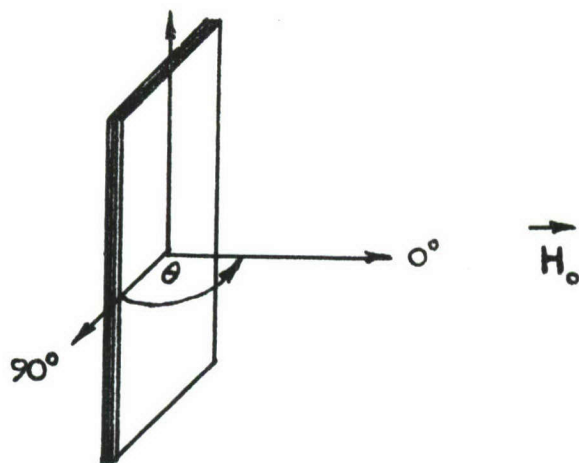


Figure 22. Crystal Orientation
in Magnetic Field

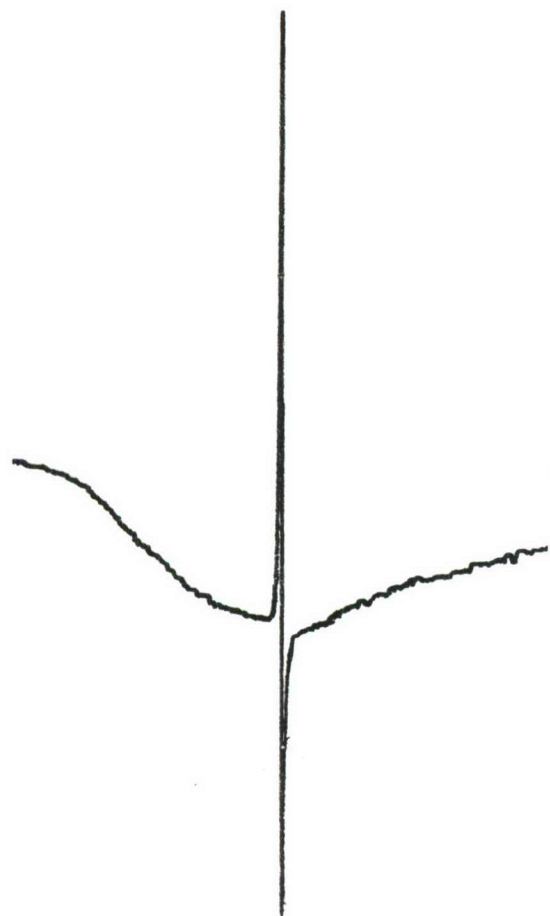


Figure 23.
 B^{11} EPR

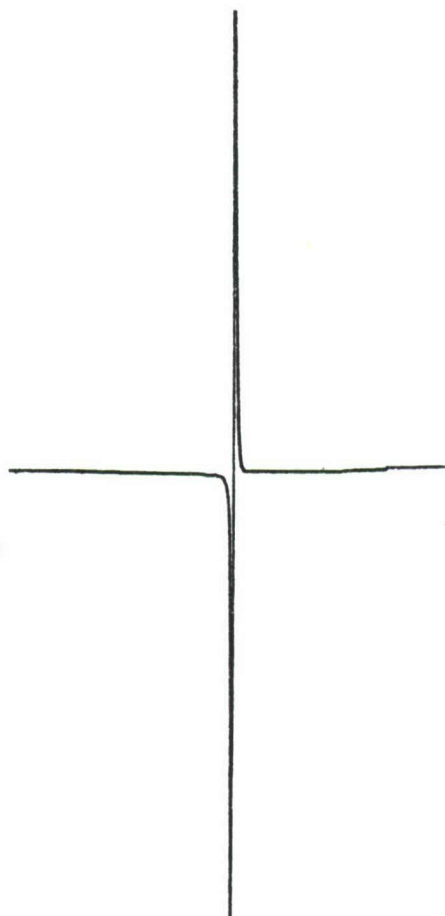


Figure 24.
 B^{11} EPR

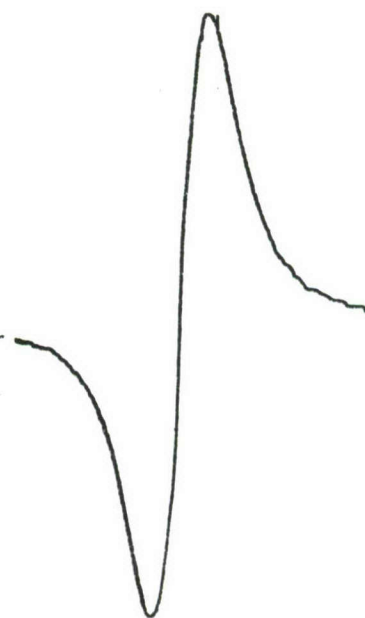


Figure 25.
 B^{11} EPR

This arrangement guaranteed that a maximum alternating magnetic field was focused on the sample and also facilitated sample orientation with respect to the static magnetic field. The angle associated with the measurements is the angle which the vector perpendicular to the width dimension makes with the static magnetic field direction. This is illustrated in Figure 22.

Boron has two isotopes, B^{10} and B^{11} , which have nuclear spins of 3 and 3/2 respectively. Since B^{11} is approximately 80% abundant, one normally would expect a spectrum consisting of sets of four equally intense lines with perhaps a background of seven weaker lines, the latter associated with the B^{10} .

Samples of high-purity boron prepared by deposition techniques on tantalum filaments were also investigated. Such samples are polymorphic and hence not suitable for crystal structure analysis. The first sample measured 9 x 12 x 1mm and the EPR spectrum obtained is illustrated in Figure 23. This signal was recorded over a magnetic field scan of 2000 - 4000 gauss. The broader resonance visible on the record is due to the presence of the tantalum ribbon on which the boron was deposited. The second sample measured 7 x 2 x 1mm and the EPR spectrum from it is illustrated in Figure 24. Notice that there is no evidence here of the tantalum ribbon. Figure 25 is a record of the EPR spectrum obtained at a reduced field scan rate and signal amplification.

A proton resonance probe was employed to measure the line width and to calculate the g-value of this EPR signal. The

linewidth (full width at half maximum of the absorption curve; or peak to peak on the derivative of the absorption curve) was found to be 12.668 gauss. The g-value was calculated from the recorded data to be 2.5452.

The EPR signal was recorded for a full range of microwave power levels, but no indication of EPR saturation was visible. This fact reduced the possibility of detecting double resonance in a pure boron sample.

A sample of Boric Acid powder dissolved in alcohol was employed to locate the B^{11} NMR signal at 3400 gauss. This sample yielded a weak, but easily recorded signal with a line width of the order of 200 milligauss. Using this as a reference point, extensive searching was done for the B^{11} NMR signal in single-, double- and poly-crystal boron and in boron slag, at room and at liquid nitrogen temperatures, at high and low levels of power, and over wide and narrow field scans. In no case was the B^{11} NMR signal detected. This negative result combined with the inability to saturate the EPR line indicates that boron is not a very promising sample for double resonance work.

4.2.4 Graphite

EPR spectra were recorded at 300° K and 77° K from both natural and artificial graphite single crystals. These crystals were obtained from Dr. Paul Bryant at Midwest Research Institute. As would be expected, the spectra are critically orientation

dependent. Resonance line shape, position and amplitude change with a change of crystal orientation. Figure 26 illustrates typical resonance signals. The fact that the line shape is Dysonian confirms that the resonance is due to the conduction electrons in the graphite. There is no indication of EPR saturation either at 300° K or at 77° K. The data obtained over a full range of microwave power levels follows the no-saturation curve of the theory exactly. The C^{13} NMR signal from these samples was not detected.

Further EPR spectra were recorded from the potassium in graphite sample. The resonance line is broad and unsaturable and thus does not seem suitable for investigation in double resonance experiments.

4.2.5 Germanium

Both NMR and EPR experiments were continued on germanium. No NMR signal was observed in crystals or in powder, at 300° K or at 77° K. The crystal sample is a 4.5 x 3 x 1.5mm section of a large crystal obtained from Texas Instruments. A finely powdered sample was made by pulverizing a piece of this crystal between steel rods. The powder same size is approximately 50mm³. Figure 27 (a) is a record of the spectrum obtained from the powdered sample at room temperature. This record was made over a magnetic field scan from 800 to 4900 gauss. Figure 27 (b) is a trace of the center portion of the signal illustrated in Figure 27 (a). The line

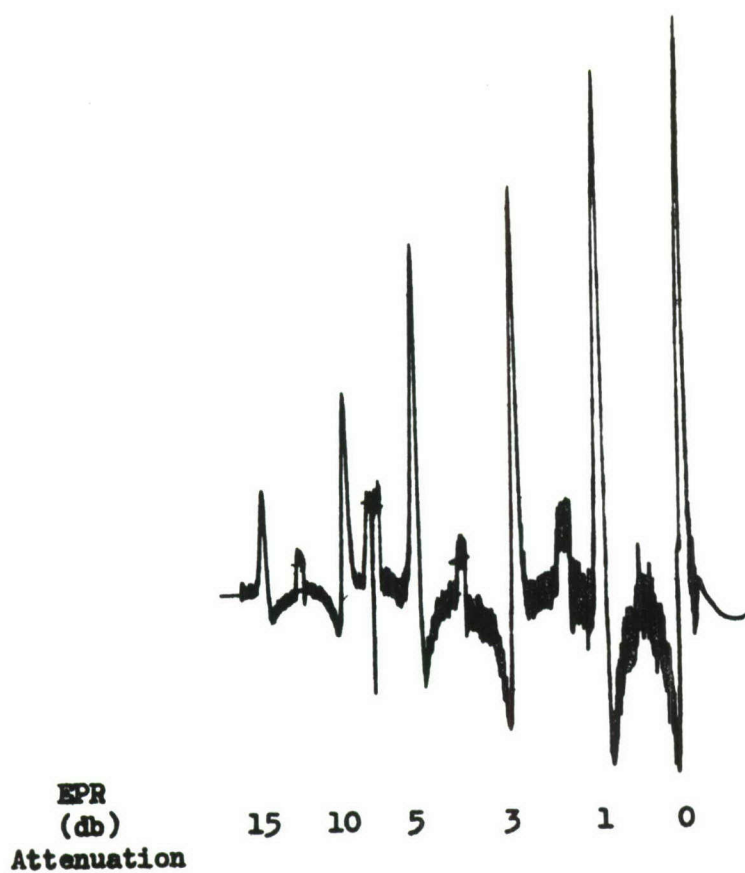


Figure 26. EPR Spectrum from Graphite Single Crystals at Different Microwave Power Levels

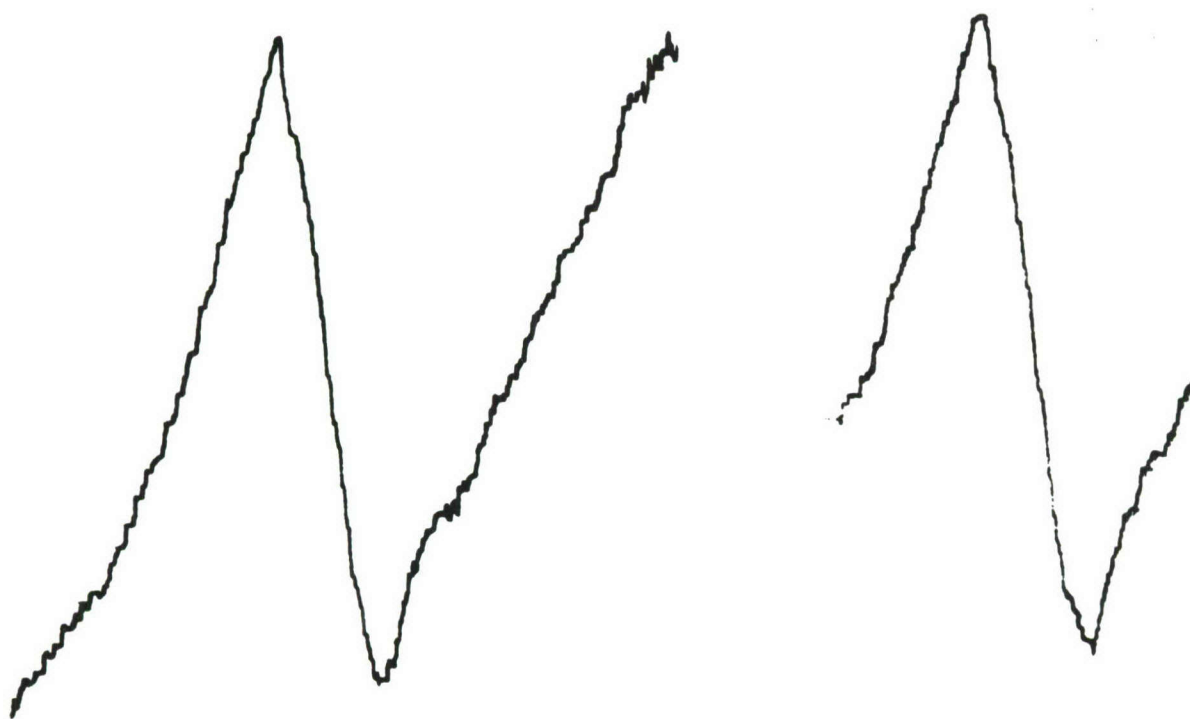


Figure 27 (a).
 Ge^{73} EPR

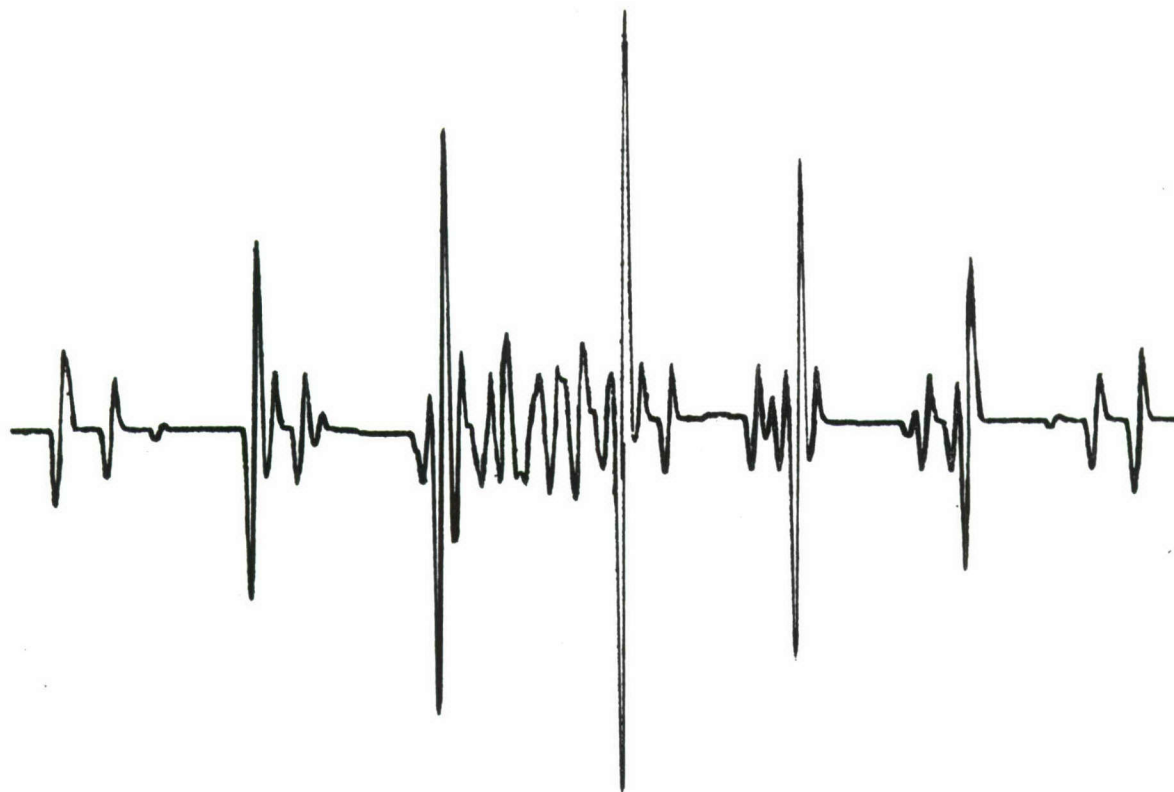
Figure 27 (b).
 Ge^{73} EPR

width from peak to peak of this signal is 527 gauss. The center of this signal corresponds to a g-value of 2.1524. It is a very strong signal. The experiment was conducted at a temperature of 300° K. When repeated at a temperature of 77° K, this entire center portion of Figure 27 (a) disappears. A steeply rising line is recorded throughout the entire field scan. We have ruled out the possibility that such a record might be due to pen recorder drift or AFC (automatic frequency control) drift, or the like. The crystal sample was then located in the cavity and the magnetic field scanned through its entire range. At both 300° K and 77° K the sharply rising signal line mentioned above for the powdered sample at 77° K was observed. At neither temperature did the center resonance (Figure 27 (b)) appear in the case of this crystal sample. The slope of this line is much greater at 77° K than at 300° K. Further work on germanium samples will continue at liquid helium temperatures.

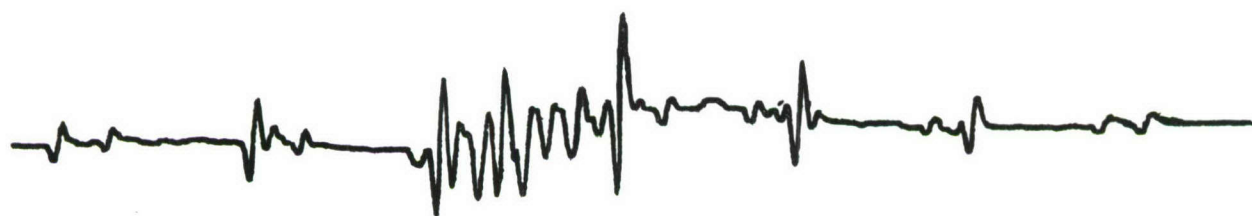
4.2.6 Potassium Chloride Crystals

The study of X_2^- centers in alkali halides has been continued. Both in our earlier Technical Notes and in previous sections of this report much theoretical and experimental data has been presented, especially on sodium chloride crystals.

Experiments were performed on K Cl crystals also. Undoped, lead-doped and thallium-doped crystals are available in our laboratory. A 2 x 2 x 10mm K Cl (Pb^{++}) crystal was carefully mounted at



(a) Attenuation 17 db.



(b) Attenuation 5 db.

Figure 28. EPR Spectra of Cl_2^- Centers in KCl (Pb^{++})
Crystal at Different Microwave Power Levels

the end of a quartz rod. It was then irradiated for nine minutes with 65 kv X-rays at 77° K. The Cl_2^- -center resonance was observed at 9400 Mc with the crystal 100 axis parallel to the magnetic field. The first derivative of the absorption was recorded for a range of microwave power levels (0 - 25 db). Figure 28 illustrates typical EPR spectrum records. The maximum signal was observed at an attenuation of 17 db. The measurements made indicated a saturation of 80%. It should be noted that this saturation value is to be associated with the allowed electronic transitions and it does not follow that the forbidden transition lines would saturate to the same degree. This is a critical point, since the forbidden transitions are the ones which must be pumped in a double resonance experiment with this type of sample. These forbidden lines occur at $\nu_e \pm \nu_n$. At a magnetic field value of 3400 gauss, the NMR frequency (ν_n) for K^{39} is 0.6756 Mc. Obviously, for a K Cl crystal sample, pumping on allowed or forbidden transitions separately will be a most difficult undertaking. The forbidden lines lie under the allowed lines. Pumping on an allowed line will involve pumping on a forbidden line simultaneously. (An inhomogeneously broadened EPR line, as is well known, may be viewed as composed of "packets" which interact minimally. If this is the case here, then there is still some hope of successfully pumping on the forbidden lines alone. It becomes a question of the frequency stability of the klystron and the width of such "packets".) If double resonance can be observed in this type of sample it will

provide an excellent opportunity to compare relaxation times and saturation behaviour of allowed and forbidden transitions in a single sample.

To date, double resonance has not been observed in these K Cl samples. The current problem is to observe the unenhanced NMR signals from either the K^{39} or Cl^{35} or Cl^{37} nuclei. Using liquid samples the NMR signals from such nuclei were detected at the frequencies associated with a field of 3400 gauss. Then, using the Robinson oscillator, a search was made for these resonances in crystals at 300° K and 77° K, at both high and low r.f. power levels, and over broad and narrow field scans. The same procedure was repeated in a magnetic field of 4600 gauss using the Varian variable frequency r.f. spectrometer in the 2 - 4 Mc range. NMR signals from the crystals were not observed.

At present a further study of these samples and of past NMR results in such samples is being made. A second Robinson oscillator, designed for low frequency operation, has been completed. A better understanding of the experimental aspects of the problem has been gleaned from the experiments on Na Cl crystals. We still feel that these K Cl crystals offer promise as double resonance samples and we plan to devote considerable time and attention to working on them.

References:

1. H. G. Beljers et al, Phys. Rev., 95, 1683 (1954).

2. E. H. Poindexter, Nature, 182, 1087 (1958); E. H. Poindexter, J. Chem. Phys., 31, 1477 (1959).
3. W. A. Anderson, Bull. Am. Phys. Soc., 4, 361 (1959).
4. E. Poindexter and J. Uebersfeld, J. Chem. Phys., 36, 2706 (1962).
5. W. A. Anderson, "Dynamic Nuclear Polarization in Liquids," Figure 9 of his paper. Cf. Reference 3.

CHAPTER 5

PREPARATION AND INVESTIGATION OF VARIOUS SAMPLES SUITABLE
FOR DMR (DOUBLE MAGNETIC RESONANCE)

5.1 GENERAL CONSIDERATIONS

The suitability of an electron-nuclear system for use in a double magnetic resonance depends on a number of factors. Obviously, one cannot arbitrarily pick a system and expect immediately to obtain enhancement of the nuclear signals. We may consider the following requirements as essential.

a) The Existence of a Dynamic Coupling Between the Electron and Nuclear Systems

The Hamiltonian of a general electron-nuclear system may be written:

$$\mathcal{H} = -g\beta\vec{H}_0\cdot\vec{S} + g_n\beta_n\vec{H}_0\cdot\vec{I} + \vec{I}\cdot\vec{A}\cdot\vec{S} + \sum_k \vec{S}_k\cdot\vec{B}_{ke}\cdot\vec{S}_e + \sum \vec{I}_m\cdot\vec{C}_{m,n}\cdot\vec{I}_n$$

where the first two terms are the electron Zeeman and nuclear Zeeman interactions of the electron and nuclear spins respectively. The magnetic field is H_0 . The third term is the electron-nuclear spin interaction energy.

The fourth term gives the interaction of the electron spin with all other electron spins, and the fifth term gives

the interaction of the nuclear spin with all other nuclei.

We have neglected interactions with the crystal field (except as they appear in the fourth term), quadrupole, and other higher order terms.

We must assume, when the perturbation of an r.f. field is applied, that cross relaxation terms exist which link the various electron-nuclear states. This condition is necessary for dynamic polarization, but not sufficient.

b) Saturability of Electron Transitions

The thermal relaxation processes considered above are usually described in terms of the longitudinal (or spin-lattice) and transverse (or spin-spin) relaxation times T_1 and T_2 . To obtain saturation of the electron spin system we must have a T_1 long enough that microwave energy is supplied to the spin system faster than it can be lost to the lattice. In this fashion we may, under suitable conditions (existence of proper cross relaxations), transfer energy to the nuclear system.

This means that we must, as far as possible, eliminate paramagnetic relaxations, i.e. processes which shorten T_1 . In this regard we will now consider the existence of paramagnetic centers. These appear in the fourth term of our

Hamiltonian. In a given sample these are of several types. The nuclei, since their magnetogyric ratio is so low, do not appreciably affect the electronic relaxations. The electron system itself is the 'pumping material' and we must be careful to have enough centers present to couple to the nuclei. The concentration of such centers will be shown to be critical. A further concern of great importance is the existence of electron paramagnetic impurities, other than the species used in pumping. The most common of these impurities is O_2 , which is paramagnetic and which often has a disastrous effect in shortening T_1 , consequently broadening EPR lines and making them unsaturable. This raises the question of sample preparation. Still, in considering paramagnetic relaxations we must look at the electron system itself.

c) Electron and Nuclear Spin Concentrations

In many cases the saturability of an EPR line is quite dependent on the concentration of the electron spins. A solution of DPPH in benzene is a very good example of this. Very concentrated solutions (1 - 10 Molar) exhibit a single, unsaturable EPR line due to the fact that the exchange interactions between electron spins dominates the hyperfine coupling between the unpaired electron and the two nearby nitrogen nuclei. As the solution strength is reduced (10^{-1} to 10^{-3} M.) the hyperfine interaction becomes

dominant and seven lines are observed. As the solution is diluted still more to 10^{-4} M., the EPR line becomes saturable to some extent.

Secondly, in order to observe nuclear enhancements, enough nuclei must "see" the electron spin. Again, DPPH in benzene is a good example. As mentioned in 4.2.1, in samples having concentrations below 10^{-4} M., there are insufficient electron spins present to affect all the protons present. As a consequence, no enhancement is observed.

Thirdly, to be observable, a sufficient concentration of nuclei is required. Consider the cases of Silicon 29 and Carbon 13. Si^{29} is approximately 4.7% abundant, C^{13} approximately 1.1%; it is thus apparent that any nuclear signals, even when enhanced, will be quite small. Samples enriched in the desired nuclei can be quite valuable in this situation.

5.2 SAMPLES PREPARED AND UNDER STUDY

5.2.1 Sugar Chars

In Technical Note No. 2 preliminary work on sugar chars was announced and further studies outlined. The main difficulty at the time was believed to be the preparation technique involved. No worthwhile amounts of the desired impurities could be adsorbed onto the chars. After some discussions with Dr. James Krebs of

the Naval Research Laboratories it was concluded that the initial chars should have been made under an inert atmosphere, and that the chars had been baked at too high a temperature. (Why this should affect them appreciably is still not apparent.) A new method of preparing samples has not yet been completely evolved.

5.2.2 Sodium Dispersion in Mineral Oil

In Technical Note No. 2 mention was made of investigations of sodium dispersions in mineral oil. In such a case where conduction electrons are present in a metal, a Knight Shift is present in the resonant field of the Na nuclei - the NMR line is shifted to a slightly lower field for the same radio frequency. In the case of the metallic dispersion the shift has been found to be several gauss. The Knight Shift is due to the contact part of the hyperfine interaction. In the Hamiltonian a term $I.S \left| \psi(0) \right|^2$ appears due to the fact that the conduction electrons in modified S-orbitals have a finite probability of being at the nucleus, in contact with it. If the EPR line due to the conduction electrons is saturated, this term disappears and the NMR line is shifted back to the field where the Na line in sodium compounds appeared. This reversing of the Knight Shift is sometimes referred to as the "Day Shift".

The magnitude of the "Day Shift" is directly proportional to the magnitude of the EPR saturation, reaching its maximum value at 100% saturation. This gives us a second method of

measuring the EPR saturation in addition to the usual method of measuring the amplitude of the EPR line. Moreover, it is not as dependent on the shape of the EPR line as is the measurement of the amplitude.

Another consideration must be mentioned in regard to the use of metallic dispersions for EPR studies. A metal, indeed any conductor, by virtue of its conductivity, attenuates by reflection an electromagnetic wave incident upon it. This can be expressed by a characteristic depth of penetration (δ).

$$\delta = \sqrt{\frac{2}{\mu \sigma \omega}}$$

where

σ = conductivity

μ = permittivity

ω = angular frequency of E-M radiation

and where (δ) is the distance within which the wave is attenuated by a factor of $1/e$. In the case of Na the depth of penetration at microwave frequencies is approximately 0.75×10^{-6} meters. If the particles in the dispersion are much above 0.75 microns in radius we cannot expect significant penetration of the sample by the microwave field. Consequently, the resulting EPR signal is reduced to some extent. The major effect is that the EPR line shape is distorted and cannot be easily saturated. Rather than the usual Lorentzian line shape, the line shape is Dysonian.

The reason for the difficulty of EPR saturation is easily explained. Upon initial application of the microwave signal, electron spins on the surface of the sample may be saturated. However, if electron spin-spin interactions are strong (and consequently spin-spin relaxation times short), the spins will diffuse to the interior of the particle where the microwave field is not available for pumping. For instance, if we make the approximation that only the electrons within one skin depth are directly affected by the microwave field, then in a particle of two skin depths radius, 87% of the electrons are "seen" by the microwave field. Similarly, for five skin depths in radius, 49% are "seen"; for 10 skin depths, 27%; for 100 skin depths, 2%.

In our investigation of the sodium dispersions, we have found a Knight Shift of the order of several gauss; when attempting to saturate the EPR line, there was no measureable shift of the NMR line, indicating that there was no saturation of the electron spins. The EPR line was quite Dysonian, retaining this shape under application of the full microwave power. The EPR line grew with increased power, indicating again little or no saturation. There was no change in the size of the NMR line, indicating no change of polarization.

From the Dysonian character of the EPR line we can infer that the metallic particles are larger than the skin depth. This indicates that they are larger than one micron in radius. Since there is no distortion of the NMR line, the particles are less

than 50 microns in size, the approximate skin depth at the resonant frequency of the nuclei.

The dispersion was diluted with mineral oil several times in an attempt to reduce the concentration of electron spins. This reduced the amplitude of both the EPR and NMR signals, but did not make saturation possible. Several experiments were attempted at liquid nitrogen temperatures, but this did not affect either the NMR or EPR to any extent. Further work on this sample has been discontinued until dispersions of much smaller particles can be prepared.

CHAPTER 6

CONCLUSIONS AND RECOMMENDATIONS

6.1 CONCLUSIONS

During the three year period in which this group has been under contract with the Rome Air Development Command, successful double magnetic resonance experiments, demonstrating a coupling between unpaired electron spins and nuclear spins, have been carried out on several samples. This has been accompanied by a considerable amount of theoretical and analytical work and by the development of suitable instrumentation and experimental techniques. Our principal effort has been concentrated on the alkali halides.

In NaCl, it is quite easy to detect the unenhanced nuclear signal from Na^{23} . Cl_2^- centers introduced by irradiation yield a well known EPR spectrum whose hyperfine components may be readily saturated. Both positive and negative enhancement of the Na^{23} signal has been observed. This was achieved by saturating forbidden transitions in which the "pump" frequency was equal to the electron spin resonance frequency plus or minus the nuclear spin resonance frequency. Analysis of the saturation and enhancement data made it possible to obtain numerical values for the concentration of Cl_2^- centers, the line width and

relaxation time of the forbidden transition, the number of sodium nuclei affected by one Cl_2^- center and the nuclear relaxation time. Mn^{++} ions are also present in our NaCl samples. These paramagnetic centers were also used to achieve a small positive enhancement of the Na^{23} resonance.

Additional samples in which DMR (Double Magnetic Resonance) was performed include DPPH in benzene, heavy fuel oil, and roofing tar dissolved in pump oil. In these three cases the unpaired electrons are associated with free radicals. Enhancement of the proton resonance signal was observed but with values smaller than those reported already in the literature by other groups.

Exploratory studies were made on a number of samples in which no DMR was achieved.

The hyperfine spectrum of Mn^{++} in CaCO_3 was observed and readily saturated. Both single ($\Delta M = \pm 1$) and double ($\Delta M = \pm 2$) transitions were detected indicating that this system is worthy of investigation as a possible maser. In addition the Redfield rotary resonance was observed at r.f. frequencies while the EPR signals were being saturated. This provides a means for measuring the amplitude of the time varying microwave signal. Attempts were made to observe the NMR frequency of Ca^{43} , C^{13} and O^{17} in CaCO_3 but were not successful probably due to the low natural abundance of these isotopes.

The EPR spectrum of Cl_2^- centers in KCl was observed and saturated. The NMR of K^{39} , Cl^{35} , and Cl^{37} was not observed.

Metallic sodium dispersed in mineral oil exhibited both an EPR and an NMR spectrum. The EPR lines were broad and not saturable. Broad EPR lines were observed in single crystals of boron, graphite, germanium, and potassium in graphite. None of these were saturable. Nuclear magnetic resonance on B^{11} , C^{13} , and Ge^{73} was attempted but no signals were detected.

6.2 RECOMMENDATIONS

A review of the first three year effort of our group indicates some guide lines for further research during the next three year period of the renewal contract.

a) Cl_2^- in NaCl

This sample offers many possibilities for extensive work. We have on hand samples of NaCl doped with various concentrations of Pb, Ag, and NO_2 ions. These are mixed into the melt when the single crystals are grown in order to inhibit F center formation and maximize Cl_2^- center concentrations. The number of Cl_2^- centers in our successful DMR experiments was estimated at between 10^{14} and 10^{15} cm^{-3} . Higher concentrations up to 10^{17} to 10^{18} cm^{-3} may be obtained by exposing the samples to more intense X-radiation. NMR enhancement should be investigated as a function of Cl_2^- concentration. The forbidden transitions associated with all seven hyperfine components should be studied for a fixed concentration in an attempt to determine

whether the enhancement at a given power level depends in a simple way on the intensities of the various hyperfine lines. These experiments should be carried out in both liquid N_2 and liquid He temperature ranges. Related theoretical studies should be undertaken in an effort to understand the mechanism of spin diffusion and to predict the concentration of paramagnetic centers which will optimize the NMR enhancement.

b) Other Alkali Halides

Cl_2^- in KCl, F_2^- in LiF, and F_2^- in NaF offer interesting possibilities comparable to the Cl_2^- in NaCl.

c) Paramagnetic Samples

The use of liquid helium temperatures is important in the study of paramagnetic Ce^{++} in magnesium lanthanum double nitrates, Cr^{+++} in Al_2O_3 and TiO_2 , etc. Although some work has been done on these, attempts should be made to enhance the NMR signal of two different nuclear species in the same sample in an effort to determine whether the coupling mechanism with the electron spin environment is the same or different for various nuclei.

d) Metal Ammonia Solutions

Na in NH_3 gives rise to very narrow, easily saturable EPR lines. This sample is worthy of study for two reasons: first, it provides a more accurate means of measuring H_1 by rotary resonance, secondly, enhancement of Na^{23} or

possibly H^2 should be compared with the enhancement of protons in the same paramagnetic environment.

e) Instrumentation

Modifications in instrumentation aimed at obtaining higher Q , more microwave power, and greater NMR signal to noise ratios should be undertaken. In particular the design and construction of a travelling wave helix for DMR is recommended.